Contents

List of Figures

List of Tables

List of Acronyms

AC	alternating current
AFM	artificial frequency mapping
AM	amplitude modulation
APFT	almost periodic Fourier transform
CMOS	complementary metal-oxide semiconductor
CW	continuous wave
DAE	differential algebraic equations
DC	direct current
DFT	discrete Fourier transform
EDGE	enhanced data rates for GSM evolution
ETHB	envelope transient harmonic balance
FDTD	finite-differences in time domain
FET	field effect transistor
FFT	fast Fourier transform
FM	frequency modulation
GMRES	generalized minimum residual
GSM	global system for mobile communications
HB	harmonic balance
IDFT	inverse discrete Fourier transform
IFFT	inverse fast Fourier transform
LSI	large scale integration
MDFT	multidimensional discrete Fourier transform
MFDTD	multivariate finite-differences in time domain
MOSFET	metal-oxide semiconductor field effect transistor

MPDAE	multirate partial differential algebraic equations
MRK	multirate Runge-Kutta
ODE	ordinary differential equations
PA	power amplifier
PLL	phase-locked loop
PM	phase modulation
PWM	pulse-width modulation
RF	radio frequency
RK	Runge-Kutta
SB	spectral balance
SoC	systems-on-a-chip
SPICE	simulation program with integrated circuit emphasis
TD-ENV	time-domain envelope following
VCO	voltage-controlled oscillator
VLSI	very large scale integration
WaMPDAE	warped multirate partial differential algebraic equations
2-D	two-dimensional
3-D	three-dimensional

Chapter 1
Introduction

1.1 Motivation

The increased use of digital signal processing and digital control techniques in current wireless transceivers, and the resulting combination of radio frequency (RF), baseband analog and digital technologies in the same circuit, created a new set of heterogeneous networks, and thus new challenges in terms of circuit simulation. In fact, both the necessity of providing increased levels of wireless systems' functionality, and the need to improve the transmitters' efficiency and linearity, have led to the extensive use of digital circuits, not only for signal processing purposes, but also for performing control operations. Current examples of these include receiver automatic gain control, transmitter output power control and look-up-table, or field-programmable-gate-arrays, based digital predistortion linearizers. This way, integrated systems-on-a-chip (SoC), combining RF and baseband analog and digital circuitry on modern complementary metal-oxide semiconductor field effect transistor (CMOS FET) technologies, are gradually reshaping current and upcoming wireless transceiver architectures.

An illustrative example where digital techniques have invaded the analog domain is the all-digital phase-locked loop (PLL) and transmitter chip recently demonstrated for GSM/EDGE hand-sets [66]. In this example, most of the conventional analog blocks were substituted by purely digital algorithms or mixed analog-digital circuits. That was the case of the power amplifier driver, in this design replaced by a high-speed digital-to-analog converter, appropriately named a digital-to-RF-amplitude converter. Other recent illustrative examples showing integration of digital techniques with traditional analog RF circuits are reported for example in [3], or [25]. The high heterogeneity and strong nonlinearity features of such networks brought a new range of challenges to circuit simulation. Because the RF, the baseband and the digital blocks are intricately mixed, it is not possible to adopt the circuit-level/system-level co-simulation methodology, in which some of the blocks are represented with a simplified system-level description, while the remaining (usually the

critical parts of the circuit) are simulated at the circuit-level, in a more or less independent way. Instead, a full circuit-level simulation technique is required, where we have to face a complex strongly nonlinear scenario, presenting heterogeneous state variables (node voltages and branch currents), evolving on widely disparate time scales.

The recent interest in envelope elimination and restoration power amplifiers [4], [18], [69], or wireless polar transmitters, has also conducted to new considerable difficulties that available RF simulators can not overcome. These are also clear examples of heterogeneous circuits where the circuit-level/system-level co-simulation technique is not applicable. In wireless polar transmitters, the amplitude, AM, and phase, PM, modulations are treated in two parallel branches. The PM branch is a traditional RF chain composed by a continuous wave (CW), sinusoidal RF carrier oscillator, a PM modulator and a highly efficient switching-mode power amplifier. Conversely, the AM path is a baseband chain whose signal is typically processed with digital over-sampling techniques [either with (sigma-delta quantizers) or without (pulse-width modulation) quantization noise shaping], which is then passed to the analog domain via fast switching power devices and a low-pass reconstruction filter. Thus, in such circuits, the RF and baseband (or even digital) circuitry are also intricately mixed. Moreover, the switching behavior of the AM power-supply modulator produces waveforms of very short rise and fall times that are extremely demanding on the number of harmonics, for a convenient frequency-domain representation. This advises the substitution of the traditional frequency-domain harmonic balance solvers (very popular in the RF and microwave community), by their time-domain rivals.

In summary, RF simulation has been led to an increasingly challenging scenario of heterogeneous broadband and strongly nonlinear wireless communication circuits, presenting a wide diversity of slowly varying and rapidly changing state variables. These circuits may also have excitation regimes with completely different formats and running on widely separated time scales [e.g., baseband information signals, AM signals, PM signals, RF carriers, digital clocks, pulse-width modulation (PWM) signals, etc.]. At present, none of the available RF tools, as the ones encountered in commercial packages, or the ones recently published in the literature, are capable of simulating this kind of circuits in an efficient way. The main reason for that is because RF tools do not perform any distinction between nodes or blocks within the circuit. Thus, since it is not possible to adopt the circuit-level/system-level co-simulation methodology, and a full circuit-level simulation technique is mandatory, all the blocks in the circuits are treated in the same way. This means that the same numerical algorithm is required to simultaneously compute the response of the digital blocks, the baseband analog blocks and the RF blocks. Obviously, this is not recommended at all in view of the fact that signals in different blocks have completely different features and evolve on widely disparate rates of change. For instance, it may be noted that, since time evolution rates of signals in different parts of a circuit may differ from three, or more, orders of magnitude,

and the sampling rate of the signals is dictated by the fastest ones, the application of the same numerical method to all the blocks will result in high inefficiency.

1.2 Objectives

In the above we have described the motivation for this thesis. We have showed that simulating some modern wireless communication systems is today a hot topic. In effect, serious difficulties arise when these nonlinear systems are highly heterogeneous circuits operating in multiple time scales. The main goal of this thesis is to develop new computer-aided design tools for the efficient numerical simulation of such circuits. In order to achieve this goal we had to go through the following intermediate steps:

- Analyze the circuits' operation in order to identify and characterize their multirate behavior (stimuli heterogeneities, time-rate disparities of the state variables, existence of different time constants in distinct parts of the circuits, possible partition into active and latent sub-circuits, etc.);
- Get a general overview on the existing simulation tools, in order to examine the main characteristics of standard simulation methods (commonly used for computing the numerical solution of classic RF problems), and carefully study the most relevant advanced simulation techniques (available for computing the solution of multirate RF problems);
- Conceive innovative numerical simulation methods capable of simulating the circuits in an efficient way;
- Test the efficiency of the proposed numerical methods by applying them to illustrative application examples, and comparing the corresponding results with the ones obtained with available RF tools.

1.3 Summary

To fulfill the above stated objectives, this thesis is organized as follows.

After this brief introductory chapter, Chapter 2 provides some general background material on standard simulation techniques commonly used for computing the numerical solution of ordinary uni-rate problems. The chapter begins with the circuit equation formulation, in which some basic concepts and definitions for both lumped and distributed problems are given. Then, numerical integration algorithms well-suited for transient analysis are addressed, and finally time and frequency-domain techniques for computing periodic steady-state solutions are discussed.

Chapter 3 presents some advanced simulation techniques for computing the numerical solution of multirate RF problems. The chapter provides a general overview on the state of the art in multirate circuit simulation, in the sense that the most relevant contributions to this research field are reported and their capabilities discussed.

Chapter 4 is devoted to the discussion of a new computer-aided design tool, especially conceived for the efficient numerical simulation of highly heterogeneous and strongly nonlinear RF circuits, considered as running in two separated time scales. The proposed numerical method operates in a bivariate framework and uses modern multirate Runge-Kutta algorithms coupled with an envelope following technique to benefit from the circuits' heterogeneity and stimuli time-rate disparities.

Since the efficiency of the method proposed in Chapter 4 degrades when more than two time scales are involved, Chapter 5 proposes an alternative powerful time-domain simulation technique to overcome that problem. The method proposed in this chapter is a robust simulation tool that is particularly suitable for highly heterogeneous and strongly nonlinear RF circuits running in three distinct time scales, and introduces an innovative multiple-line double multirate shooting technique operating within a 3-D framework.

Chapter 6 is dedicated to the discussion of two innovative time-domain techniques that operate within a bivariate framework of a periodic fast time scale and two aperiodic slow time scales, mixed in the same dimension. The methods are tailored for simulating strongly nonlinear RF circuits whose state variables are all fluctuating in the fast carrier time scale, but, in opposition, are presenting different rates of variation in the slow envelope time dimension. An alternative concept of time-domain latency is exploited in this chapter.

Chapter 7 describes a new mixed frequency-time technique, especially conceived for the efficient simulation of moderately nonlinear RF circuits. This new and efficient approach combines multitime envelope transient harmonic balance (ETHB) with a purely time-marching engine, to process some state variables in a bivariate mixed frequency-time domain, while others are treated in a single-time manner.

Finally, Chapter 8 concludes this thesis by summarizing its most relevant achievements, and pointing some future work directions as a continuation of this research.

1.4 Original Contributions

This thesis is believed to represent an important contribution to the RF and microwave circuit simulation area. The theoretical and experimental work carried out in this research have conducted to the development of some innovative computational tools, which demonstrated to be very powerful and appropriate to face the increasingly challenging simulation scenarios brought by modern wireless communication technologies.

The major contributions of this thesis can be summarized as the numerical methods described in Chapters 4, 5 and 7. The first and the second are innovative purely time-domain techniques, which allow the efficient simulation of highly heterogeneous RF circuits operating under strong nonlinear regimes. The third contribution consists in the development of a new mixed frequency-

time technique, which is more appropriate to deal with circuits presenting moderately nonlinearities.

We disseminated the main contributions of this research through the publication of papers in some major peer reviewed international conferences and journals. These are listed in the following.

Papers in International Conferences:

Oliveira, J. F., and J. C. Pedro, "A New Time-Domain Simulation Method for Highly Heterogeneous RF Circuits," *Proc. 37th European Microwave Conference*, Munich, Oct. 2007, pp. 1161-1164.

Oliveira, J. F., and J. C. Pedro, "An Innovative Time-Domain Simulation Technique for Strongly Nonlinear Heterogeneous RF Circuits Operating in Diverse Time Scales," *Proc. 38th European Microwave Conference*, Amsterdam, Oct. 2008, pp. 1557-1560.

Papers in International Journals:

Oliveira, J. F., and J. C. Pedro, "An Efficient Time-Domain Simulation Method for Multirate RF Nonlinear Circuits," *IEEE Transactions on Microwave Theory and Techniques*, vol. 55, no. 11, Nov. 2007, pp. 2384-2392.

Oliveira, J. F., and J. C. Pedro, "A Multiple-Line Double Multirate Shooting Technique for the Simulation of Heterogeneous RF Circuits," *IEEE Transactions on Microwave Theory and Techniques*, vol. 57, no. 2, Feb. 2009, pp. 421-429.

Chapter 2
Background Material

2.1 Introduction

This chapter is intended to provide some background material on standard simulation techniques that may be used for computing the numerical solution of ordinary uni-rate problems. Section 2.2 is devoted to the circuit equation formulation, i.e., to the construction of a mathematical model that describes the operation of a generic electronic circuit. Then, the presentation of the various circuit analysis and simulation methods is organized by dividing them in two groups. The first one, described in Section 2.3, is devoted to the examination of the transient analysis of the circuits, in which the classic time-step integration techniques (the SPICE-like simulation engines) are focused. The second group, addressed in Section 2.4, is dedicated to the discussion of numerical algorithms for computing the steady-state solutions. We first examine some time-domain techniques, as shooting, or finite-differences in time domain (FDTD), to then analyze the most commonly used frequency-domain technique in the RF and microwave community: the harmonic balance (HB) method. A comparison between various aspects of the performance of the methods will be provided to make clear each of their strengths and weaknesses. Also, a comparison between the time and frequency-domain approaches will be made to elucidate the corresponding advantages and disadvantages.

2.2 Mathematical Model of an Electronic Circuit

2.2.1 Lumped Problems

The behavior of an electronic circuit can be described with a system of equations involving voltages, currents, charges and fluxes. This system of equations can be constructed from a circuit description using, for example, nodal analysis, which involves applying the Kirchoff current law to each node in the circuit, and applying the constitutive or branch equations to each circuit element.

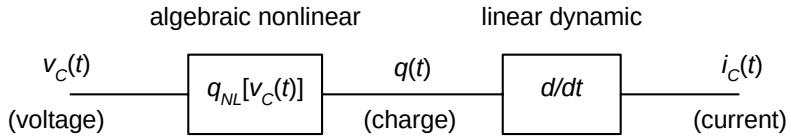

Figure 2.1 Quasi-static model for a nonlinear capacitance.

Under the *quasi-static assumption*, [27], [56], systems generated this way have, in general, the following form,

$$\boldsymbol{p}\left[\boldsymbol{y}(t)\right]+\frac{d\boldsymbol{q}\left[\boldsymbol{y}(t)\right]}{dt}=\boldsymbol{x}(t), \tag{2.1}$$

where $\boldsymbol{x}(t)\in\mathbb{R}^n$ and $\boldsymbol{y}(t)\in\mathbb{R}^n$ stand for the excitation (independent voltage and current sources) and state variable (node voltages and branch currents) vectors, respectively. $\boldsymbol{p}\left[\boldsymbol{y}(t)\right]$ stands for all memoryless linear or nonlinear elements, as resistors, nonlinear voltage-controlled current sources, etc., while $\boldsymbol{q}\left[\boldsymbol{y}(t)\right]$ models dynamic linear or nonlinear elements, as capacitors (represented as linear or nonlinear voltage-dependent electric charges), or inductors (represented as linear or nonlinear current-dependent magnetic fluxes).

The quasi-static assumption is invariably used when modeling nonlinear devices. In this approximation, all quantities in nonlinear circuit elements are assumed to be functions only of instantaneous values of the controlling variables [27], [56]. It should be noted that a quasi-static circuit element does not have to be memoryless. For instance, a capacitor is considered as quasi-static if its charge, and, consequently, its incremental capacitance, are only functions of the instantaneous voltage across its terminals. This way, its current-voltage dependence can be modeled by the cascade of a linear dynamic operator and an algebraic nonlinear function. Please see Figure 2.1.

The system of (2.1) is, in general, a *differential algebraic equations'* (DAE) system. For achieving an intuitive explanation of the mathematical formulation of (2.1), let us consider the basic illustrative example depicted in Figure 2.2. This circuit is composed of a current source connected to a linear inductance and two nonlinear circuit elements commonly used when modeling semi-conductor devices (a nonlinear capacitance and a nonlinear voltage-dependent current source). These nonlinearities are assumed as quasi-static and thus are described by algebraic constitutive relations of voltage-dependent charge and voltage-dependent current. A nodal analysis of this circuit leads to the following system of equations in the node voltage $v_O(t)$ and the inductor current $i_L(t)$:

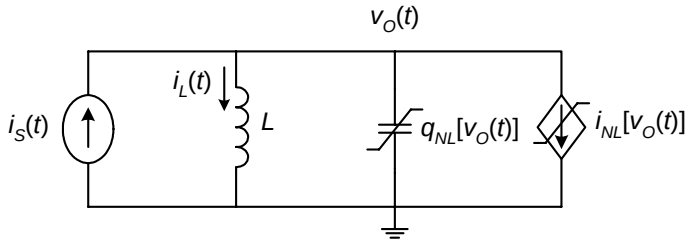

Figure 2.2 Nonlinear dynamic circuit example.

$$\begin{cases} i_{NL}\left[v_O(t)\right] + i_L(t) + \dfrac{d}{dt} q_{NL}\left[v_O(t)\right] = i_S(t) \\ v_O(t) + \dfrac{d}{dt}\left[-L \cdot i_L(t)\right] = 0 \end{cases} \tag{2.2}$$

This system can be seen as a particular case (in $\mathbb{R}^2$) of the DAE system of (2.1), in which the excitation vector, $\boldsymbol{x}(t)$, and the vector of state variables, $\boldsymbol{y}(t)$, are given by

$$\boldsymbol{x}(t) = \begin{bmatrix} i_S(t) \\ 0 \end{bmatrix}, \qquad \boldsymbol{y}(t) = \begin{bmatrix} v_O(t) \\ i_L(t) \end{bmatrix}. \tag{2.3}$$

The DAE system of (2.1) may obviously be written in other forms. For instance, if we apply the chain differentiation rule to the dynamic term of its left hand side, we can obtain

$$\frac{d\boldsymbol{q}(\boldsymbol{y})}{d\boldsymbol{y}} \frac{d\boldsymbol{y}(t)}{dt} = \boldsymbol{x}(t) - \boldsymbol{p}\left[\boldsymbol{y}(t)\right], \tag{2.4}$$

or,

$$\boldsymbol{M}\left[\boldsymbol{y}(t)\right] \frac{d\boldsymbol{y}(t)}{dt} = \boldsymbol{x}(t) - \boldsymbol{p}\left[\boldsymbol{y}(t)\right], \tag{2.5}$$

in which $\boldsymbol{M}\left[\boldsymbol{y}(t)\right]$ is usually known as the *mass matrix*. If this matrix is nonsingular, then the DAE system of (2.4) may degenerate into the following *ordinary differential equations'* (ODE) system,

$$\frac{d\boldsymbol{y}(t)}{dt} = \boldsymbol{M}\left[\boldsymbol{y}(t)\right]^{-1} \left(\boldsymbol{x}(t) - \boldsymbol{p}\left[\boldsymbol{y}(t)\right]\right), \tag{2.6}$$

which can be rewritten in the classical form

$$\frac{d\boldsymbol{y}(t)}{dt} = \boldsymbol{f}\left[\boldsymbol{t}, \boldsymbol{y}(t)\right], \tag{2.7}$$

commonly used in the mathematical literature. When $\boldsymbol{M}\left[\boldsymbol{y}(t)\right]$ is singular, the DAE system of (2.4) will not degenerate into a ODE system, but it is often possible to express it as a set of algebraic equations combined with a set of differential equations of the form of (2.7).

From the above we conclude that, in some cases, electronic circuits may be described by ODE systems instead of DAE systems. For example, if we return to the simple nonlinear dynamic circuit of Figure 2.2, and rewrite (2.2) as

$$\begin{cases} \dfrac{dq_{NL}(v_O)}{dv_O}\dfrac{dv_O(t)}{dt} = i_S(t) - i_{NL}\left[v_O(t)\right] - i_L(t) \\ L\dfrac{di_L(t)}{dt} = v_O(t) \end{cases} \tag{2.8}$$

or, in its vector-matrix form, as

$$\begin{bmatrix} \dfrac{dq_{NL}(v_O)}{dv_O} & 0 \\ 0 & L \end{bmatrix} \begin{bmatrix} \dfrac{dv_O(t)}{dt} \\ \dfrac{di_L(t)}{dt} \end{bmatrix} = \begin{bmatrix} i_S(t) - i_{NL}\left[v_O(t)\right] - i_L(t) \\ v_O(t) \end{bmatrix} \tag{2.9}$$

we can easily see that if $dq_{NL}(v_O)/dv_O \neq 0$ then the mass matrix is nonsingular, and the circuit may be described by an ODE system expressed in the classical form of (2.7), which, in this case, will simply result in

$$\begin{cases} \dfrac{dv_O(t)}{dt} = \left[\dfrac{dq_{NL}(v_O)}{dv_O}\right]^{-1}\left[i_S(t) - i_{NL}\left[v_O(t)\right] - i_L(t)\right] \\ \dfrac{di_L(t)}{dt} = \dfrac{1}{L}v_O(t) \end{cases} \tag{2.10}$$

2.2.2 Distributed Devices

Practical RF and microwave circuits typically include linear time-invariant *distributed devices* such as nonideal transmission lines. For instance, when two distant points of a printed circuit board are connected by a conductor, the conductor will be (most of the times) physically implemented with a strip of metal which passes over, but is insulated from, a ground plane. This metal strip may be long enough so that the voltages and currents vary appreciably over its length. The metal strip, the insulator and the ground plane form an approximation to a transmission line, which is the most common distributed device used in modeling circuits. The distribution of the voltages and currents along the metal strip affects the circuit performance. So, since it cannot be seen as an ideal conductor, it is necessary to consider its nonideal behavior. The behavior of a transmission line can be computed by solving the wave equation system that describes the voltages and currents along its length,

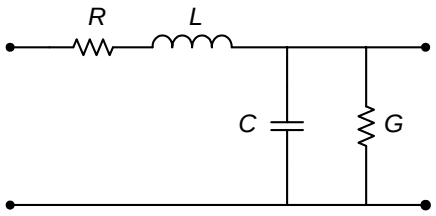

Figure 2.3 A lumped equivalent circuit to an infinitesimal section of a transmission line.

$$\begin{cases} L\dfrac{\partial i(z,t)}{\partial t}+\dfrac{\partial v(z,t)}{\partial z}+Ri(z,t)=0 \\ C\dfrac{\partial v(z,t)}{\partial t}+\dfrac{\partial i(z,t)}{\partial z}+Gv(z,t)=0 \end{cases} \tag{2.11}$$

where $v(z,t)$ and $i(z,t)$ are the voltage and current as a function of the position z along its length and time t. R, L, G and C, are the series resistance and inductance, and shunt conductance and capacitance, per unit length, respectively. To solve for the entire time evolution of the currents and voltages in the transmission line, boundary conditions must be established at its ends, and the initial distribution of voltages and currents over its length must be known.

In order to simulate circuits with transmission lines, (2.11) must be numerically solved for each line. One standard algorithm for solving (2.11) consists in approximating the transmission line with several sections of a resistor-conductor-inductor-capacitor network, as the one shown in Figure 2.3, and then simulating the resulting nondistributed (*lumped*) equivalent circuit with standard simulation techniques. A second approach to simulate circuits with transmission lines can be obtained by taking advantage of the fact that only the voltages and currents at the ends, or terminals, of the line ($z = 0$ and $z = l$) have an effect on the rest of the circuit. In the case of linear time-invariant transmission lines, the terminal currents can be computed from the terminal voltages by convolution with impulse responses. This means that a term of the form

$$\int_{-\infty}^{t} \boldsymbol{h}(t-\tau)\,\boldsymbol{y}(\tau)\,d\tau, \tag{2.12}$$

in which $\boldsymbol{h}(t)$ is the *matrix-valued impulse response* of the linear time-invariant distributed devices in the circuit, will be included in the left hand side of (2.1) if this technique is adopted.

The lumped equivalent circuit approach, as also the convolution integral technique, can be both computationally expensive. Although they seem particularly simple to incorporate in time-domain circuit simulators, they involve substantial additional data. In the first case, this is due to the fact that the distributed devices commonly present in RF circuits can only be represented accurately by lumped equivalent models with a large number of nodes, which means that a large number of state variables is added to the circuit equation formulation of (2.1). In the case of the convolution

integral technique, the considerable amount of data results from the fact that to calculate currents using the convolution integral, the voltages for all past are needed. Since none of these two strategies are adequate to deal with distributed devices, in this thesis we have decided to adopt the compact DAE formulation of (2.1), or possibly (2.7), for the general time-domain mathematical description of the circuits.

In order to simulate circuits with transmission lines in an efficient way, a frequency-domain approach is mandatory. Indeed, if it is possible to perform numerical computations directly in the frequency-domain, then linear time-invariant distributed devices can be easily included. Since the distributed devices are considered as linear, superposition allows each frequency to be handled individually. Consequently, the frequency-domain constitutive relations between currents and voltages are still algebraic, just like in lumped devices, which means that it is relatively easy to develop frequency-domain models for distributed devices. To illustrate this point, consider the wave equation system at the frequency ω,

$$\begin{cases} \left(L\frac{\partial}{\partial t} + R \right) I(z) e^{j\omega t} + \frac{\partial}{\partial z} V(z) e^{j\omega t} = 0 \\ \left(C\frac{\partial}{\partial t} + G \right) V(z) e^{j\omega t} + \frac{\partial}{\partial z} I(z) e^{j\omega t} = 0 \end{cases} \tag{2.13}$$

in which the voltage and the current take the form $V(z)e^{j\omega t}$ and $I(z)e^{j\omega t}$. $V(z)$ and $I(z)$ are complex phasors, and the system of (2.13) can be simplified to

$$\begin{cases} (R + j\omega L) I(z) e^{j\omega t} + \frac{\partial}{\partial z} V(z) e^{j\omega t} = 0 \\ (G + j\omega C) V(z) e^{j\omega t} + \frac{\partial}{\partial z} I(z) e^{j\omega t} = 0 \end{cases} \tag{2.14}$$

where the time derivatives were evaluated symbolically. This way, the partial differential system of (2.13) is converted into a simple ordinary differential system in space for the phasors. But, because only the terminal voltages and currents of the line affect the whole circuit in which it is inserted, (2.14) needs only to evaluated at $z = 0$ and $z = l$, and the line becomes described by a much simpler purely algebraic model.

Frequency-domain techniques are thus the right choice to handle distributed elements. These techniques differ form their time-domain rivals in many basic aspects and will be addressed later in Section 2.4.2.

2.3 Transient Analysis

2.3.1 Time-Step Integration

Let us consider the DAE system of (2.1), describing the behavior of a generic electronic circuit. Obtaining the solution to (2.1) over a specified time interval $[t_0, t_{Final}]$ from a specific initial

condition $\boldsymbol{y}(t_0) = \boldsymbol{y}_0$, is what is usually known as an *initial value problem*, and computing such solution is frequently referred to as *transient analysis*. The most natural way to evaluate $\boldsymbol{y}(t)$ is to numerically time-step integrate (2.1) directly in time domain. One possible way to do so consists in simply converting the differential equations into difference equations, in which the time derivatives are approximated by appropriate incremental ratios. With this strategy, the nonlinear differential algebraic equations' system of (2.1) is converted into a purely nonlinear algebraic system. For example, if we discretize the time *t* using a uniform grid (a set of a successive equally spaced time instants) defined as $t_i = t_0 + i \cdot h$, and use the backward Euler rule (the popular implicit finite-differences scheme of order 1 [24]) to approximate the time derivatives of (2.1), we obtain

$$\boldsymbol{p}(\boldsymbol{y}_i) + \frac{\boldsymbol{q}(\boldsymbol{y}_i) - \boldsymbol{q}(\boldsymbol{y}_{i-1})}{h} = \boldsymbol{x}(t_i), \tag{2.15}$$

where $\boldsymbol{y}_i$ denotes an approximation to the exact solution $\boldsymbol{y}(t_i)$, and the parameter $h = t_i - t_{i-1}$ is the time-step integration size. Small step sizes can provide a good accuracy in the simulation results but may conduct to large computation times. On the contrary, large step sizes will reduce the computation time but will definitely conduct to poorer accuracy. A good compromise between accuracy and simulation time is achieved when h is dynamically selected according to the to solution's rate of change. Once the solution $\boldsymbol{y}_{i-1}$ at the time instant t_{i-1} is known, the nonlinear algebraic system given by (2.15) must be solved to compute $\boldsymbol{y}_i$. The iterative Newton-Raphson algorithm [19], [45], is usually employed to solve (2.15). In summary, $\boldsymbol{y}(t)$ is evaluated for a set of successive time grid instants t_i within the $[t_0, t_{Final}]$ interval, beginning with the knowledge of the initial condition $\boldsymbol{y}(t_0) = \boldsymbol{y}_0$, and then solving the system of (2.15) for each time step.

The above formulation derives directly from the intuitive idea that derivatives can be approximated, and thus simply replaced, by finite-differences schemes. Although this technique can be used to compute the transient response of a generic electronic circuit described by (2.1), there is as alternative strategy which is more often employed to find the solution of initial value problems. Such strategy consists in using initial value solvers, as linear multistep methods [16], [24], or Runge-Kutta methods [16], [24] (the most popular time-step integrators). Both classes of theses methods can provide a wide variety of explicit and implicit numerical schemes, with very distinct properties in terms of order (accuracy) and numerical stability. Consequently, for the same time-step length h, solutions obtained with these methods can be extremely more accurate than the ones obtained with the backward Euler differentiation rule described above, which has order 1. Nevertheless, it must be noted that, instead of the backward Euler rule, an higher order finite-differences scheme could be used in (2.15). Because of substantial part of the research work described in this thesis is based on modern multirate Runge-Kutta schemes, we will restrict our presentation only on Runge-Kutta methods. Linear multistep methods will not be addressed here.

2.3.2 Runge-Kutta Methods

In view of the fact that the well-established theory of numerical integration is oriented toward the solution of standard ODEs, we will now consider the form of (2.7) for the mathematical description of a circuit's operation. So, let us consider a generic initial value problem with n state variables, expressed in its classical form by the system of (2.7) and the initial condition $\boldsymbol{y}(t_0) = \boldsymbol{y}_0$, i.e.,

$$\frac{d\boldsymbol{y}(t)}{dt} = \boldsymbol{f}\left[t, \boldsymbol{y}(t)\right], \quad \boldsymbol{y}(t_0) = \boldsymbol{y}_0, \quad t_0 \le t \le t_{Final}, \quad \boldsymbol{y}(t) \in \mathbb{R}^n. \tag{2.16}$$

Definition 2.1: Runge-Kutta (RK) method. A standard *s*-stage RK method expressed by its Butcher tableau $(\boldsymbol{b}, \boldsymbol{A}, \boldsymbol{c})$ [24]

$$\begin{array}{c|cccc} c_1 & a_{11} & a_{12} & \cdots & a_{1s} \\ c_2 & a_{21} & a_{22} & \cdots & a_{2s} \\ \vdots & \vdots & \vdots & & \vdots \\ c_s & a_{s1} & a_{s2} & \cdots & a_{ss} \\ \hline & b_1 & b_2 & \cdots & b_s \end{array} \tag{2.17}$$

for obtaining the numerical solution of (2.16) at the time instant $t_1 = t_0 + h$, is defined as [15], [24]:

$$\boldsymbol{y}(t_0 + h) \simeq \boldsymbol{y}_1 = \boldsymbol{y}_0 + h\sum_{i=1}^{s} b_i \boldsymbol{k}_i, \tag{2.18}$$

where

$$\boldsymbol{k}_i = \boldsymbol{f}\left(t_0 + c_i h, \boldsymbol{y}_0 + h\sum_{j=1}^{s} a_{ij}\boldsymbol{k}_j\right), \quad i = 1, 2, \ldots, s. \tag{2.19}$$

The algorithm defined by (2.18), (2.19), allows the numerical solution $\boldsymbol{y}_i$ at any generic time instant t_i to be evaluated from its previous calculated value $\boldsymbol{y}_{i-1}$. If we have $a_{ij} = 0$ for $j \ge i$, $i = 1, 2, \ldots, s$, then each of the $\boldsymbol{k}_i$ in (2.19) is given explicitly in terms of the previously computed $\boldsymbol{k}_j$, $j = 1, 2, \ldots, i-1$, and the method is then an explicit Runge-Kutta method. If this is not the case then the method is implicit and, in general, it is necessary to solve a nonlinear system of $n \times s$ algebraic equations to simultaneously compute all the $\boldsymbol{k}_i$. In general, any iterative technique (e.g., fixed point iteration [19], [45], or Newton-Raphson iteration) may be used to solve the nonlinear system of (2.19).

Runge-Kutta methods are universally utilized for time-step integrating initial value problems, and differ from linear multistep methods in several aspects. Since they present a genuine one-step format, one of their main advantages is that there is no difficulty in changing the steplength in a dynamic time-step integration process (in opposition to multistep methods where considerable

difficulties may be encountered when we want to change steplength [24]). The automatic step size control is based on the estimation of local errors, for which diverse techniques can be used, such as extrapolation techniques, or embedded RK formulas. All theoretical and technical details of implementation of these techniques, as also many other aspects of the RK methods, as consistency, convergence, order conditions, numerical stability, etc., are out of the scope of this thesis. They can be seen, for example, in [15], or [24].

2.3.3 Conventional Transient Simulation Technique: SPICE

In the above we have seen that the most natural way of simulating an electronic circuit is to numerically time-step integrate, in time domain, the ordinary differential system describing its operation. So, it should be of no surprise that this straightforward technique was used in the first digital computer programs of circuit analysis and is still nowadays the most widely used numerical method for that purpose. It is present in all SPICE or SPICE-like computer programs.

SPICE (which means Simulation Program with Integrated Circuit Emphasis) was initially developed at the Electronics Research Laboratory of the University of California, Berkeley, in the early 1970's. The real popularity of SPICE started with SPICE2 [32] in 1975, which was a much-improved program than its original version (SPICE1), containing several analyses (AC analysis, DC analysis, DC transfer curve analysis, transient analysis, etc.) and device models needed to design integrated circuits of that time. SPICE2 transient analysis used either the trapezoidal rule [24] or the Gear integration method [24], for the time-step integration of (2.1) with dynamic step size control.

Other versions of SPICE have been developed along the years and today many commercial simulators are based on SPICE. However, its application to RF circuits may cause some problems resulting from the specific behavior of RF systems. To understand that we must recall that RF signals are typically narrowband signals. This means that a data signal with a relatively low bandwidth is transmitted at a very high carrier frequency. To simulate a sufficient portion of the data signal a large number of carrier periods must be time-step integrated, and thus a very large number of time samples is required (a large amount of memory and computational time consumption). Some of the major limitations of SPICE transient analysis are overcome with the methods described in the following section.

2.4 Steady-State Simulation Engines

Although some simulation tools focus on transient analysis (SPICE-like simulation), the steady-state behavior of the circuits is typically of primary interest to RF and microwave designers. The main reason for that is because certain aspects of system performance are easier to characterize and verify in steady-state. For instance, distortion, noise, power, and transfer characteristics such as

gain, or impedance, are examples of quantities that are best measured, or simply only defined, when a circuit is in steady-state.

Time-step integration engines, as the ones described in the previous section, which were tailored for finding the circuit's transient response, are not adequate for computing the steady-state. As seen, time-step integration is a numerical implementation for obtaining the solution of an initial value problem, because it evaluates $\boldsymbol{y}(t)$ for a set of successive time instants (time steps) from the knowledge of an initial condition $\boldsymbol{y}(t_0)$. However, if the objective is the determination of the steady-state, there is no other way than to pass through the lengthy process of integrating all transients, and expecting them to vanish. In circuits presenting extremely different time constants, or high *Q* resonances, as is typically the case of RF and microwave circuits, time-step integration can be very inefficient. Indeed, in such cases frequencies in steady-state response are much higher than the rate at which the circuit approaches steady-state, or the ratio between the highest and the lowest frequency is very large. Thus, the number of discretization time steps used by the numerical integration scheme will be enormous, because the time interval over which the differential equations must be numerically integrated is set by the lowest frequency, or by how long the circuit takes to achieve steady-state, while the size of the time steps is constrained by the highest frequency component.

Before beginning to present some common steady-state simulation techniques, it must be noted that there are several different kinds of steady-state behavior that may be of interest. The first one is *DC steady-state*. Here the solution obviously does not vary with time. Stable linear circuits driven by sinusoidal sources may exhibit a *sinusoidal steady-state* regime, which is characterized as being purely sinusoidal except, possibly, for some DC offset. If the steady-state response of a circuit consists of generic waveforms presenting a common period, then the circuit is said to be in *periodic steady-state*. If a nonlinear circuit is excited by several periodic sources at uncommensurated frequencies, the circuit will typically have a *quasiperiodic steady-state* regime. The computation of quasiperiodic responses, which consist of linear combinations of the sum and difference frequencies of a finite set of fundamental frequencies and their harmonics, will be discussed in the next chapter.

The periodic steady-state regime is the one that will be addressed in this section. In the following subsections we will briefly describe some standard steady-state simulation engines that compute the periodic steady-state solution in a much more efficient way than numerically integrating the circuit's associated differential system from some arbitrary initial condition. Time-domain methods will be presented first. Then, frequency-domain techniques will be addressed.

2.4.1 Time-Domain Techniques

Computing the periodic steady-state response of an electronic circuit involves finding the initial condition, $\boldsymbol{y}(t_0)$, for the differential system that describe the circuit's operation, such that the

solution at the end of one period matches the initial condition, i.e., $\boldsymbol{y}(t_0) = \boldsymbol{y}(t_0 + T)$, where T is the period. Problems of this form, those of finding the solution to a system of ordinary differential equations that satisfies constraints at two or more distinct points in time, are referred to as *boundary value problems*. In this particular case, we have a *periodic boundary value problem* that can be formulated as

$$\boldsymbol{p}\left[\boldsymbol{y}(t)\right] + \frac{d\boldsymbol{q}\left[\boldsymbol{y}(t)\right]}{dt} = \boldsymbol{x}(t), \quad \boldsymbol{y}(t_0) = \boldsymbol{y}(t_0 + T), \quad t_0 \le t \le t_0 + T, \quad \boldsymbol{y}(t) \in \mathbb{R}^n, \tag{2.20}$$

or, in the classical ODE form, as

$$\frac{d\boldsymbol{y}(t)}{dt} = \boldsymbol{f}\left[t, \boldsymbol{y}(t)\right], \quad \boldsymbol{y}(t_0) = \boldsymbol{y}(t_0 + T), \quad t_0 \le t \le t_0 + T, \quad \boldsymbol{y}(t) \in \mathbb{R}^n, \tag{2.21}$$

where the condition $\boldsymbol{y}(t_0) = \boldsymbol{y}(t_0 + T)$ is known as the *periodic boundary condition*.

Solving (2.21) involves computing a numerical solution that simultaneously satisfies the differential system and the two point periodic boundary condition. Certainly, there is no shortage of mathematical literature describing methods for solving boundary value problems. However, certain methods have been found especially useful for electronic circuit problems. We will examine here the two standard time-domain alternatives that may be used for computing periodic steady-state responses of electronic circuits [21], [44]: the *shooting* method and the *finite-differences in time domain* (FDTD) method.

2.4.1.1 The Shooting Method

The time-domain method most commonly used for numerically evaluating the periodic steady-state solution of an electronic circuit is the shooting method. Shooting solves boundary value problems by computing the solution to a succession of initial value problems with progressively improved guesses at an initial condition, which ultimately results in steady-state. In a circuit's steady-state simulation, shooting begins by simulating the circuit for one period using some guessed initial condition (generally determined from a previous DC analysis). Then, the computed solution at the end of the period is checked, and if it does not agree with the initial condition, the initial condition is wisely modified. The circuit is then re-simulated with the adjusted initial condition, and this process is repeated until the solution after one period matches the initial condition.

In order to provide some mathematical details on the implementation of the shooting method, let us consider (2.21). Now suppose that we want to numerically time-step integrate the differential system in (2.21) with an initial value solver. As stated above, time-step integration is tailored for transient analysis, but is inadequate for computing steady-state responses. The problem comes from the fact that we don't know a priori which initial condition $\boldsymbol{y}(t_0)$ must be considered that will lead to the steady-state solution in the period T, i.e., that will satisfy the periodic boundary condition $\boldsymbol{y}(t_0) = \boldsymbol{y}(t_0 + T)$. So, we are trying to solve a boundary value problem with an initial value

solution technique. One possible way to convert the initial value solution procedure into a boundary value problem solver consists of guessing the initial estimate of $\boldsymbol{y}(t_0)$, or shooting for $\boldsymbol{y}(t_0)$, time-step integrating the differential system from $t = t_0$ until $t = t_0 + T$, comparing the resulting $\boldsymbol{y}(t_0 + T)$ with $\boldsymbol{y}(t_0)$, and then wisely update the initial estimate. So, shooting is an iterative solver that uses an initial value technique to solve a boundary value problem. In the end, it relies on finding the solution of

$$\boldsymbol{y}(t_0) = \boldsymbol{y}(t_0 + T) \Leftrightarrow \boldsymbol{y}(t_0) - \boldsymbol{y}(t_0 + T) = 0. \tag{2.22}$$

Let us now define $\boldsymbol{y}(t_0 + T) = \phi\left[\boldsymbol{y}(t_0), T\right]$ and rewritte (2.22) as

$$\phi\left[\boldsymbol{y}(t_0), T\right] - \boldsymbol{y}(t_0) = 0, \tag{2.23}$$

where ϕ is the *state-transition function* [21], [44]. An easy way to solve (2.23) consists in using the fixed-point iteration solver, which, in this case, would simply result in

$$\boldsymbol{y}^{[r+1]}(t_0) = \phi\left[\boldsymbol{y}^{[r]}(t_0), T\right]. \tag{2.24}$$

However, shooting with the fixed-point iteration technique is obviously equivalent to integrating the original differential system from $t = t_0$ until all transients decay. So, it is generally a useless technique because the convergence to the periodic steady-state solution may be extremely slow. A well known tactic to accelerate the route to steady-state, i.e., to accelerate the convergence of (2.23) to its solution, is the so-called *shooting-Newton* technique. As any other shooting technique, shooting-Newton is based on guessing initial conditions. However, it can take advantage of the fact that, although electronic circuits can be strongly nonlinear, their state-transition functions are usually quite linear. This means that slight perturbations on the initial condition (starting state) produce almost proportional perturbations in the subsequent time states. Taking this in to account, it is easy to conclude that (2.23) can be iteratively solved in an efficient way with the Newton's method, which in this case will lead us to

$$\phi\left[\boldsymbol{y}^{[r]}(t_0), T\right] - \boldsymbol{y}^{[r]}(t_0) + \left[\frac{\partial \phi\left[\boldsymbol{y}(t_0), T\right]}{\partial \boldsymbol{y}(t_0)} - I\right]\Bigg|_{\boldsymbol{y}(t_0) = \boldsymbol{y}^{[r]}(t_0)} \left[\boldsymbol{y}^{[r+1]}(t_0) - \boldsymbol{y}^{[r]}(t_0)\right] = 0, \tag{2.25}$$

where I is the $n \times n$ identity matrix. The only entity of (2.25) that is difficult to compute is the derivative of the state-transition function (usually referred to as the *sensitivity matrix*). In order to compute this matrix we must take into consideration the chain differentiation rule. In fact, since in practice $\phi\left[\boldsymbol{y}(t_0), T\right]$ is nothing more than the numerical value $\boldsymbol{y}_K$, with K being the total number of time steps in the interval $[t_0, t_0 + T]$, which depends on the previous value $\boldsymbol{y}_{K-1}$, which, itself, depends on $\boldsymbol{y}_{K-2}$, and so forth, the sensitivity matrix can be given by

$$\frac{\partial \phi\left[\boldsymbol{y}(t_0), T\right]}{\partial \boldsymbol{y}(t_0)} = \frac{\partial \boldsymbol{y}_K}{\partial \boldsymbol{y}_{K-1}} \cdot \frac{\partial \boldsymbol{y}_{K-1}}{\partial \boldsymbol{y}_{K-2}} \cdot \cdots \cdot \frac{\partial \boldsymbol{y}_1}{\partial \boldsymbol{y}_0}. \tag{2.26}$$

It is easy to see that all the matrices in (2.26) can be individually computed along the time-step integration process. For concreteness, let us suppose that a standard Runge-Kutta method (2.18), (2.19), is being used to perform time-step integration on the consecutive iterations of the shooting method. If, for example, we want to evaluate the first matrix, then we have

$$\frac{\partial \boldsymbol{y}_1}{\partial \boldsymbol{y}_0} = I + h\sum_{i=1}^{s} b_i \frac{\partial \boldsymbol{k}_i}{\partial \boldsymbol{y}_0}. \tag{2.27}$$

Now, if we rewrite (2.19) as

$$\boldsymbol{k}_i = \boldsymbol{f}\left(t_0 + c_i h, \boldsymbol{y}_0 + h\sum_{j=1}^{s} a_{ij}\boldsymbol{k}_j \right) = \boldsymbol{f}\left(t_0 + c_i h, \boldsymbol{Y}_i\right), \quad i = 1,2,\ldots,s, \tag{2.28}$$

we obtain

$$\frac{\partial \boldsymbol{k}_i}{\partial \boldsymbol{y}_0} = \left.\frac{\partial \boldsymbol{f}}{\partial \boldsymbol{y}}\right|_{t_0 + c_i h, \boldsymbol{Y}_i} \cdot \frac{\partial \boldsymbol{Y}_i}{\partial \boldsymbol{y}_0}, \quad i = 1,2,\ldots,s. \tag{2.29}$$

In an explicit Runge-Kutta method each one of the $\partial \boldsymbol{k}_i / \partial \boldsymbol{y}_0$ may be evaluated in terms of previously computed $\partial \boldsymbol{k}_j / \partial \boldsymbol{y}_0$, $j = 1,2,\ldots,i-1$. In an implicit Runge-Kutta method all the $\partial \boldsymbol{k}_i / \partial \boldsymbol{y}_0$ in (2.29) must be computed simultaneously.

Although solving (2.25) and computing the sensitivity matrix may involve some extra computational cost, shooting-Newton converges to the steady-state solution much faster than the normal time-step integration procedure (shooting with fixed-point iteration). This is the reason why it is the time-domain steady-state engine most widely used in circuit simulation.

Beyond shooting-Newton, there is another well known technique that may be used to accelerate the convergence of the shooting method. Such technique is based on extrapolation methods, and will not be addressed in this thesis. All of its details of implementation can be seen in for example in [21].

2.4.1.2 FDTD

Finite-differences in time domain (FDTD) is an alternative technique that can be utilized to determine the solution of a boundary value problem, and thus may be used to compute the periodic steady-state response of an electronic circuit. FDTD methods consist in defining a time grid over the entire time interval, to then impose a discretization of the differential system, replacing its derivatives with finite-difference approximations. With this strategy, the differential system describing the circuit's operation is converted into a nonlinear algebraic equations' system, which can be solved iteratively. A brief explanation of the FDTD methods is provided in the following.

Let us consider (2.20). Let us also consider the discretization of the $[t_0, t_0 + T]$ time interval defined by the grid

$$t_0 < t_1 < t_2 < \cdots < t_{i-1} < t_i < \cdots < t_K = t_0 + T, \qquad h_i = t_i - t_{i-1}, \tag{2.30}$$

which has a total of $K+1$ grid points and may be, in general, nonuniform. If we impose a finite-differences discretization to (2.20), using, for example, the backward Euler rule, then we obtain

$$\boldsymbol{p}(\boldsymbol{y}_i)+\frac{\boldsymbol{q}(\boldsymbol{y}_i)-\boldsymbol{q}(\boldsymbol{y}_{i-1})}{h_i}=\boldsymbol{x}(t_i),\quad i=1,\ldots,K, \tag{2.31}$$

with $\boldsymbol{y}_i \simeq \boldsymbol{y}(t_i)$, together with the condition describing the periodic regime

$$\boldsymbol{y}_0 = \boldsymbol{y}_K. \tag{2.32}$$

The system of (2.31) is a nonlinear algebraic system of $n\times K$ equations in $n\times(K+1)$ unknowns, $\boldsymbol{y}_0$, $\boldsymbol{y}_1$, …, $\boldsymbol{y}_K$. By substituting (2.32) into (2.31), these systems can then be rewritten jointly as a nonlinear algebraic system of $n\times K$ equations in $n\times K$ unknowns

$$\begin{aligned}
&\boldsymbol{p}(\boldsymbol{y}_1)+\frac{\boldsymbol{q}(\boldsymbol{y}_1)-\boldsymbol{q}(\boldsymbol{y}_0)}{h_1}=\boldsymbol{x}(t_1)\\
&\boldsymbol{p}(\boldsymbol{y}_2)+\frac{\boldsymbol{q}(\boldsymbol{y}_2)-\boldsymbol{q}(\boldsymbol{y}_1)}{h_2}=\boldsymbol{x}(t_2)\\
&\vdots\\
&\boldsymbol{p}(\boldsymbol{y}_0)+\frac{\boldsymbol{q}(\boldsymbol{y}_0)-\boldsymbol{q}(\boldsymbol{y}_{K-1})}{h_K}=\boldsymbol{x}(t_K)
\end{aligned} \tag{2.33}$$

The solution of this system may be evaluated with a $n\times K$ - dimensional Newton-Raphson iterative solver. For that, it starts with some estimate $\left[\boldsymbol{y}_0^{[0]},\boldsymbol{y}_1^{[0]},\ldots,\boldsymbol{y}_{K-1}^{[0]}\right]$ and hopefully expects that it iteratively converges to the steady-state solution.

As we can see, unlike the shooting methods, in which all intermediate iterations verify the differential system but not the boundary condition, in the FDTD approach the boundary condition is always satisfied, but the differential system is not. Another important feature of the FDTD methods, which is not shared by the shooting methods, is that they attempt to solve for all $\left[\boldsymbol{y}_0,\boldsymbol{y}_1,\ldots,\boldsymbol{y}_{K-1}\right]$ simultaneously. This is the reason why they rely on $n\times K$ - dimensional Newton-Raphson iteration schemes, while shooting-Newton involves only n - dimensional Newton-Raphson iterative solvers. Consequently, the amount of storage required for FDTD is obviously much larger than the one needed for shooting-Newton. This has prevented the use of FDTD in general-purpose simulators.

2.4.2 Frequency-Domain Techniques

Frequency-domain methods differ from time domain steady-state techniques in the way that, instead of representing waveforms as a collection of time samples, they represent them using coefficients of sinusoids in trigonometric series. The main advantage of the trigonometric-series approach is that the steady-state solution can often be represented accurately with a small number of terms. For example, if the circuit is linear and its inputs are all sinusoidal of the same frequency, only two terms (magnitude and phase) of the trigonometric series will represent the solution

exactly, whereas an approximate time-domain solution would require a much larger number of sample points. Actually, in such case, the computation of the coefficients of the trigonometric series would be equivalent to phasor analysis.

In general, the advantage of operating directly in the frequency-domain is that linear dynamic operations like differentiation and integration are converted into simple algebraic operations such as multiplying or dividing by frequency, respectively. For example, when analyzing linear time-invariant circuit devices the coefficients of the response are easily evaluated by exploiting superposition within phasor analysis. These calculations are trivial for any lumped elements, and are still simple for any distributed devices or other elements described in a purely frequency-domain manner. Computing the response of nonlinear devices is obviously more difficult than for linear devices, in part because superposition no longer applies, and also because, in general, the coefficients of the response cannot be computed directly from the coefficients of the stimulus. Nevertheless, in the case of moderate nonlinearities, the steady-state solution is typically achieved much more easily in frequency-domain than in time-domain simulators.

Several frequency-domain techniques for analyzing RF and microwave circuits have become popular in recent years. The two most important are called *harmonic balance* (HB) and *Volterra series*. The first one, HB, is indeed the most used frequency-domain simulation technique in the RF and microwave community. This is due to the fact that, unlike the conventional transient SPICE-like engines, as also the time-domain steady-state techniques addressed above, HB handles the circuit, its excitation, and its state variables in the frequency-domain, which is the format normally adopted by RF designers. Because of that, it also benefits from allowing the direct inclusion of distributed devices (like dispersive transmission lines), or other circuit elements that do not have an exact time-domain representation. The second one, the Volterra-series analysis, will not be addressed in this thesis. It is a technique that does not rely on any iterative procedure, being, in contrast, a recursive method. Actually, it allows analysis in both time and frequency-domains and, contrary to any other nonlinear method, it enables handy calculations and provides closed-form expressions for the solutions of circuits obtained via polynomial approximations of their nonlinearities. Therefore, in terms of practical application, Volterra series is restricted to small-signal distortion analysis (where the referred polynomial approximations are accurate enough), being almost unknown out of this field. An extensive and detailed explanation of the Volterra-series analysis can be seen for example in [27], or [44].

2.4.2.1 Harmonic Balance

Harmonic balance (HB) is nowadays a mature computer simulation tool with a large number of different implementations. However, we will restrict our presentation to *nodal harmonic balance* with its *harmonic-Newton* algorithm. Other HB variants (as *piecewise harmonic balance*), or continuation techniques (as *source-stepping*), as well as a lot of technical details of implementation

that will not be presented here, can be seen for example in [21], [27], [33], [44], or [56]. Also a special version of HB, usually known as *spectral balance* (SB) to distinguish it from the conventional HB, that obviates the need for Fourier transformations, and that has the ability to handle any type of input spectrum and to operate with dynamic nonlinearities, i.e., nonlinearities that may not be expressed by the quasi-static approximation (the cascade of a linear dynamic operator and an algebraic nonlinear function), will not be addressed in this thesis and can be seen for example in [44].

In order to provide a brief and illustrative explanation of the conventional HB theory let us start by considering again the boundary value problem of (2.20), describing the periodic steady-state regime of an electronic circuit. For simplicity, let us momentarily suppose that we are dealing with a scalar problem, i.e., that we have a simple circuit described with a unique state variable $y(t)$, and that this circuit is driven by a single source $x(t)$, verifying the periodic condition $x(t)=x(t+T)$. Since the steady-state response of the circuit will be also periodic with period T, both the excitation and the steady-state solution can be expressed as the Fourier series

$$x(t)=\sum_{k=-\infty}^{+\infty} X_k e^{jk\omega_0 t}, \qquad y(t)=\sum_{k=-\infty}^{+\infty} Y_k e^{jk\omega_0 t}, \tag{2.34}$$

where $\omega_0 = 2\pi/T$ is the fundamental frequency. By substituting (2.34) into (2.20), and adopting a convenient harmonic truncation at some order $k = K$, we will obtain

$$p\left(\sum_{k=-K}^{+K} Y_k e^{jk\omega_0 t}\right)+\frac{d}{dt}\left[q\left(\sum_{k=-K}^{+K} Y_k e^{jk\omega_0 t}\right)\right]=\sum_{k=-K}^{+K} X_k e^{jk\omega_0 t}. \tag{2.35}$$

The HB method consists in converting this differential system into the frequency-domain, in way to obtain an algebraic system of $2K+1$ equations, in which the unknowns are the Fourier coefficients Y_k. Is must be noted that, since p and q are, in general, nonlinear functions, it is not possible to directly compute the Fourier coefficients Y_k in this system. In fact, we only now a priori the trivial solution $y(t)=0$ for $x(t)=0$. So, we can possibly guess an initial estimate to $y(t)$ and then adopt an iterative procedure to compute the steady-state response of the circuit. For that, we use a first order Taylor-series expansion, in which each initial expansion point corresponds to the previous iterated solution. Indeed, we expand the left hand side of the DAE system in (2.20) to obtain

$$\begin{aligned} &p\left[y^{[r]}(t)\right]+\frac{dq\left[y^{[r]}(t)\right]}{dt}+\underbrace{\left.\frac{dp(y)}{dy}\right|_{y=y^{[r]}}}_{g\left(y^{[r]}\right)}\left[y^{[r+1]}(t)-y^{[r]}(t)\right] \\ &\quad+\frac{d}{dt}\underbrace{\left.\frac{dq(y)}{dy}\right|_{y=y^{[r]}}}_{c\left(y^{[r]}\right)}\left[y^{[r+1]}(t)-y^{[r]}(t)\right]=x(t), \end{aligned} \tag{2.36}$$

which results in

$$\begin{aligned} & p\left(\sum_{k=-K}^{K} Y_k^{[r]} e^{jk\omega_0 t}\right) + \frac{d}{dt}\left[q\left(\sum_{k=-K}^{K} Y_k^{[r]} e^{jk\omega_0 t}\right)\right] \\ & + g\left(\sum_{k=-K}^{K} Y_k^{[r]} e^{jk\omega_0 t}\right)\left[\sum_{k=-K}^{K}\left(Y_k^{[r+1]} - Y_k^{[r]}\right) e^{jk\omega_0 t}\right] \\ & + \frac{d}{dt}\left[c\left(\sum_{k=-K}^{K} Y_k^{[r]} e^{jk\omega_0 t}\right)\left[\sum_{k=-K}^{K}\left(Y_k^{[r+1]} - Y_k^{[r]}\right) e^{jk\omega_0 t}\right]\right] = \sum_{k=-K}^{K} X_k e^{jk\omega_0 t}. \end{aligned} \tag{2.37}$$

The difficulty now arising in solving (2.37) is that we want to transform this system entirely into the frequency-domain but we don't know how to compute the Fourier coefficients of $p(\cdot)$, $q(\cdot)$, $g(\cdot)$ and $c(\cdot)$ at each iteration r. So, one possible way to do that consists of computing each of these nonlinear functions in the time domain, and then calculate their Fourier coefficients. Therefore, according to the properties of the Fourier transform, the time-domain products $g\left(y^{[r]}\right)\cdot\left[y^{[r+1]}(t) - y^{[r]}(t)\right]$ and $c\left(y^{[r]}\right)\cdot\left[y^{[r+1]}(t) - y^{[r]}(t)\right]$ will become spectral convolutions, which can be represented as matrix-vector products using the *conversion matrix* formulation [27], [44]. This way, (2.37) can be expressed in the form

$$\mathbf{P}^{[r]} + j\Omega\mathbf{Q}^{[r]} + \mathbf{G}^{[r]}\left[\mathbf{Y}^{[r+1]} - \mathbf{Y}^{[r]}\right] + j\Omega\mathbf{C}^{[r]}\left[\mathbf{Y}^{[r+1]} - \mathbf{Y}^{[r]}\right] = \mathbf{X}, \tag{2.38}$$

where

$$\mathbf{Y} = \begin{bmatrix} Y_{-K} \\ \vdots \\ Y_0 \\ \vdots \\ Y_K \end{bmatrix}, \qquad \mathbf{X} = \begin{bmatrix} X_{-K} \\ \vdots \\ X_0 \\ \vdots \\ X_K \end{bmatrix}, \qquad j\Omega = \operatorname{diag}\left(-jK\omega_0, \ldots, 0, \ldots, jK\omega_0\right).$$

In (2.38) $\mathbf{P}$ and $\mathbf{Q}$ are vectors containing the Fourier coefficients of $p\left[y(t)\right]$ and $q\left[y(t)\right]$, respectively, and $\mathbf{G}$ and $\mathbf{C}$ denote the $(2K+1)\times(2K+1)$ conversion matrices (Toeplitz) [44] corresponding to $g\left[y(t)\right]$ and $c\left[y(t)\right]$. If we rewrite (2.38) as

$$\underbrace{\mathbf{P}^{[r]} + j\Omega\mathbf{Q}^{[r]} - \mathbf{X}}_{\mathbf{F}\left(\mathbf{Y}^{[r]}\right)} + \underbrace{\mathbf{G}^{[r]} + j\Omega\mathbf{C}^{[r]}}_{\mathbf{J}\left(\mathbf{Y}^{[r]}\right)}\left[\mathbf{Y}^{[r+1]} - \mathbf{Y}^{[r]}\right] = 0, \tag{2.39}$$

we can obtain

$$\mathbf{F}\left(\mathbf{Y}^{[r]}\right) + \left.\frac{d\mathbf{F}(\mathbf{Y})}{d\mathbf{Y}}\right|_{\mathbf{Y}=\mathbf{Y}^{[r]}}\left[\mathbf{Y}^{[r+1]} - \mathbf{Y}^{[r]}\right] = 0, \tag{2.40}$$

in which

$$\mathbf{F}(\mathbf{Y}) = \mathbf{P}(\mathbf{Y}) + j\Omega\mathbf{Q}(\mathbf{Y}) - \mathbf{X} = 0 \tag{2.41}$$

is known as the *harmonic balance equation*, and the $(2K+1)\times(2K+1)$ composite conversion matrix

$$\mathbf{J}(\mathbf{Y}) = \frac{d\mathbf{F}(\mathbf{Y})}{d\mathbf{Y}} = \mathbf{G}(\mathbf{Y}) + j\Omega\mathbf{C}(\mathbf{Y}) \tag{2.42}$$

is known as the *Jacobian matrix* of the error function $\mathbf{F}(\mathbf{Y})$.

The iterative procedure of (2.36)-(2.42) is the so-called *harmonic-Newton* algorithm. In order to achieve the final solution of the problem, we have to do the following operations at each iteration r: (i) perform inverse Fourier transformation to obtain $y^{[r]}(t)$ from $\mathbf{Y}^{[r]}$; (ii) evaluate $p\left[y^{[r]}(t)\right]$, $q\left[y^{[r]}(t)\right]$, $g\left[y^{[r]}(t)\right]$ and $c\left[y^{[r]}(t)\right]$ in time domain; (iii) calculate their Fourier coefficients to obtain $\mathbf{P}\left(\mathbf{Y}^{[r]}\right)$, $\mathbf{Q}\left(\mathbf{Y}^{[r]}\right)$, $\mathbf{G}\left(\mathbf{Y}^{[r]}\right)$ and $\mathbf{C}\left(\mathbf{Y}^{[r]}\right)$, and thus $\mathbf{F}\left(\mathbf{Y}^{[r]}\right)$ and $\mathbf{J}\left(\mathbf{Y}^{[r]}\right)$; (iv) solve the linear system of $(2K+1)$ algebraic equations of (2.40) to compute the next estimate $\mathbf{Y}^{[r+1]}$. Consecutive iterations will be conducted until a final solution $\mathbf{Y}^{[f]}$ satisfies the HB equation of (2.41) with a desired accuracy, i.e., until

$$\left\|\mathbf{F}\left(\mathbf{Y}^{[f]}\right)\right\| = \left\|\mathbf{P}\left(\mathbf{Y}^{[f]}\right) + j\Omega\mathbf{Q}\left(\mathbf{Y}^{[f]}\right) - \mathbf{X}\right\| < tol, \tag{2.43}$$

where tol is an allowed error ceiling, and $\|\mathbf{F}(\bullet)\|$ stands for some norm of the error function $\mathbf{F}(\bullet)$.

Since in a digital computer both time and frequency domains are represented by discrete quantities, the mathematical tools used to perform Fourier and inverse Fourier transformations are, respectively, the discrete Fourier transform (DFT) and the inverse discrete Fourier transform (IDFT), or their fast algorithms, the fast Fourier transform (FFT) and the inverse fast Fourier transform (IFFT).

The system of (2.40) is typically a sparse linear system in the case of a generic circuit with n state variables. In general, several methods can be used to solve this system, such as direct solvers, sparse solvers, or iterative solvers. However, for very large systems, iterative solvers are usually preferred. Krylov subspace techniques [68] are a class of iterative methods for solving sparse linear systems of equations. An advantage of Krylov techniques is that (2.40) do not need to be fully solved in each iteration. The iterative process needs only to proceed until $\mathbf{Y}^{[r+1]} - \mathbf{Y}^{[r]}$ is such that $\mathbf{Y}^{[r+1]}$ decreases the error function. This approach to the solution, called *inexact Newton*, can provide significantly improved efficiency. Today, there is a general consensus that a technique called the *generalized minimum residual* (GMRES) [61], is the preferred one, of the many available Krylov subspace techniques, for harmonic-balance analysis [52]-[54].

The generalization of the above described harmonic-Newton algorithm to the case of a generic electronic circuit with n state variables is obviously straightforward. Indeed, in such case we will simply have

$$\mathbf{Y} = \left[\mathbf{Y}_1^T, \mathbf{Y}_2^T, \ldots, \mathbf{Y}_n^T\right]^T, \tag{2.44}$$

where each one of the $\mathbf{Y}_v$, $v=1,\ldots,n$, is a $(2K+1)\times 1$ vector containing the Fourier coefficients of the corresponding state variable $y_v(t)$. The $j\boldsymbol{\Omega}$ matrix will be defined as

$$j\boldsymbol{\Omega} = \operatorname{diag}\left(\underbrace{-jK\omega_0,\ldots,jK\omega_0}_{v=1}, \underbrace{-jK\omega_0,\ldots,jK\omega_0}_{v=2}, \ldots, \underbrace{-jK\omega_0,\ldots,jK\omega_0}_{v=n} \right), \tag{2.45}$$

and the Jacobian matrix $\mathbf{J}(\mathbf{Y}) = d\mathbf{F}(\mathbf{Y})/d\mathbf{Y}$ will have a block structure, consisting of an $n\times n$ matrix of square submatrices (blocks), each of one with dimension $(2K+1)$. Each block contains information on the sensitivity of changes in a component of the error function $\mathbf{F}(\mathbf{Y})$, resulting from changes in a component of $\mathbf{Y}$. The general block of row m and column l can be expressed as

$$\frac{d\mathbf{F}_m(\mathbf{Y})}{d\mathbf{Y}_l} = \frac{d\mathbf{P}_m(\mathbf{Y})}{d\mathbf{Y}_l} + j\Omega\frac{d\mathbf{Q}_m(\mathbf{Y})}{d\mathbf{Y}_l}, \tag{2.46}$$

where $d\mathbf{P}_m(\mathbf{Y})/d\mathbf{Y}_l$ and $d\mathbf{Q}_m(\mathbf{Y})/d\mathbf{Y}_l$ denote, respectively, the Toeplitz conversion matrices [44] of the vectors containing the Fourier coefficients of $dp_m[y(t)]/dy_l(t)$ and $dq_m[y(t)]/dy_l(t)$.

As a final remark, it may be noted that if we would opt to include the convolutive term of (2.12) in the DAE formulation of (2.20), then it would simply result in the addition of a linear term of the form $\mathbf{H}\cdot\mathbf{Y}$ in the HB equation of (2.41), i.e.,

$$\mathbf{F}(\mathbf{Y}) = \mathbf{P}(\mathbf{Y}) + j\Omega\mathbf{Q}(\mathbf{Y}) + \mathbf{H}\cdot\mathbf{Y} - \mathbf{X} = 0 \tag{2.47}$$

and the addition of the constant $\mathbf{H}$ in the Jacobian matrix defined by (2.41), i.e.,

$$\mathbf{J}(\mathbf{Y}) = \frac{d\mathbf{F}(\mathbf{Y})}{d\mathbf{Y}} = \mathbf{G}(\mathbf{Y}) + j\Omega\mathbf{C}(\mathbf{Y}) + \mathbf{H}, \tag{2.48}$$

where $\mathbf{H}$ is the diagonal form of the matrix-valued frequency response of the linear time-invariant distributed devices contained in the circuit.

2.4.3 Comparisons

Each of the three classes of methods discussed in this section (shooting, FDTD and HB) for computing the periodic steady-state solution of an electronic circuit, present some advantages and disadvantages. Some of them were already mentioned above. Nevertheless, in order to complete our discussion and to get a more realistic idea, we will now summarize in the following the most important strengths and weakness of the methods.

Shooting methods convert boundary value problems into a sequence of initial value problems. Because of that, they do not compute the solution of the differential system all at once but only need to access to a small piece of it at any time instant. As a result, they need considerably less memory than FDTD. A very important characteristic of the shooting methods is that they converge quickly and reliably if the state-transition function is almost linear, which is quite often the case,

even when the overall circuit behavior is not. A negative aspect of shooting methods is that they are not able to deal with convolutive operations, and so they cannot handle distributed devices unless these devices are replaced with lumped approximations. The question is that lumped equivalent circuits contain in general so many additional nodes that they significantly increase the cost of using shooting methods.

FDTD methods solve boundary value problems by discretizing the differential system on a finite set of time instants (grid points) covering the simulation interval. FDTD methods can generate large systems of equations, especially if either the number of unknown waveforms or the number of grid points is large. Because of the large number of equations and unknowns involved, the amount of memory required by FDTD often constrains the size of the circuit that can be simulated. So, although they are well known in the mathematics community, they have received minor attention from the circuit simulation community. FDTD also tends to have more Newton-Raphson convergence problems than shooting. In fact, in general, shooting-Newton requires less iterations to converge than FDTD, and thus it can be more robust and fast. On the other hand, because FDTD deals with all time grid instants simultaneously, it is able to handle convolutive operations. This may be useful for computing (in time domain) steady-state solutions of RF and microwave circuits having linear time-invariant distributed devices, or elements having only a frequency-domain representation, as they can be characterized by their impulse responses (the inverse Fourier transforms of the corresponding frequency-domain transfer functions).

HB represents signals using coefficients of sinusoids rather than a sampled-data representation. It can often be extremely accurate with a small number of terms, especially if the circuits are nearly linear. HB also shares with any other frequency-domain methods an important advantage that is particularly significant to RF and microwave circuits. It can handle directly circuit elements having a frequency-domain representation (dispersive transmission lines, transmission line discontinuities, or, in general, any admittance or scattering matrix coming from laboratory network analysis). HB presents, however, a serious drawback for lumped circuits: it is not suitable for dealing with strong nonlinearities. In fact, when facing strongly nonlinear regimes the large number of terms required in the trigonometric-series expansions can make frequency-domain methods very inefficient, both in memory storage and simulation time. In contrast, time-domain methods do not suffer from these limitations.

Chapter 3
Advanced Simulation Techniques for Multirate RF Problems

3.1 Introduction

This chapter addresses some advanced simulation techniques especially conceived for computing the numerical solution of multirate RF problems. Several specific situations for which the solution of the problem is typically hard to compute with the standard simulation techniques presented in the previous chapter, and that can be computed efficiently with the specialized methods described in this chapter, will be now analyzed. In this sense, this chapter provides a general overview on the state of the art in multirate simulation, in view of the fact that the most relevant contributions to this research field are here reported.

Section 3.2 is dedicated to the examination of problems exhibiting state variables with disparate rates of variation, i.e., circuits presenting slow (latent) and fast-varying (active) voltages and currents, and the benefits obtained from the use of modern multirate Runge-Kutta (MRK) algorithms when time-step integrating such problems. Section 3.3 describes the exploitation of latency in the frequency-domain circuit analysis, which is based on a multirate sampling technique for the FFT in the HB method, according to the smoothness of the waveforms. Section 3.4 is devoted to the analysis of problems having multirate signals, i.e., signals (state variables or stimuli) containing components that vary at two or more widely separated rates. A brief description of some simulation techniques that may be used to overcome the difficulties encountered in such problems is provided. Section 3.5 introduces the recent multivariate formulation theory, in which the one-dimensional time is converted into a set of multiple time variables, turning mathematical circuit models into partial differential algebraic systems, within a scenario of multivariate representations. Several powerful numerical methods based on the multivariate strategy, operating in time, frequency, or hybrid (combination) domains, are presented. Finally, Section 3.6 addresses the warped time formulation technique, which can be seen as a modification of the straightforward

multivariate formulation strategy described in Section 3.5, with the purpose of accommodating phase modulated signals in the multivariate framework.

3.2 Time-Domain Latency

3.2.1 State Variables with Different Rates of Variation

Dynamical behavior of some electronic circuits involves signals with widely separated rates of variation. Analog circuits presenting extremely different time constants, coupled systems of analog and digital networks, or combined technologies of RF and baseband analog (or even digital) blocks in the same circuit, are typical examples where the corresponding state variables may evolve according to very distinct time scales. In such cases node voltages or branch currents presenting slow (*latent*) and very fast (*active*) time evolution rates may coexist in the same problem. This phenomenon, the one of some state variables varying very slowly (or being even practically constant) within a specific time interval, while other variables exhibit fast variations in that interval, is frequently referred to as *time-domain latency*. Another common situation where time-domain latency can be found refers to purely digital circuits. For example, in large scale integration (LSI) or very large scale integration (VLSI) applications, usually, only a small part of the circuits (a small number of state variables) is active in a certain time interval, whereas the major part is latent (a large number of state variables may possibly remain practically constant within that interval). In summary, many kinds of electronic circuits may exhibit time-domain latency.

In Chapter 2 we have seen that time-step integration is a classical technique that is still used nowadays by all SPICE-like computer programs for simulating electronic circuits. However, when integrating systems whose components (state variables) evolve according to different time scales one would like to use numerical schemes that do not expend unnecessary work on slowly changing (latent) components. In fact, in such cases traditional time-step integrators, like standard Runge-Kutta or linear multistep methods, which use the same step size for all system's components, become inefficient and numerical schemes with different time-step sizes are required.

In order to provide an illustrative explanation of the issues under discussion in this section, let us consider a generic electronic circuit with n state variables, described by the initial value problem of (2.16), that we rewrite here for convenience

$$\frac{d\boldsymbol{y}(t)}{dt} = \boldsymbol{f}(t, \boldsymbol{y}), \quad \boldsymbol{y}(t_0) = \boldsymbol{y}_0, \quad t_0 \le t \le t_{Final}, \quad y \in \mathbb{R}^n. \tag{3.1}$$

If some state variables of the circuit are very fast, while others are much slower, then this disparity can be exploited by multirate schemes, in view of the fact that they will integrate components of the slow subsystem with a larger step size than the one used for the fast subsystem. The key idea is to split the differential system into a pair of coupled active and latent subsystems, obtaining

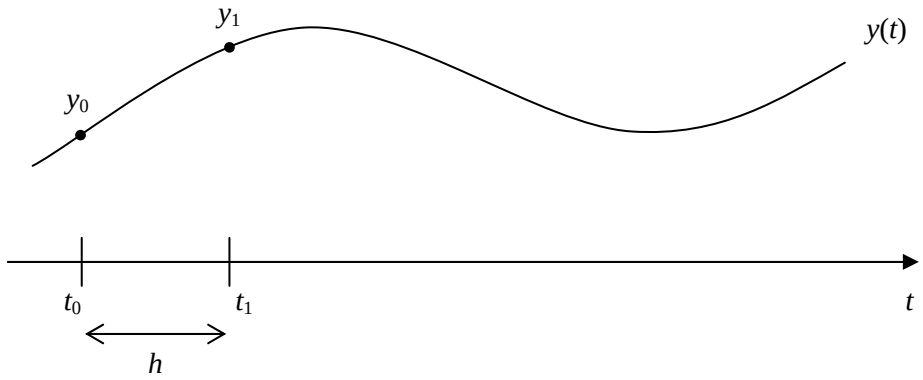

Figure 3.1 Single step in a standard Runge-Kutta integrator.

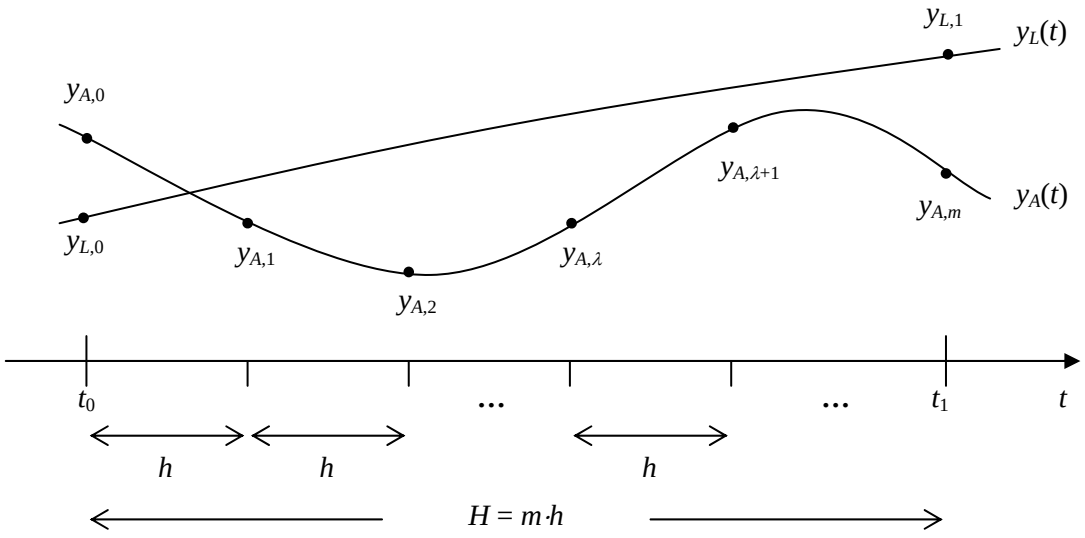

Figure 3.2 Micro and macrosteps in a multirate Runge-Kutta integrator.

$$\begin{aligned} \frac{d\boldsymbol{y}_A(t)}{dt} &= \boldsymbol{f}_A(t, \boldsymbol{y}_A, \boldsymbol{y}_L), \quad \boldsymbol{y}_A(t_0) = \boldsymbol{y}_{A,0} \\ \frac{d\boldsymbol{y}_L(t)}{dt} &= \boldsymbol{f}_L(t, \boldsymbol{y}_A, \boldsymbol{y}_L), \quad \boldsymbol{y}_L(t_0) = \boldsymbol{y}_{L,0}, \end{aligned} \tag{3.2}$$

with

$$\boldsymbol{y} = \begin{bmatrix} \boldsymbol{y}_A \\ \boldsymbol{y}_L \end{bmatrix}, \quad \boldsymbol{y}_A \in \mathbb{R}^{n_A}, \quad \boldsymbol{y}_L \in \mathbb{R}^{n_L}, \quad n_A + n_L = n, \tag{3.3}$$

where $\boldsymbol{y}_A$ is the active (fast-varying) state-variable components' vector and $\boldsymbol{y}_L$ the latent (slowly varying) state-variable components' vector. The active components will be integrated with a small step size h (*microstep*) while the latent components will be integrated with a much larger step size H (*macrostep*). The number of microsteps within each macrostep is an integer that we will denote by m; thus, $H = m \cdot h$.

3.2.2 Time-Step Integration using MRK Methods

For achieving an intuitive explanation of the fundamentals of multirate schemes, let us start by considering the first order and one stage explicit Runge-Kutta scheme, also known as the forward Euler method. In that case, the numerical solution of (3.1) at $t_1 = t_0 + h$ is given by

$$\begin{aligned} \boldsymbol{y}(t_0 + h) \simeq \boldsymbol{y}_1 &= \boldsymbol{y}_0 + h\boldsymbol{k}, \\ \boldsymbol{k} &= \boldsymbol{f}(t_0, \boldsymbol{y}_0). \end{aligned} \tag{3.4}$$

This is illustrated in Figure 3.1. The corresponding multirate version of the forward Euler scheme for the numerical solution of the partitioned system of (3.2) would be given by

$$\begin{aligned} \boldsymbol{y}_L(t_0 + H) \simeq \boldsymbol{y}_{L,1} &= \boldsymbol{y}_{L,0} + H\boldsymbol{k}_L, \\ \boldsymbol{k}_L &= \boldsymbol{f}_L(t_0, \boldsymbol{y}_{A,0}, \boldsymbol{y}_{L,0}), \end{aligned} \tag{3.5}$$

for the latent components, and by

$$\begin{aligned} \boldsymbol{y}_A(t_0 + h) \simeq \boldsymbol{y}_{A,1} &= \boldsymbol{y}_{A,0} + h\boldsymbol{k}_A^0, \\ \boldsymbol{k}_A^0 &= \boldsymbol{f}_A(t_0, \boldsymbol{y}_{A,0}, \boldsymbol{y}_{L,0}), \\ \boldsymbol{y}_A(t_0 + 2h) \simeq \boldsymbol{y}_{A,2} &= \boldsymbol{y}_{A,1} + h\boldsymbol{k}_A^1, \\ \boldsymbol{k}_A^1 &= \boldsymbol{f}_A(t_0 + h, \boldsymbol{y}_{A,1}, \boldsymbol{y}_{L,0} + h\boldsymbol{k}_L), \\ &\vdots \\ \boldsymbol{y}_A(t_0 + \lambda h + h) \simeq \boldsymbol{y}_{A,\lambda+1} &= \boldsymbol{y}_{A,\lambda} + h\boldsymbol{k}_A^\lambda, \\ \boldsymbol{k}_A^\lambda &= \boldsymbol{f}_A(t_0 + \lambda h, \boldsymbol{y}_{A,\lambda}, \boldsymbol{y}_{L,0} + \lambda h\boldsymbol{k}_L), \\ \lambda &= 0, 1, \ldots, m-1, \end{aligned} \tag{3.6}$$

for the active components. As defined in (3.6) and illustrated in Figure 3.2, the vector of active state variables at each of the time instants $t_0 + \lambda h$, defined in a fine grid, is calculated from its previous values and the respective time derivatives, $\boldsymbol{k}_A^{\lambda-1}$. On the other hand, the vector of latent state variables is only evaluated in the coarse time instant $t_0 + H$, assuming that its time derivatives, $\boldsymbol{k}_L$, are constant within that interval.

The algorithm defined by (3.5) and (3.6) constitutes the simplest form of a *multirate Runge-Kutta scheme*. A general definition of a multirate Runge-Kutta time-step integrator is presented in the following.

Definition 3.1: Multirate Runge-Kutta (MRK) method. Consider two Runge-Kutta methods of s and $\bar{s}$ stages, that can be, but do not necessarily have to be, the same, expressed by their Butcher tableaus $(\boldsymbol{b}, \boldsymbol{A}, \boldsymbol{c})$ and $(\bar{\boldsymbol{b}}, \bar{\boldsymbol{A}}, \bar{\boldsymbol{c}})$,

$$\begin{array}{c|cccc} c_1 & a_{11} & a_{12} & \cdots & a_{1s} \\ c_2 & a_{21} & a_{22} & \cdots & a_{2s} \\ \vdots & \vdots & \vdots & & \vdots \\ c_s & a_{s1} & a_{s2} & \cdots & a_{ss} \\ \hline & b_1 & b_2 & \cdots & b_s \end{array} \qquad \begin{array}{c|cccc} \overline{c}_1 & \overline{a}_{11} & \overline{a}_{12} & \cdots & \overline{a}_{1s} \\ \overline{c}_2 & \overline{a}_{21} & \overline{a}_{22} & \cdots & \overline{a}_{2s} \\ \vdots & \vdots & \vdots & & \vdots \\ \overline{c}_s & \overline{a}_{s1} & \overline{a}_{s2} & \cdots & \overline{a}_{ss} \\ \hline & \overline{b}_1 & \overline{b}_2 & \cdots & \overline{b}_s \end{array} \tag{3.7}$$

The resulting multirate Runge-Kutta method for obtaining the numerical solution of the partitioned system of (3.2), using a microstep h and the active components and a macrostep H for the latent components, is defined as follows [22], [23].

The active (fast-varying) components $\boldsymbol{y}_A$ are given by

$$\boldsymbol{y}_A\left(t_0+\lambda h+h\right) \simeq \boldsymbol{y}_{A,\lambda+1} = \boldsymbol{y}_{A,\lambda} + h\sum_{i=1}^{s} b_i \boldsymbol{k}_{A,i}^{\lambda}, \qquad \lambda = 0,1,\ldots,m-1, \tag{3.8}$$

$$\boldsymbol{k}_{A,i}^{\lambda} = \boldsymbol{f}_A\left(t_0+\lambda h+c_i h, \boldsymbol{y}_{A,\lambda} + h\sum_{j=1}^{s} a_{ij}\boldsymbol{k}_{A,j}^{\lambda}, \tilde{\boldsymbol{Y}}_{L,i}^{\lambda}\right), \qquad i = 1,2,\ldots s, \tag{3.9}$$

with $\tilde{\boldsymbol{Y}}_{L,i}^{\lambda} \simeq \boldsymbol{y}_L\left(t_0+\lambda h+c_i h\right)$.

The latent (slowly varying) components $\boldsymbol{y}_L$ are given by

$$\boldsymbol{y}_L\left(t_0+H\right) \simeq \boldsymbol{y}_{L,1} = \boldsymbol{y}_{L,0} + H\sum_{i=1}^{\overline{s}} \overline{b}_i \boldsymbol{k}_{L,i}, \tag{3.10}$$

$$\boldsymbol{k}_{L,i} = \boldsymbol{f}_L\left(t_0+\overline{c}_i H, \tilde{\boldsymbol{Y}}_{A,i}, \boldsymbol{y}_{L,0} + H\sum_{j=1}^{\overline{s}} \overline{a}_{ij}\boldsymbol{k}_{L,j}\right), \qquad i = 1,2,\ldots,\overline{s}, \tag{3.11}$$

with $\tilde{\boldsymbol{Y}}_{A,i} \simeq \boldsymbol{y}_A\left(t_0+\overline{c}_i H\right)$.

As can be seen, the coupling between the active and latent subsystems is performed by the intermediate stage values $\tilde{\boldsymbol{Y}}_{L,i}^{\lambda}$ and $\tilde{\boldsymbol{Y}}_{A,i}$. There are several strategies for computing these values, as the ones suggested in [12], [13], which are based on interpolation and/or extrapolation techniques, or the ones more recently proposed in [14], [22], or [23], which are based on coupling coefficients.

It must be noted that, in general, the partition into fast and slow subsystems, as well as the number of microsteps within a macrostep, may vary throughout the integration process. Technical details of MRK code implementation, such as active-latent partitioning strategies, step size control tools, or even stiffness detection stratagems, can be seen in detail for example in [22], [38], or [39].

3.3 Frequency-Domain Latency

Periodic steady-state regimes of electronic systems can sometimes have waveforms with distinct degrees of smoothness within the same circuit. This means that if one wants to represent the state variables of such circuits in the frequency-domain, some of them will require a significant number of harmonic components, while others will be represented by a few quantity of harmonics. This property is defined as *frequency-domain latency*.

As stated in Chapter 2, HB is the most widely used frequency-domain simulation technique in the RF and microwave community. However, standard HB algorithms do not perform any distinction between the circuit's state variables, i.e., they process all node voltages and branch currents in the same manner. As seen, in the harmonic balance analysis the DFT and the IDFT (or their fast algorithms, the FFT and the IFFT) are used to perform conversion between time and frequency domains of nonlinear functions and Jacobian elements, in which the same number of harmonic components is assumed for every variable in the circuit. So, when many harmonics are required, Jacobian matrices become large at each harmonic-Newton iteration step. As a result, too much computation time and memory storage are involved.

To obviate the above difficulties, a strategy for exploiting latency in frequency-domain analysis was initially proposed in [1], [2] and [28]. This strategy takes advantage of the fact that, in some applications, the number of harmonics needed to represent each circuit's variable may be not the same. So, it suggests the use of an individualized number of harmonics for each voltage or current. This means that the DFT and its inverse, the IDFT, (or the FFT and the IFFT), are evaluated with a specific number of sampling points for each of the circuit's variables, according to the corresponding degree of smoothness. This technique is referred to as *multirate sampling* [1], [2], [28], and is illustrated in Figure 3.3.

In the example depicted in Figure 3.3 we consider that the fast Fourier-transform algorithm (FFT), is used to obtain the frequency components from the time waveforms. One requirement of the FFT is that the number of harmonics must always be an integer power of two. Another requirement, consequence of the sampling theorem, is that the number of time samples must be at least twice the number of frequency components. For those reasons, a sample rate of 4 time samples per cycle is used in $y_1(t)$, which is assumed as being sinusoidal with some DC offset, and a sample rate of 16 time samples per cycle is used in $y_2(t)$, which is assumed as being represented accurately with an harmonic truncation at the order $K = 7$.

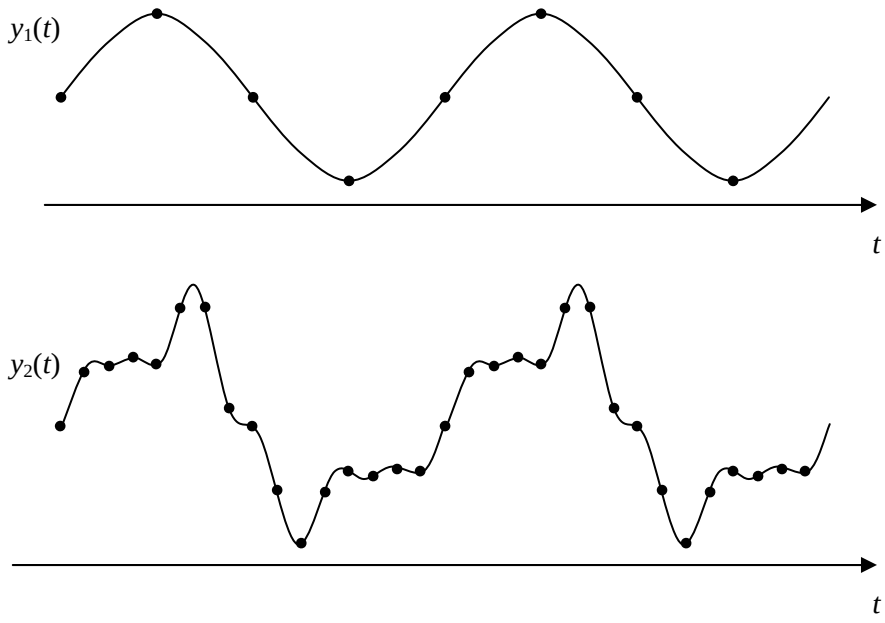

Figure 3.3 Multirate sampling technique.

The use of a small number of harmonics in some parts of the circuits can conduct to substantial reductions in the size of the HB systems. Consequently, significant reductions in the sizes of the Jacobian matrices can be achieved, and thus considerable computation and memory savings can be obtained. The strategy suggested in [1], [2], and [28] is no more than an adaptive version of the standard HB engine that exploits frequency-domain disparities by using a different number of harmonics in each state variable when computing the corresponding steady-state solutions. Some of its technical details of implementation, as well as some practical applications, can be seen in these references. Other applications exploiting frequency-domain latency are also addressed for example in [17], [37], or [71].

3.4 Multirate Signals

Signals containing components that vary themselves at two or more widely separated rates are usually referred to as *multirate signals* (e.g., a very fast rectangular wave with a slowly changing duty cycle, a high frequency sinusoid with a slowly varying envelope, etc.). Such signals arise in many kind of electronic circuits, such as switched-power converters, switched-capacitor filters, voltage-controlled oscillators, pulse-width modulators, phase locked loops, etc., and have a special incidence in RF and microwave communication applications, such as mixers (up/down converters), modulators, demodulators, power amplifiers, etc. Circuits like these are very difficult to simulate using the standard simulation techniques described in the previous chapter. The main difficulty derives from the fact that following the fast-varying signal components long enough to obtain

information about the slowly varying ones is usually computationally expensive or prohibitive. Another significant limitation is that numerical errors can enlarge considerably over the long simulation process, even in the presence of tight local error control.

Multirate signals can appear in RF systems due to the existence of excitation regimes of widely separated time scales (e.g., baseband stimuli and high frequency local oscillators), because the stimuli can be, themselves, multirate signals (e.g., circuits driven by modulated signals), or as a result of the particular characteristics of the circuits' operation (e.g., voltage-controlled oscillators). In this section and in the following ones we will describe a wide variety of numerical techniques that were specially conceived to overcome the difficulties that emerge when simulating problems containing multirate signals. We first begin to address some mature multirate techniques focused on the classical cases of amplitude and/or phase modulated solutions and quasiperiodic solutions. Then, in Sections 3.5 and 3.6, we will present a collection of methods based on a recent multivariate strategy, which can be appropriate to deal with any kind of multirate signals.

3.4.1 Modulated Signals

Signals handled by wireless communication systems can usually be described by a high frequency RF carrier modulated by some kind of baseband information signals, as amplitude and/or phase signals. The general form of an amplitude and phase modulated signal can be defined as

$$x(t) = e(t)\cos\left[\omega_C t + \phi(t)\right], \tag{3.12}$$

where $e(t)$ and $\phi(t)$ are, respectively, the amplitude, or envelope, and phase slowly varying baseband signals, modulating the $\cos(\omega_C t)$ fast-varying carrier.

Circuits driven by amplitude and/or phase modulated signals, or presenting themselves state variables of this type, are common in RF and microwave applications. Since the baseband signals have a spectral content of much lower frequency than the carrier, i.e., because they are typically slowly varying signals while the carrier is a fast-varying entity, simulating nonlinear circuits containing this kind of signals is often a very challenging issue. Because the aperiodic nature of the signals obviates the use of any steady-state technique, one might think that conventional time-step integration (SPICE-like transient simulation) would be the natural method for simulating such circuits, as long as the time scale of slowly varying components of the signals is comparable to the larger time constants involved. However, the large time constants of the bias networks determine long transient regimes and, as a result, the obligation of simulating a large number of carrier periods. In addition, computing the RF carrier oscillations long enough to obtain information about its envelope and phase properties is, itself, a colossal task. Time-step integration is thus inadequate for simulating this kind of problems.

3.4.2 Mixed Frequency-Time ETHB Technique

The *envelope transient harmonic balance* (ETHB) [36], [51], [63], is a mixed frequency-time technique that was conceived to overcome the inefficiency revealed by SPICE-like engines when simulating circuits driven by modulated signals. It consists in calculating the response of the circuit to the baseband and the carrier, by treating the envelope and phase in the time domain and the carrier in the frequency-domain. For that, it assumes that the envelope and phase baseband signals are extremely slow when compared to the carrier, so that they can be considered as practically constant during many carrier periods. Taking this into account, ETHB samples the baseband signals in an appropriately slow time rate and assumes a staircase version of both amplitude and phase, which will conduct to a new modulated version of these signals. The steady-state response of the circuit to this new modulated version is then computed at each time step with the frequency-domain HB engine.

In order to provide a very brief theoretical description of the ETHB technique let us suppose that we have a circuit driven by a single source of the form of $x(t)$ in (3.12). If we rewrite $x(t)$ as

$$x(t) = e(t)\sum_{k=-1}^{1} A_k e^{jk\left[\omega_C t+\phi(t)\right]} = \sum_{k=-1}^{1} e(t) A_k e^{jk\phi(t)} e^{jk\omega_C t} = \sum_{k=-1}^{1} X_k(t) e^{jk\omega_C t}, \tag{3.13}$$

and assume that the circuit is stable, then all its state variables can be expressed as time-varying Fourier series

$$y(t) = \sum_k Y_k(t) e^{jk\omega_C t}, \tag{3.14}$$

where $Y_k(t)$ represents the time-varying Fourier coefficients of $y(t)$, which are slowly varying in the baseband time scale. Now, if we take into consideration the disparity between the baseband and the carrier time scales, and assume that they are also uncorrelated, which is normally the case, then we can rewritte (3.12) and (3.14) as

$$x(t_E, t_C) = e(t_E)\cos\left[\omega_C t_C + \phi(t_E)\right], \tag{3.15}$$

and

$$y(t_E, t_C) = \sum_k Y_k(t_E) e^{jk\omega_C t_C}, \tag{3.16}$$

where t_E is the slow baseband time scale and t_C is the fast carrier time scale. Then, if we discretize the slow baseband time scale using a grid of successive time instants $t_{E,i}$, and adopt a convenient harmonic truncation at some order $k = K$, we will obtain for each $t_{E,i}$ a periodic boundary value problem that can be solved in the frequency-domain with HB. In order to compute the whole response of the circuit a set of successive HB equations of the form

$$\mathbf{F}\left[\mathbf{Y}(t_{E,i})\right] = \mathbf{P}\left[\mathbf{Y}(t_{E,i})\right] + j\Omega\mathbf{Q}\left[\mathbf{Y}(t_{E,i})\right] - \mathbf{X}(t_{E,i}) = 0 \tag{3.17}$$

have to be solved, in which $\mathbf{X}(t_{E,i})$ and $\mathbf{Y}(t_{E,i})$ represent the vectors containing the time-varying Fourier coefficients of the excitation and of the solution, respectively.

ETHB is, nowadays, a mature technique in the RF simulation community. However, its basic assumption constitutes its major drawback. By requiring the envelope and phase to be extremely slowly varying signals when compared to the carrier frequency, this mixed frequency-time technique becomes restricted to circuits whose stimuli occupy only a small fraction of the available bandwidth. In Section 3.5 we will present an alternative ETHB formulation that does not suffer from this bandwidth restriction.

3.4.3 Quasiperiodic Signals

If a nonlinear circuit is excited by several distinct periodic sources at uncommensurated frequencies (or is driven by a multitone signal having two or more uncommensurated tones) then the circuit will typically have a quasiperiodic steady-state response. In this kind of regime, the signals involved in the circuit consist of linear combinations at the sum and difference frequencies of a finite set of fundamental frequencies and their harmonics. A general definition of a *m*-tone quasiperiodic signal is presented in the following [59].

Definition 3.2: Quasiperiodic signal. $y(t)$ is *m*-tone quasiperiodic if it can be expressed in the form

$$y(t) = \sum_{k_1,k_2,\ldots,k_m} Y_{k_1,k_2,\ldots,k_m} e^{j(k_1\omega_1 + k_2\omega_2 + \cdots + k_m\omega_m)t}, \tag{3.18}$$

where $Y_{k_1,k_2,\ldots,k_m}$ are real- or complex-valued constants and the frequencies $\omega_1, \omega_2, \ldots, \omega_m$, are not harmonics of some single fundamental frequency.

Quasiperiodic steady-state regimes arise in many kinds of communication circuits (e.g., mixers). In general, input signals present in mixers are not harmonically related, and thus the signals found in mixers are not periodic, but rather quasiperiodic. Analyzing circuits with multitone stimuli is also of incontestable practical interest in the design and test of RF and microwave applications (e.g., intermodulation distortion evaluation in power amplifiers). However, simulating circuits presenting quasiperiodic steady-state regimes may be a very challenging issue. First, because the standard steady-state techniques described in Chapter 2, as shooting, FDTD, or HB, are only suitable to analyze circuits with periodic steady-state responses, which is not the case here. Second, because time-step integration (SPICE) can be extremely inefficient. For example, when frequency tones are either widely separated, or very closely spaced, the time interval over which the differential equations must be numerically integrated is dramatically large compared to the time-step size used by the numerical integration scheme.

Some mature multirate techniques that operate in the frequency-domain have been developed to efficiently compute quasiperiodic steady-state solutions. These techniques are widely known in the RF and microwave community as distinct forms of implementation of a general technique commonly denoted as *generalized harmonic balance* or *multitone harmonic balance* [27].

3.4.4 Quasiperiodic Steady-State Solutions: the Multitone HB

Conventional HB was initially conceived to compute periodic steady-state solutions of nonlinear circuits with single tone excitations. Due to the restrictions imposed by the DFT, this standard technique is only capable of handling periodic signals. However, it is possible to generate time-to-frequency transforms which do not require the frequency components of the signals to be harmonically related, and thus appropriate to deal with uncommensurated frequencies.

In order to achieve clarity in the explanation of multitone HB, let us consider the simple case of a two-tone source having frequencies ω_1 and ω_2,

$$x(t) = A_1 \cos(\omega_1 t + \phi_1) + A_2 \cos(\omega_2 t + \phi_2), \tag{3.19}$$

where the uncommensurated frequencies' condition $k_1\omega_1 + k_2\omega_2 \neq 0$ is satisfied for any nonsimultaneous null integers k_1 and k_2. The state variables of a nonlinear circuit excited by this source will be of the form

$$y(t) = \sum_{k_1,k_2} Y_{k_1,k_2} e^{j(k_1\omega_1 + k_2\omega_2)t}, \tag{3.20}$$

where two distinct strategies can be considered for the necessary harmonic truncation. *Box truncation* [21] assumes that k_1 and k_2 are such that $|k_1| \leq K_1$ and $|k_2| \leq K_2$. *Diamond truncation* [21] considers, instead, that $|k_1| + |k_2| \leq K$, and thus requires fewer terms. As stated above, since $y(t)$ is not periodic, uniformly sampling this signal and calculating its spectrum using the DFT is not possible. Three distinct alternative techniques to the use of the DFT can efficiently overcome this difficulty: the *almost periodic Fourier transform* (APFT), the *multidimensional discrete Fourier transform* (MDFT), and the *artificial frequency mapping* (AFM) technique.

3.4.4.1 Almost Periodic Fourier Transform

The almost periodic Fourier transform (APFT) is a linear operator that is an extension to the standard discrete Fourier transform (DFT), in which the restriction of harmonically related frequencies is removed. It is based on the intuitive idea that, in principle, $(2K+1)$ Fourier coefficients ($2K$ real numbers for the positive frequencies plus one for DC component) can be obtained from $(2K+1)$ time samples.

Let us consider the quasiperiodic signal of (3.20). According to the adopted harmonic truncation, we are able to consider the finite set of positive frequencies defined by $k_1\omega_1 + k_2\omega_2$ (containing individual harmonic terms and mixing products, truncated at some order), which, for

convenience, we now denote by $\{\omega_1, \omega_2, \ldots, \omega_K\}$. The Fourier coefficients of $y(t)$ can be obtained by solving the following linear system of $(2K+1)$ equations [65],

$$\begin{bmatrix} 1 & 2\cos(\omega_1 t_1) & -2\sin(\omega_1 t_1) & \cdots & 2\cos(\omega_K t_1) & -2\sin(\omega_K t_1) \\ 1 & 2\cos(\omega_1 t_2) & -2\sin(\omega_1 t_2) & \cdots & 2\cos(\omega_K t_2) & -2\sin(\omega_K t_2) \\ 1 & 2\cos(\omega_1 t_3) & -2\sin(\omega_1 t_3) & \cdots & 2\cos(\omega_K t_3) & -2\sin(\omega_K t_3) \\ \vdots & \vdots & \vdots & & \vdots & \vdots \\ 1 & 2\cos(\omega_1 t_S) & -2\sin(\omega_1 t_S) & \ldots & 2\cos(\omega_K t_S) & -2\sin(\omega_K t_S) \end{bmatrix} \begin{bmatrix} Y_0 \\ Y_{1,r} \\ Y_{1,i} \\ \vdots \\ Y_{K,r} \\ Y_{K,i} \end{bmatrix} = \begin{bmatrix} y(t_1) \\ y(t_2) \\ y(t_3) \\ \vdots \\ y(t_S) \end{bmatrix} \tag{3.21}$$

with $S = 2K+1$, and $Y_k = Y_{k,r} + jY_{k,i}$, $k = 1, \ldots, K$.

In the case of the DFT and periodic signals, the $S = 2K+1$ time samples are equally spaced along one period. However, trying to adopt this uniform sampling strategy to quasiperiodic signals is usually not recommended because the system of (3.21) becomes ill conditioned. This means that the rows of the matrix in (3.21) are nearly linearly dependent, the system is close to be undetermined and the transform can greatly magnify arithmetic round off errors or aliasing. Some techniques that can be adopted to choose a set of time samples that results in well-conditioned transform matrices can be seen, for example, in [21], [27], or [65].

3.4.4.2 Multidimensional DFT

The multidimensional discrete Fourier transform (MDFT) is the generalization of the DFT to the generic case of signals that are function of two, or more, independent variables. As we will see, it constitutes an alternative technique to the use of the above related APFT, because it is possible to treat our unique independent variable, time, as two, or more, independent parameters [8], [49].

Let us consider again the two-tone quasiperiodic signal of (3.20). If we define the parameters $\theta_1 = \omega_1 t$ and $\theta_2 = \omega_2 t$, we can rewrite this signal as a double periodic two-dimensional signal,

$$y(\theta_1, \theta_2) = \sum_{k_1, k_2} Y_{k_1,k_2} e^{jk_1\theta_1} e^{jk_2\theta_2}, \tag{3.22}$$

in which the conditions $y(\theta_1, \theta_2) = y(\theta_1 + \omega_1 T_1, \theta_2) = y(\theta_1, \theta_2 + \omega_2 T_2)$ are verified for $T_1 = 2\pi/\omega_1$ and $T_2 = 2\pi/\omega_2$. If a harmonic box truncation is adopted in (3.22), i.e., if $|k_1| \le K_1$ and $|k_2| \le K_2$, and a collection of time samples of $y(\theta_1, \theta_2)$ is uniformly taken on a rectangular grid defined as

$$\begin{aligned} t_{s_1} &= \frac{T_1}{2K_1+1} s_1, \quad s_1 = -K_1, \ldots, K_1, \\ t_{s_2} &= \frac{T_2}{2K_2+1} s_2, \quad s_2 = -K_2, \ldots, K_2, \end{aligned} \tag{3.23}$$

then the two-dimensional Fourier coefficients of $y(\theta_1, \theta_2)$ can be calculated by solving the following linear system of $(2K_1+1)(2K_2+1)$ equations

$$y\left(t_{s_1},t_{s_2}\right)=\sum_{k_1=-K_1}^{K_1}\sum_{k_2=-K_2}^{K_2}Y_{k_1,k_2}e^{jk_1\omega_1 t_{s_1}}e^{jk_2\omega_2 t_{s_2}}. \tag{3.24}$$

This is the definition of the two-dimensional IDFT. If we invert (3.24) then we obtain the two-dimensional DFT

$$Y_{k_1,k_2}=\frac{1}{\left(2K_1+1\right)\left(2K_2+1\right)}\sum_{s_1=-K_1}^{K_1}\sum_{s_2=-K_2}^{K_2}y\left(t_{s_1},t_{s_2}\right)e^{-jk_1\omega_1 t_{s_1}}e^{-jk_2\omega_2 t_{s_2}}. \tag{3.25}$$

Contrary to the APFT, the multidimensional DFT does not suffer from ill-conditioning problems. However, since the application of the MDFT is restricted to box truncation, the number of arithmetic operations required to compute this transform increases exponentially with the number of tones involved. This is a serious limitation, which, in practice, usually inhibits the use of MDFT to more than three tones.

3.4.4.3 Artificial Frequency Mapping

Artificial Frequency Mapping (AFM) is a strategy that allows the use of the one-dimensional DFT for harmonic balance analysis of circuits with quasiperiodic steady-state regimes [9], [21], [41], [44], [56]. With AFM actual base frequencies are replaced by artificially selected frequencies so that the original spectrum (which can be extremely sparse) is converted into a periodic and dense spectrum. This means that the correspondent artificial time-domain waveforms are periodic, and so their Fourier coefficients can be efficiently computed with the DFT.

Artificial Frequency Mapping techniques rely on the assumption that the nonlinearities of the circuit are memoryless and time-invariant, and thus can be expressed in the form $y(t)=f\left[x(t)\right]$ where $f(\cdot)$ is an algebraic function. In order to exemplify the trick behind mapping techniques let us consider an illustrative example, in which $x(t)$ is the two-tone quasiperiodic signal of (3.19) and $f(\cdot)=(\cdot)^2$. In that case, we will have

$$\begin{aligned}y(t)=&\frac{A_1^2+A_2^2}{2}+\frac{A_1^2}{2}\cos\left(2\omega_1 t+2\phi_1\right)+A_1A_2\cos\left(\omega_1 t-\omega_2 t+\phi_1-\phi_2\right)\\&+A_1A_2\cos\left(\omega_1 t+\omega_2 t+\phi_1+\phi_2\right)+\frac{A_2^2}{2}\cos\left(2\omega_2 t+2\phi_2\right).\end{aligned} \tag{3.26}$$

Now, we must note that the DC component and the magnitudes and phases of the cosines, i.e., the Fourier coefficients of the response signal, $y(t)$, are independent of the frequencies ω_1 and ω_2. Hence, for the purpose of evaluating nonlinear devices, the values of the actual base frequencies are irrelevant and can be chosen freely. Taking this into account, artificial frequencies can be chosen to be multiples of some arbitrary frequency, so that the correspondent artificial time-domain signal is periodic. Once artificial frequencies are chosen in this way, the DFT can be used.

With the above considerations in mind, we can relax on the need for the either ill-conditioned APFT or computationally expensive MDFT. An important advantage of artificial frequency

mapping is, indeed, its applicability to problems having a large number of uncommensurated excitations. Mapping techniques, for both box and diamond truncation, that make possible to convert the frequency mixing components' vector into another one where the original proportions between frequency positions are preserved, and which is both dense and harmonically related, can be seen, for example, in [21], or [44].

3.5 Multivariate Formulation

In this section we will introduce a powerful strategy for analyzing nonlinear circuits handling multirate signals. This strategy is suitable to deal with the above amplitude and/or phase modulated signals and quasiperiodic signals, as with any other kind of multirate signals. It uses multiple time variables to describe multirate behavior, and it is based on the fact that multirate signals can be represented much more efficiently if they are defined as functions of two or more time variables, i.e., if they are defined as *multivariate functions* [57], [59]. With this multivariate formulation, circuits will be no longer described by ordinary differential algebraic equations in the one-dimensional time *t*, but, instead, by partial differential algebraic systems.

Several powerful numerical techniques based on the multivariate strategy, operating in time, frequency, or hybrid (combination) domains, will be presented. The strategies adopted to each case are essentially dependent on two aspects: (i) the existence (or not) of periodicity in the components of the signals; (ii) the degree of the circuits' nonlinearities, which is intricately related with the smoothness of the signals.

3.5.1 Multivariate Representations

The multidimensional strategy is easily illustrated by applying it to a bi-dimensional problem. So, let us consider, for example, an amplitude modulated RF carrier of the form

$$x(t) = e(t)\sin(2\pi f_C t), \tag{3.27}$$

where $e(t)$ is an envelope, slowly varying in time, while $\sin(2\pi f_C t)$ is a fast-varying RF carrier. As seen, simulating a circuit with this kind of stimulus, using conventional time-step integration schemes, tends to be highly inefficient because it requires time steps closely spaced in time (for representing each fast RF cycle accurately) and during a very long time window determined by the envelope. Let us now consider a bivariate representation for $x(t)$, defined as

$$\hat{x}(t_1, t_2) = e(t_1)\sin(2\pi f_C t_2), \tag{3.28}$$

where t_1 is the slow envelope time scale and t_2 is the fast carrier time scale. In this particular case $\hat{x}(t_1, t_2)$ is a periodic function with respect to t_2 but not to t_1, i.e.,

$$\hat{x}(t_1, t_2) = \hat{x}(t_1, t_2 + T_2), \quad T_2 = 1/f_C. \tag{3.29}$$

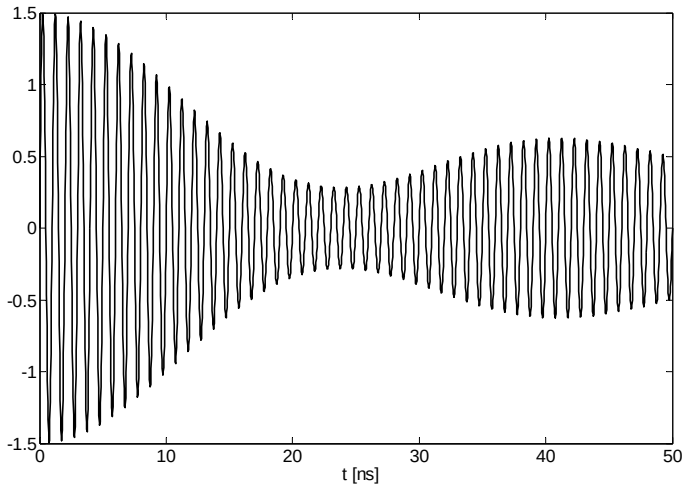

Figure 3.4 Envelope modulated signal in the univariate time.

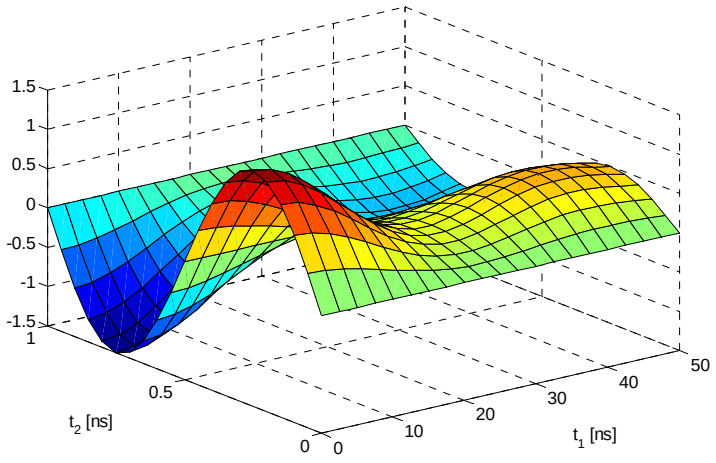

Figure 3.5 Bivariate representation of the envelope modulated signal.

The univariate and bivariate forms of $x(t)$, with $e(t)=\text{sinc}\left(60\times10^{6}t\right)+0.5$ and $f_C=1\,\text{GHz}$, are plotted in Figures 3.4 and 3.5, for a $[0,50\,\text{ns}]$ time interval, and a rectangular region $[0,50\,\text{ns}]\times[0,T_2]$, respectively. There, it can be appreciated that $\hat{x}(t_1,t_2)$ does not have as many undulations as $x(t)$, allowing thus a more compact representation with fewer samples. Furthermore, due to the periodicity of $\hat{x}(t_1,t_2)$ in t_2, we know that its plot repeats over the rest of this time axis. Thus, the bivariate form plotted in Figure 3.5 contains all the information necessary to recover the original univariate form depicted in Figure 3.4.

In general, the multivariate form of a multirate signal can require far fewer points to represent numerically the original signal, especially when its time scales are widely separated. This is not only true for signals with a compact frequency-domain representation (as the above illustrative

example), but also for those that can not be represented efficiently in the frequency-domain (e.g., a high frequency PWM signal with a duty cycle controlled by a slow information signal). However, it must be noted that this is not universally true. For example, phase modulated (PM) signals are not compact in a simple bivariate representation. For that reason they will be addressed separately in Section 3.6.

3.5.2 MPDAE

Let us consider a general nonlinear RF circuit described by the differential algebraic equations' (DAE) system of (2.1), that we rewrite here for convenience,

$$\boldsymbol{p}\left[\boldsymbol{y}(t)\right]+\frac{d\boldsymbol{q}\left[\boldsymbol{y}(t)\right]}{dt}=\boldsymbol{x}(t), \tag{3.30}$$

and let us suppose that this circuit is driven by the envelope modulated signal of (3.27). Taking the above considerations into account, we will adopt the following procedure: for the slowly varying parts (envelope time scale) of the expressions of $\boldsymbol{x}(t)$ and $\boldsymbol{y}(t)$, t is replaced by t_1; for the fast-varying parts (RF carrier time scale) t is replaced by t_2. The application of this bivariate strategy to the DAE system of (3.30) converts it into the following *multirate partial differential algebraic equations'* (MPDAE) system [57], [59]:

$$\boldsymbol{p}\left[\hat{\boldsymbol{y}}(t_1,t_2)\right]+\frac{\partial\boldsymbol{q}\left[\hat{\boldsymbol{y}}(t_1,t_2)\right]}{\partial t_1}+\frac{\partial\boldsymbol{q}\left[\hat{\boldsymbol{y}}(t_1,t_2)\right]}{\partial t_2}=\hat{\boldsymbol{x}}(t_1,t_2). \tag{3.31}$$

The mathematical relation between (3.30) and (3.31) establishes that, if $\hat{\boldsymbol{x}}(t_1,t_2)$ and $\hat{\boldsymbol{y}}(t_1,t_2)$ satisfy (3.31), then the univariate forms $\boldsymbol{x}(t)=\hat{\boldsymbol{x}}(t,t)$ and $\boldsymbol{y}(t)=\hat{\boldsymbol{y}}(t,t)$ satisfy (3.30) [59]. Therefore, univariate solutions of (3.30) are available on diagonal lines $t_1=t$, $t_2=t$, along the bivariate solutions of (3.31), i.e., $\boldsymbol{y}(t)$ may be retrieved from its bivariate form $\hat{\boldsymbol{y}}(t_1,t_2)$, by simply setting $t_1=t_2=t$. Consequently, if one wants to obtain the univariate solution in the generic $\left[0,t_{Final}\right]$ interval, due to the periodicity of the problem in the t_2 dimension we will have

$$\boldsymbol{y}(t)=\hat{\boldsymbol{y}}(t,t\bmod T_2) \tag{3.32}$$

on the rectangular domain $\left[0,t_{Final}\right]\times\left[0,T_2\right]$, where $t\bmod T_2$ represents the remainder of division of t by T_2.

The generalization of this bivariate strategy to a multidimensional problem with more than two time scales is straightforward. In fact, if the signals in the circuit present m separate rates of change, then m time scales will be used. In that case, (3.31) assumes the generic form

$$\boldsymbol{p}\left[\hat{\boldsymbol{y}}(t_1,t_2,\ldots,t_m)\right]+\frac{\partial\boldsymbol{q}\left[\hat{\boldsymbol{y}}(t_1,t_2,\ldots,t_m)\right]}{\partial t_1}+\cdots+\frac{\partial\boldsymbol{q}\left[\hat{\boldsymbol{y}}(t_1,t_2,\ldots,t_m)\right]}{\partial t_m}=\hat{\boldsymbol{x}}(t_1,t_2,\ldots,t_m), \tag{3.33}$$

and the univariate solution, $\boldsymbol{y}(t)$, may be recovered from its multivariate form, $\hat{\boldsymbol{y}}(t_1,t_2,\ldots,t_m)$, by setting $t_1=t_2=\cdots=t_m=t$.

This generic MPDAE formulation can be employed to solve many types of multirate problems. Depending on the numerical method chosen to compute the solution of (3.33), it can be adopted to deal with either weakly or strongly nonlinear regimes, as with a large class of multirate signals. The main advantage of this MPDAE approach is that it can result in significant improvements in simulation speed when compared to DAE-based alternatives [38], [40], [57], [59], [60].

3.5.3 Boundary Conditions

In order to compute the multivariate solutions, some boundary conditions must be added to the MPDAE system. These boundary conditions are intricately related with the existence (or not) of periodicity in the components of the signals. Once again, we will assume the bi-dimensional case to guarantee explanation clarity. The generalization to the *m* multidimensional case is straightforward.

3.5.3.1 Envelope Modulated Regimes

Envelope modulated responses to excitations of the form of (3.27) correspond to a combination of initial and periodic boundary conditions for the MPDAE. This means that the bivariate forms of these solutions can be obtained by numerically solving the following initial-boundary value problem [59]

$$\begin{aligned} \boldsymbol{p}\left[\hat{\boldsymbol{y}}\left(t_1,t_2\right)\right]+\frac{\partial \boldsymbol{q}\left[\hat{\boldsymbol{y}}\left(t_1,t_2\right)\right]}{\partial t_1}+\frac{\partial \boldsymbol{q}\left[\hat{\boldsymbol{y}}\left(t_1,t_2\right)\right]}{\partial t_2}&=\hat{\boldsymbol{x}}\left(t_1,t_2\right)\\ \hat{\boldsymbol{y}}\left(0,t_2\right)&=\boldsymbol{g}\left(t_2\right)\\ \hat{\boldsymbol{y}}\left(t_1,0\right)&=\hat{\boldsymbol{y}}\left(t_1,T_2\right)\end{aligned} \tag{3.34}$$

on the rectangle $\left[0,t_{Final}\right]\times\left[0,T_2\right]$. $g\left(\cdot\right)$ is a given initial-condition function defined on $\left[0,T_2\right]$, satisfying $\boldsymbol{g}\left(0\right)=\boldsymbol{g}\left(T_2\right)=\boldsymbol{y}\left(0\right)$, and the periodic boundary condition $\hat{\boldsymbol{y}}\left(t_1,0\right)=\hat{\boldsymbol{y}}\left(t_1,T_2\right)$ is due to the periodicity of the problem in the t_2 fast carrier time scale.

The reason why bivariate envelope modulated solutions do not need to be evaluated on the entire $\left[0,t_{Final}\right]\times\left[0,t_{Final}\right]$ domain (which would be computationally very expensive and would turn the multivariate strategy useless), and are restricted to the rectangle $\left[0,t_{Final}\right]\times\left[0,T_2\right]$, is because the solutions repeat along the t_2 time axis. The way how univariate solutions are recovered from their multivariate forms was already defined above by (3.32) and it is illustrated in Figure 3.6.

3.5.3.2 Quasiperiodic Regimes

Bivariate quasiperiodic steady-state solutions are captured using bi-periodic boundary conditions for the MPDAE. In order to illustrate that, let us consider the quasiperiodic signal of (3.20) and let us define its bivariate form as

$$\hat{y}\left(t_1,t_2\right)=\sum_{k_1,k_2}Y_{k_1,k_2}e^{j\left(k_1\omega_1 t_1+k_2\omega_2 t_2\right)}. \tag{3.35}$$

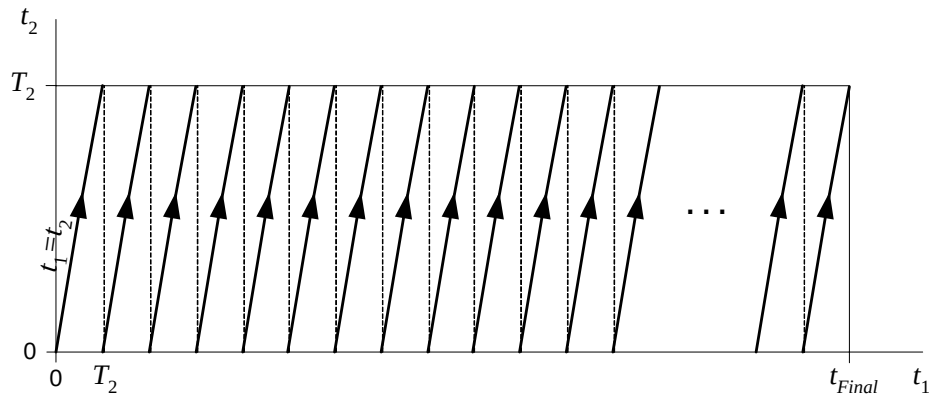

Figure 3.6 Sawtooth path in the $t_1 t_2$ plane for envelope modulated signals.

It is easy to see that $\hat{y}(t_1,t_2)$ satisfies the condition $\hat{y}(t_1,t_2)=\hat{y}(t_1+T_1,t_2+T_2)$ for all t_1,t_2, with $T_1=2\pi/\omega_1$ and $T_2=2\pi/\omega_2$. Thus, this bivariate signal is bi-periodic, i.e., it is periodic with respect to both t_1 and t_2 arguments.

The conversion of quasiperiodicity for univariate signals into bi-periodicity for bivariate signals is the key that allows the computation of the MPDAE solutions to be restricted to the $[0,T_1]\times[0,T_2]$ rectangular domain. Indeed, if we would evaluate the bivariate solution of a circuit under a quasiperiodic steady-state regime, on the entire $[0,t_{Final}]\times[0,t_{Final}]$ domain, we would conclude that such solution repeats over the t_1,t_2 plane. So, bivariate forms of these solutions can be obtained by numerically solving the following bi-periodic boundary value problem [59]

$$\begin{aligned} \boldsymbol{p}\left[\hat{\boldsymbol{y}}(t_1,t_2)\right]+\frac{\partial \boldsymbol{q}\left[\hat{\boldsymbol{y}}(t_1,t_2)\right]}{\partial t_1}+\frac{\partial \boldsymbol{q}\left[\hat{\boldsymbol{y}}(t_1,t_2)\right]}{\partial t_2}&=\hat{\boldsymbol{x}}(t_1,t_2)\\ \hat{\boldsymbol{y}}(0,t_2)&=\hat{\boldsymbol{y}}(T_1,t_2)\\ \hat{\boldsymbol{y}}(t_1,0)&=\hat{\boldsymbol{y}}(t_1,T_2) \end{aligned} \tag{3.36}$$

on the rectangle $[0,T_1]\times[0,T_2]$.

The original univariate solution $\boldsymbol{y}(t)$ is now retrieved from $\hat{\boldsymbol{y}}(t_1,t_2)$ by setting

$$\boldsymbol{y}(t)=\hat{\boldsymbol{y}}(t \bmod T_1, t \bmod T_2). \tag{3.37}$$

This is illustrated in Figure 3.7(a) for widely separated fundamental frequencies, ω_1 and ω_2, and in Figure 3.7(b) for closely spaced frequencies.

3.5.3.3 Other Multirate Regimes Containing Periodic Components

There are many other kinds of multirate signals beyond the two cases just presented above. With some exceptions (e.g., the case of PM signals addressed bellow in Section 3.6), the MPDAE formulation that can be obtained for handling generic multirate signals may be one of the above described for the case of envelope modulated signals or quasiperiodic signals. Indeed, the conditions that must be applied to the MPDAE system are merely dependent on the existence (or

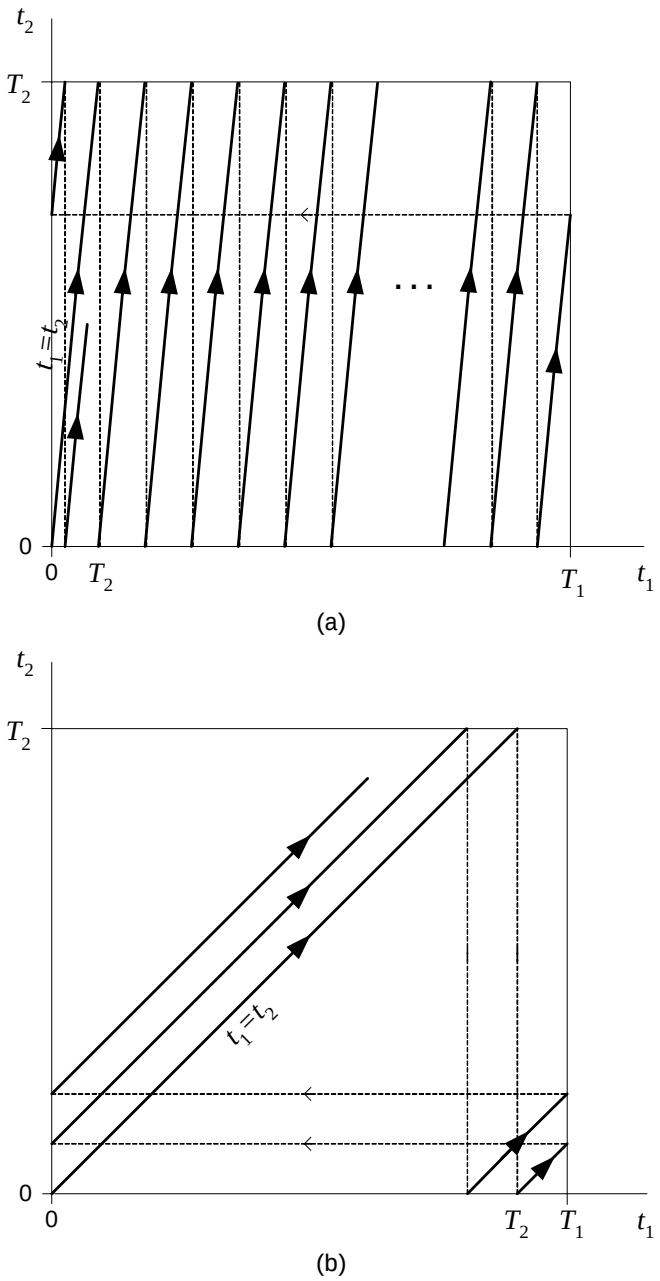

Figure 3.7 Sawtooth path in the $t_1 t_2$ plane for quasiperiodic signals: (a) widely separated tones and (b) closely spaced tones.

not) of periodicity on the components of the signals. For instance, in a circuit excited by a fast PWM source whose duty cycle is controlled by a slow aperiodic information signal, we will have an initial-boundary value problem, with an initial condition in the slow time scale and a periodic boundary condition in the fast time scale. On the contrary, if the duty cycle of the PWM changes periodically, then we will have a bi-periodic boundary value problem, with periodic boundary conditions in both time dimensions.

3.5.3.4 Aperiodic Multirate Regimes

Let $y(t)$ be a multirate state variable in a circuit, defined as

$$y(t) = e_1(t) + e_2(t), \tag{3.38}$$

in which $e_1(t)$ and $e_2(t)$ are two aperiodic functions of widely separated rates of change. Let us consider, for instance, that $e_2(t)$ is fast-varying in time, which requires N_2 time samples to be represented accurately in a generic $[0, t_{Final}]$ time interval, and $e_1(t)$ is a slowly varying signal, that needs only $N_1 << N_2$ time samples to be represented in the same interval. Since the sampling rate of a multirate signal is dictated by its fastest component, it is easy to see that the number of time samples required to represent $y(t)$ accurately will be N_2.

Now, let us consider the bivariate form of $y(t)$, defined as

$$\hat{y}(t_1, t_2) = e_1(t_1) + e_2(t_2). \tag{3.39}$$

In view of the fact that $\hat{y}(t_1, t_2)$ does not evidence any periodicity in t_1 or t_2, it must be represented in the entire $[0, t_{Final}] \times [0, t_{Final}]$ domain. So, a much higher total of $N_1 \times N_2$ sample points will be now required. Therefore, it is straightforward to conclude that the multivariate strategy is completely useless when the multirate signals do no evidence any periodicity in their components.

3.5.4 Techniques for Computing the Solution of the MPDAE

We will now finally present several numerical techniques that can be used to evaluate the solution of the MPDAE. Techniques operating in a purely time-domain framework will be suitable to deal with strong nonlinearities, whereas techniques operating in frequency or hybrid domains will be more adequate to handle moderately nonlinear regimes. Since these techniques are more easily illustrated by applying them to bi-dimensional problems, we will focus again our presentation on the bivariate formulation (the generalization to the *m* multivariate formulation is straightforward). We will first consider the case of the initial-boundary value problems described by (3.34), to then address the bi-periodic boundary value problems of the form defined by (3.36).

3.5.4.1 Envelope Transient over Shooting

The *envelope transient over shooting* is a purely time-domain method that can be used to obtain the numerical solution of the initial-boundary value problem of (3.34). This method is a particular implementation of a general technique that is often referred to as *envelope following* or *envelope transient oriented technique*. In this case we have a time domain envelope following (TD-ENV) method [10], [59]. For achieving an intuitive explanation of the envelope transient over shooting method, let us start by considering the semi-discretization of the rectangular domain $[0, t_{Final}] \times [0, T_2]$ in the t_1 slow time dimension defined by the grid

$$0 = t_{1,0} < t_{1,1} < \cdots < t_{1,i-1} < t_{1,i} < \cdots < t_{1,K_1} = t_{Final}, \quad h_{1,i} = t_{1,i} - t_{1,i-1}, \tag{3.40}$$

where K_1 is the total number of steps in t_1. If we replace the derivatives of the MPDAE in t_1 with a finite-differences approximation (e.g., the Backward Euler rule), then we obtain for each slow time instant $t_{1,i}$, from $i=1$ to $i=K_1$, the periodic boundary value problem defined by

$$\begin{gathered} \boldsymbol{p}\left[\hat{\boldsymbol{y}}_i(t_2)\right] + \frac{\boldsymbol{q}\left[\hat{\boldsymbol{y}}_i(t_2)\right] - \boldsymbol{q}\left[\hat{\boldsymbol{y}}_{i-1}(t_2)\right]}{h_{1,i}} + \frac{d\boldsymbol{q}\left[\hat{\boldsymbol{y}}_i(t_2)\right]}{dt_2} = \hat{\boldsymbol{x}}(t_{1,i}, t_2), \\ \hat{\boldsymbol{y}}_i(0) = \hat{\boldsymbol{y}}_i(T_2), \end{gathered} \tag{3.41}$$

where $\hat{\boldsymbol{y}}_i(t_2) \simeq \hat{\boldsymbol{y}}(t_{1,i}, t_2)$. This means that, once $\hat{\boldsymbol{y}}_{i-1}(t_2)$ is known, the solution on the next level, $\hat{\boldsymbol{y}}_i(t_2)$, is obtained by solving (3.41), and thus for obtaining the whole solution $\hat{\boldsymbol{y}}$ in the entire domain $[0, t_{Final}] \times [0, T_2]$ a total of K_1 boundary value problems have to be solved. With the envelope transient over shooting technique each of the periodic boundary value problems of (3.41) is solved using the shooting method.

3.5.4.2 Envelope Transient over FDTD

Another purely time-domain technique that can be suitable to solve initial-boundary value problems of the form of (3.34) is the *envelope transient over FDTD*. This is a TD-ENV technique that is very similar to envelope transient over shooting. The basic difference is that, instead of the shooting method, each one of the periodic boundary value problems of (3.41) is here numerically solved with FDTD.

The advantages and disadvantages of these two techniques are analogous to the ones already discussed for their univariate versions (one-dimensional shooting and one-dimensional FDTD). As stated in Chapter 2, although FDTD has the ability to deal with linear time-invariant distributed devices, it can generate large systems of equations, especially if either the number of unknown waveforms or the number of grid points is large. So, envelope transient over shooting is, in general, a more preferable technique than envelope transient over FDTD.

3.5.4.3 Multitime Envelope Transient Harmonic Balance

Let us consider again the initial-boundary value problem of (3.34) and the above strategy of replacing t_1 derivatives with finite-differences approximations, which has conducted to the periodic boundary value problems defined by (3.41). When waveforms are not extremely demanding on the number of harmonics for a convenient frequency-domain representation, an alternative way to the use of shooting or FDTD methods for computing efficiently the solution of (3.41) consists in using the HB method. By doing so, we will obtain the following HB system for each slow time instant $t_{1,i}$,

$$\mathbf{P}\left[\hat{\mathbf{Y}}(t_{1,i})\right] + \frac{\mathbf{Q}\left[\hat{\mathbf{Y}}(t_{1,i})\right] - \mathbf{Q}\left[\hat{\mathbf{Y}}(t_{1,i-1})\right]}{h_{1,i}} + j\boldsymbol{\Omega}\mathbf{Q}\left[\hat{\mathbf{Y}}(t_{1,i})\right] = \hat{\mathbf{X}}(t_{1,i}), \tag{3.42}$$

in which $\hat{\mathbf{X}}\left(t_{1,i}\right)$ and $\hat{\mathbf{Y}}\left(t_{1,i}\right)$ are the vectors containing the Fourier coefficients of the excitation and of the solution, respectively, at $t_1 = t_{1,i}$.

With this strategy we have an envelope following method that handles the solution dependence on t_2 in frequency-domain, while treating the course of the solution to t_1 in time domain. So, this is a mixed frequency-time technique, which is similar to the ETHB engine previously reported in Section 3.4.2. In order to distinguish the two versions, we will denote this new mixed frequency-time technique as *multitime envelope transient harmonic balance* (multitime ETHB).

An important advantage of multime ETHB over conventional ETHB is that it does not suffer from bandwidth limitations [42], [43]. For example, in circuits driven by envelope modulated signals, the only restriction that has to be imposed is that the modulating signal and the carrier must not be correlated in time (which is typically the case).

3.5.4.4 Multivariate FDTD

The *multivariate FDTD* (MFDTD) is a purely time-domain technique that can be utilized to obtain the numerical solution of multidimensional boundary value problems. It can be seen as the generalization of the univariate FDTD presented in Chapter 2, to a framework with two, or more, time dimensions.

Thus, let us consider now the bi-periodic boundary value problem of (3.36). Let us also consider the discretization of the rectangular domain $\left[0,T_1\right]\times\left[0,T_2\right]$ in both the t_1 and t_2 dimensions, defined by

$$0 = t_{1,0} < t_{1,1} < \cdots < t_{1,i-1} < t_{1,i} < \cdots < t_{1,K_1} = T_1, \quad h_{1,i} = t_{1,i} - t_{1,i-1}, \tag{3.43}$$

$$0 = t_{2,0} < t_{2,1} < \cdots < t_{2,j-1} < t_{2,j} < \cdots < t_{2,K_2} = T_2, \quad h_{2,j} = t_{2,j} - t_{2,j-1}, \tag{3.44}$$

with a total of $\left(K_1+1\right)\times\left(K_2+1\right)$ grid points. If we impose a finite-differences scheme (e.g., the Backward Euler rule) to approximate both the differentiation operators of the MPDAE, then we obtain

$$\boldsymbol{p}\left(\hat{\boldsymbol{y}}_{i,j}\right) + \frac{\boldsymbol{q}\left(\hat{\boldsymbol{y}}_{i,j}\right) - \boldsymbol{q}\left(\hat{\boldsymbol{y}}_{i-1,j}\right)}{h_{1,i}} + \frac{\boldsymbol{q}\left(\hat{\boldsymbol{y}}_{i,j}\right) - \boldsymbol{q}\left(\hat{\boldsymbol{y}}_{i,j-1}\right)}{h_{2,j}} = \hat{\boldsymbol{x}}_{i,j} \qquad \begin{matrix} i = 1,\ldots,K_1, \\ j = 1,\ldots,K_2, \end{matrix} \tag{3.45}$$

where $\hat{\boldsymbol{x}}_{i,j} = \hat{\boldsymbol{x}}\left(t_{1,i},t_{2,j}\right)$ and $\hat{\boldsymbol{y}}_{i,j} \simeq \hat{\boldsymbol{y}}\left(t_{1,i},t_{2,j}\right)$, together with the conditions describing the bi-periodic regime

$$\hat{\boldsymbol{y}}_{0,j} = \hat{\boldsymbol{y}}_{K_1,j}, \qquad \hat{\boldsymbol{y}}_{i,0} = \hat{\boldsymbol{y}}_{i,K_2}. \tag{3.46}$$

By substituting (3.46) into (3.45) we can obtain a nonlinear system of $n\times K_1\times K_2$ algebraic equations, where n is the number of state variables of the circuit. Such system can be solved with a $n\times K_1\times K_2$-dimensional Newton-Raphson iterative solver.

MFDTD suffers from a serious drawback, which is precisely the difficulty inherent to univariate FDTD, but now in an augmented proportion. Because of the large number of equations and unknowns involved, the amount of memory required by MFDTD severely constrains the size of the circuit. For example, in multitone analysis, the use of MFDTD is usually restricted to circuits of very small size under a two-tone excitation.

3.5.4.5 Hierarchical Shooting

A different approach for solving the bi-periodic boundary value problem of (3.36) in a purely time-domain way is to use *hierarchical shooting* [59]. Hierarchical shooting is the multivariate version of classical one-dimensional shooting. As seen, shooting consists in guessing initial conditions, by comparing and wisely updating them, after successive time-step integrations (shooting loop). Hierarchical shooting consists in performing shooting in one dimension, say t_2, nested in the other dimension, t_1. This means that, by considering the semi-discretization of the $[0,T_1]\times[0,T_2]$ rectangular domain defined by (3.43), and replacing the derivatives of the MPDAE in t_1 with a finite-differences approximation, we obtain a set of successive periodic boundary value problems of the form of (3.41) that we solve by shooting. So, first we have to go through successive shooting iterations for each one of the consecutive vertical lines $t_{1,i},t_2$ (inner loop), starting from $t_{1,0},t_2$ until t_{1,K_1},t_2. Then, we have to compare and update the initial solution on the left side of the rectangle, according to the solution obtained on the right side, to afterwards repeat the vertical line shooting process all over the domain, until a bi-periodic solution is achieved (outer loop).

One advantage of hierarchical shooting over MFDTD is that the amount of storage required is much smaller. Therefore, and even though the total computation time is dependent on the number of shooting iterations needed to achieve the final solution, hierarchical shooting is, comparably, a more suitable technique to solve (3.36) than MFDTD.

3.5.4.6 Multidimensional HB

The *multidimensional harmonic balance* is a frequency-domain technique that can be used to solve *m*-periodic boundary value problems, when strong nonlinearities are not present. This technique is the generalization of classical one-dimensional HB to the case of problems involving two, or more, time dimensions. Thus it can be viewed as the technique already reported in Section 3.4.4 for the computation of quasiperiodic steady-state solutions, referred to as harmonic balance based on the multidimensional discrete Fourier transform (MDFT).

In order to provide a brief and intuitive explanation of bi-dimensional HB, let us consider a scalar ($n=1$) bi-periodic boundary value problem of the form of (3.36). Since both the bivariate forms $\hat{x}(t_1,t_2)$ and $\hat{y}(t_1,t_2)$ are bi-periodic, they can be expressed as two-dimensional Fourier series, i.e.,

$$\hat{x}(t_1,t_2)=\sum_{k_1,k_2} X_{k_1,k_2} e^{jk_1\omega_1 t_1} e^{jk_2\omega_2 t_2}, \qquad \hat{y}(t_1,t_2)=\sum_{k_1,k_2} Y_{k_1,k_2} e^{jk_1\omega_1 t_1} e^{jk_2\omega_2 t_2}. \tag{3.47}$$

If a harmonic box truncation is adopted, i.e., if $|k_1|\le K_1$ and $|k_2|\le K_2$, the one-dimensional HB equation of (2.41) can be converted into its bi-dimensional form

$$\mathbf{F}(\hat{\mathbf{Y}})=\mathbf{P}(\hat{\mathbf{Y}})+ j\Omega_1\mathbf{Q}(\hat{\mathbf{Y}})+ j\Omega_2\mathbf{Q}(\hat{\mathbf{Y}})-\hat{\mathbf{X}}=0, \tag{3.48}$$

where

$$\hat{\mathbf{X}}=\left[X_{-K_1,-K_2},\ldots,X_{K_1,-K_2},\ldots,X_{-K_1,0},\ldots,X_{K_1,0},\ldots,X_{-K_1,K_2},\ldots,X_{K_1,K_2}\right]^T,$$

$$\hat{\mathbf{Y}}=\left[Y_{-K_1,-K_2},\ldots,Y_{K_1,-K_2},\ldots,Y_{-K_1,0},\ldots,Y_{K_1,0},\ldots,Y_{-K_1,K_2},\ldots,Y_{K_1,K_2}\right]^T,$$

and

$$j\Omega_1=\mathrm{diag}\left(\underbrace{-jK_1\omega_1,\ldots,jK_1\omega_1}_{k_2=-K_2},\ldots,\underbrace{-jK_1\omega_1,\ldots,jK_1\omega_1}_{k_2=0},\ldots,\underbrace{-jK_1\omega_1,\ldots,jK_1\omega_1}_{k_2=K_2}\right),$$

$$j\Omega_2=\mathrm{diag}\left(\underbrace{-jK_2\omega_2,\ldots,-jK_2\omega_2}_{k_1\text{ elements}},\ldots,\underbrace{0,\ldots,0}_{k_1\text{ elements}},\ldots,\underbrace{jK_2\omega_2,\ldots,jK_2\omega_2}_{k_1\text{ elements}}\right).$$

The solution of (3.48) can be iteratively computed with the Newton-Raphson algorithm (2.40), in which the Jacobian matrix of (2.42) is now given by

$$\mathbf{J}(\hat{\mathbf{Y}})=\frac{d\mathbf{F}(\hat{\mathbf{Y}})}{d\hat{\mathbf{Y}}}=\mathbf{G}(\hat{\mathbf{Y}})+ j\Omega_1\mathbf{C}(\hat{\mathbf{Y}})+ j\Omega_2\mathbf{C}(\hat{\mathbf{Y}}). \tag{3.49}$$

In the same way as mentioned in Section 3.4.4, since this technique is restricted to box truncation the number of arithmetic operations required to compute the solution increases exponentially with the number of time scales involved. So, in general it is not used for periodic boundary value problems with more than two or three time dimensions.

3.6 Warped Time Formulation

The key to the efficiency of the numerical techniques presented in the previous section relies on the fact that multivariate representations of multirate signals can have a much more compact description than their original univariate forms. Although this is valid for a large class of signals, such as the ones addressed above, this is not universally true. For example, phase modulated (PM) signals can not, in general, be represented compactly in a multivariate framework.

To illustrate this situation let us consider the PM signal

$$x(t)=\cos\left[2\pi f_C t+k_p s(t)\right], \tag{3.50}$$

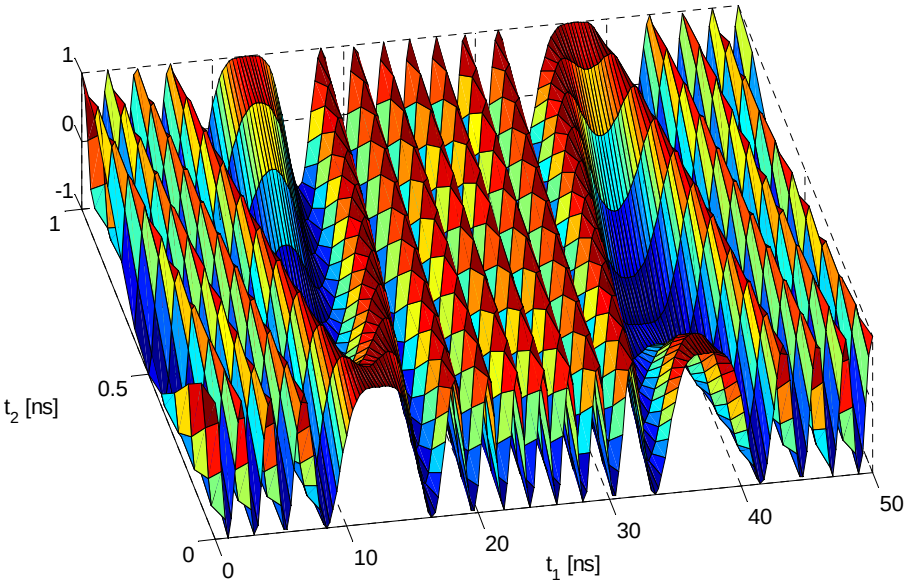

Figure 3.8 Bivariate representation of the PM signal.

where $s(t)$ is a slowly varying modulating signal and f_C is the frequency of the fast-varying RF carrier. By adopting the same procedure as for (3.27) and (3.28), we can obtain the bivariate form

$$\hat{x}(t_1,t_2)=\cos\left[2\pi f_C t_2 + k_p s(t_1)\right], \tag{3.51}$$

which is plotted in Figure 3.8 for a carrier frequency of $f_C = 1\,\text{GHz}$, a modulation index of $k_p = 8\pi$ and $s(t)=\sin(2\pi f_0 t)$ (a low frequency sinusoid of $f_0 = 20$ MHz). Now we can see that $\hat{x}(t_1,t_2)$ has a high density of fluctuations, unlike the simple surface shown in Figure 3.5. Furthermore, the number of these fluctuations could even be larger if k_p was increased.

To effectively handle PM signals, we make use of the concept of *warped time* [34], [35], [46]-[48], within the bivariate formulation. The employment of this recently proposed technique dynamically rescales (warps) the fast time axis to considerably reduce the number of fluctuations of the PM signals. For instance, let us now consider the new bivariate form

$$\hat{x}(\tau_1,\tau_2)=\cos(2\pi\tau_2), \tag{3.52}$$

together with the warping function

$$\phi(\tau_1)= f_C\tau_1 + \frac{k_p}{2\pi}s(\tau_1). \tag{3.53}$$

The plot of $\hat{x}(\tau_1,\tau_2)$ will be a simple surface and the original univariate form $x(t)$ may be recovered as $x(t)=\hat{x}\left[t,\phi(t)\right]$. This strategy eases the compact representation of PM signals on a two-dimensional grid and leads to a framework of multirate partial differential algebraic equations in warped and unwarped time scales, together with a mapping between multitime and single-time

functions. Indeed, if we take the above considerations into account we can adopt the following procedure: for the slowly-varying parts of the expressions of $\boldsymbol{x}(t)$ and $\boldsymbol{y}(t)$ in (3.30) t is replaced by $\tau_1 = t$; for the fast-varying parts t is replaced by $\tau_2 = \phi(t)$, where $\phi(t)$ is any appropriate rescaling function (the so-called *warped time*). This results in warped bivariate representations for the excitation and the solution that we will now denote by $\hat{\boldsymbol{x}}(\tau_1, \tau_2)$ and $\hat{\boldsymbol{y}}(\tau_1, \tau_2)$, respectively, and the differential algebraic system of (3.30) becomes converted into the following *warped multirate partial differential algebraic equations'* (WaMPDAE) system [34], [35], [46]-[48]

$$\boldsymbol{p}\left[\hat{\boldsymbol{y}}(\tau_1, \tau_2)\right] + \frac{\partial \boldsymbol{q}\left[\hat{\boldsymbol{y}}(\tau_1, \tau_2)\right]}{\partial \tau_1} + \omega(\tau_1)\frac{\partial \boldsymbol{q}\left[\hat{\boldsymbol{y}}(\tau_1, \tau_2)\right]}{\partial \tau_2} = \hat{\boldsymbol{x}}(\tau_1, \tau_2), \tag{3.54}$$

in which $\omega(\tau_1) = d\phi(\tau_1)/d\tau_1$. It is easy to show that if $\hat{\boldsymbol{x}}(\tau_1, \tau_2)$ and $\hat{\boldsymbol{y}}(\tau_1, \tau_2)$ satisfy (3.54), then the univariate forms $\boldsymbol{x}(t) = \hat{\boldsymbol{x}}\left[t, \phi(t)\right]$ and $\boldsymbol{y}(t) = \hat{\boldsymbol{y}}\left[t, \phi(t)\right]$ satisfy (3.30) [35]. Consequently, the univariate solutions $\boldsymbol{y}(t)$ are available on paths of parametric equations $\tau_1 = t$, $\tau_2 = \phi(t)$, along the bivariate solutions $\hat{\boldsymbol{y}}(\tau_1, \tau_2)$ in the τ_1, τ_2 space.

This warped multitime approach can be seen as the generalization of the straightforward multiple time formulation presented in Section 3.5. In fact, if we would unwarp the fast time axis making $\phi(t) = t$, then (3.54) would degenerate into (3.31). It must be noted that the choice of the coupled warped bivariate form (3.52) and warping function (3.53) is not unique. In effect, any warping function can be chosen as long as it guarantees that the resulting warped bivariate representation is compact, i.e., it has the desired property of being easy to sample. In some problems, as is the case of oscillators (e.g., VCOs), $\phi(t)$ is not even known a priori. It is computed jointly with the solution of the the WaMPDAE, by simultaneously solving (3.54) and an additional slowly varying phase condition [31], [34], [35], which ensures a compact numerical representation for the warped bivariate forms.

The generalization of the above warped bivariate formulation to the case of m time scales is straightforward. In that case, the *m*-dimensional WaMPDAE can be defined to be

$$\begin{aligned} &\boldsymbol{p}\left[\hat{\boldsymbol{y}}(\tau_1, \tau_2, \ldots, \tau_m)\right] + \frac{\partial \boldsymbol{q}\left[\hat{\boldsymbol{y}}(\tau_1, \tau_2, \ldots, \tau_m)\right]}{\partial \tau_1} + \cdots + \frac{\partial \boldsymbol{q}\left[\hat{\boldsymbol{y}}(\tau_1, \tau_2, \ldots, \tau_m)\right]}{\partial \tau_l} \\ &+ \omega_{l+1}(\tau_1)\frac{\partial \boldsymbol{q}\left[\hat{\boldsymbol{y}}(\tau_1, \tau_2, \ldots, \tau_m)\right]}{\partial \tau_{l+1}} + \cdots + \omega_m(\tau_1)\frac{\partial \boldsymbol{q}\left[\hat{\boldsymbol{y}}(\tau_1, \tau_2, \ldots, \tau_m)\right]}{\partial \tau_m} = \hat{\boldsymbol{x}}(\tau_1, \tau_2, \ldots, \tau_m), \end{aligned} \tag{3.55}$$

in which $\tau_{l+1}, \ldots, \tau_m$ are warped time scales, whereas $\tau_1, \ldots, \tau_l$ are unwarped time scales. Univariate solutions $\boldsymbol{y}(t)$ are retrieved from their multivariate forms $\hat{\boldsymbol{y}}(\tau_1, \tau_2, \ldots, \tau_m)$ by setting $\tau_i = t$, $i = 1, \ldots, l$, and $\tau_i = \phi_i(t)$, $i = l+1, \ldots, m$, with $\omega_i(\tau_1) = d\phi_i(\tau_1)/d\tau_1$.

Chapter 4
An Efficient Time-Domain Simulation Method

4.1 Introduction

This chapter is dedicated to the discussion of a new computer-aided design tool especially conceived for the efficient time-domain simulation of highly heterogeneous nonlinear wireless communication networks, combining RF and baseband analog circuitry and digital components. Thus, a first approach to cope with the current RF circuit simulation challenging scenario described in the introduction of this thesis is here advanced. Due to the strongly nonlinear regimes of the circuits under analysis (e.g., switching-mode operations), the possibility of using any frequency-domain technique was completely discarded. A time-domain description is here mandatory. The proposed numerical method uses the modern multirate Runge-Kutta algorithms presented in Section 3.2.2, applied to the envelope transient method over the shooting time-domain periodic steady-state engine, to efficiently resolve such strongly nonlinear heterogeneous circuits, which are excited by a complex combination of forcing functions of diverse types and of very distinct time scales, and exhibit slow (latent) and fast-varying (active) state variables.

Until now, multirate Runge-Kutta methods were only used to obtain the numerical solution of univariate initial value problems (transient electronic circuit simulation in the one-dimensional time) [12]-[14], [22], [23]. Here, we will make use of them in a bivariate framework. As we will see in the next sections, in the technique addressed in this chapter we will consider a multirate scheme (different time-step integration sizes to state variables that present significantly disparate rates of change) coupled with a multirate excitation regime (multiple time-scale representations). This way, we managed to first efficiently resolve strongly nonlinear circuits excited by forcing functions of very distinct time scales using multiple time variables, and then dramatically reduce the simulation time attributing different time steps to the slowly varying (latent) and fast-varying (active) state variables. In addition, the use of a warped time domain will also allow the accommodation of the phase modulated RF carrier of the polar transmitter PA used in Section 4.3

for illustration of the method. Indeed, the adopted circuit simulation case study - a wireless transmitter based on the modern polar architectures - shows how the benefits of this novel simulation technique can be felt in today's RF circuits of unarguable practical interest.

4.2 Innovative Simulation Method

4.2.1 Bivariate Warped Time Formulation

The method proposed in this chapter is especially conceived for circuits operating in a periodic fast time scale and an aperiodic slow time scale. This way, in order to exploit the bivariate nature of the circuits' operation, a bi-dimensional time framework will be used. However, we will not make use of the straightforward bivariate formulation described by the multitime partial differential algebraic system of (3.31). It is so because the case study that will be presented in Section 4.3 has a mixture of diverse types of periodic and aperiodic stimuli (baseband signals, RF carrier, digital clock, pulse-width modulation signals and PM signals). As explained in Chapter 3, PM signals are not compact in the simple bivariate representation of (3.31). As seen, bivariate forms of PM/FM signals have many fluctuations (i.e., high frequency components), which is the reason why they cannot be sampled efficiently on a basic two-dimensional grid. Thus, the direct application of the straightforward multiple time approach is not well suited to analyze our illustrative application example (the polar transmitter PA).

Taking the above into account, we will make use of the concept of warped time within the bivariate formulation. As seen, the employment of this technique dynamically rescales (warps) the fast time axis to considerably reduce the number of fluctuations of the PM signals. In this case we will adopt the procedure described in Section 3.6, i.e., we will replace t by $\tau_1 = t$ in the slowly varying parts of the expressions of the excitation, $\boldsymbol{x}(t)$, and the solution, $\boldsymbol{y}(t)$, and we will substitute t by $\tau_2 = \phi(t)$ (the so-called warped time), in their fast-varying parts. In this context the original univariate DAE system of (2.1) describing the circuit's operation will be converted into the WaMPDAE system of (3.54), i..e,

$$\boldsymbol{p}\left[\hat{\boldsymbol{y}}(\tau_1,\tau_2)\right] + \frac{\partial \boldsymbol{q}\left[\hat{\boldsymbol{y}}(\tau_1,\tau_2)\right]}{\partial \tau_1} + \omega(\tau_1)\frac{\partial \boldsymbol{q}\left[\hat{\boldsymbol{y}}(\tau_1,\tau_2)\right]}{\partial \tau_2} = \hat{\boldsymbol{x}}(\tau_1,\tau_2). \tag{4.1}$$

Once we want to obtain the solution of the circuit in some $[0, t_{Final}]$ single-time interval, we must solve (4.1) on the rectangular domain $[0, t_{Final}] \times [0, T_2]$, where T_2 is the period of the excitation and the solution in the τ_2 fast warped time scale. In view of the fact that univariate solutions are recovered from their bivariate forms by setting $\boldsymbol{y}(t) = \hat{\boldsymbol{y}}(t, \phi(t))$, according to the periodicity of the problem in the τ_2 dimension we will have here

$$\boldsymbol{y}(t) = \hat{\boldsymbol{y}}(t, \phi(t) \bmod T_2). \tag{4.2}$$

4.2.2 Envelope Transient over Shooting in a Warped Time Domain

Warped multitime based methods can efficiently simulate systems with heterogeneous forcing functions (AM sources, PM sources, etc.) of widely separated time scales and, in general, numerical computations can be performed using time-domain, frequency-domain, or hybrid (combination) methods. However, the strongly nonlinear regimes of the circuits under analysis in this chapter, and so the probable existence of waveforms of very short rise and fall times (which are extremely demanding on the number of harmonics for a convenient representation), advises the substitution of frequency-domain solvers by their time-domain rivals. In this case, we will solve (4.1) taking profit of the periodicity of the problem in the τ_2 fast time dimension using an envelope transient oriented method (the envelope transient over shooting). For that, similarly to what has been presented in Section 3.5.4, we first consider the semi-discretization of the rectangular domain $[0, t_{Final}] \times [0, T_2]$ in the τ_1 dimension according to the grid

$$0 = \tau_{1,0} < \tau_{1,1} < \cdots < \tau_{1,i-1} < \tau_{1,i} < \cdots < \tau_{1,K_1} = t_{Final}, \quad h_{1,i} = \tau_{1,i} - \tau_{1,i-1}, \tag{4.3}$$

where K_1 is the total number of steps in τ_1. Then, the derivatives of (4.1) in the τ_1 slow time scale are replaced with finite-differences approximations, so that we have for each slow time instant $\tau_{1,i}$, from $i = 1$ to $i = K_1$, the ordinary differential algebraic system

$$\boldsymbol{p}\left[\hat{\boldsymbol{y}}_i(\tau_2)\right] + \frac{\boldsymbol{q}\left[\hat{\boldsymbol{y}}_i(\tau_2)\right] - \boldsymbol{q}\left[\hat{\boldsymbol{y}}_{i-1}(\tau_2)\right]}{h_{1,i}} + \omega(\tau_{1,i}) \frac{d\boldsymbol{q}\left[\hat{\boldsymbol{y}}_i(\tau_2)\right]}{d\tau_2} = \hat{\boldsymbol{x}}_i(\tau_2), \tag{4.4}$$

where $\hat{\boldsymbol{x}}_i(\tau_2) = \hat{\boldsymbol{x}}(\tau_{1,i}, \tau_2)$ and $\hat{\boldsymbol{y}}_i(\tau_2) \simeq \hat{\boldsymbol{y}}(\tau_{1,i}, \tau_2)$, with the periodic boundary condition

$$\hat{\boldsymbol{y}}_i(0) = \hat{\boldsymbol{y}}_i(T_2). \tag{4.5}$$

For obtaining the whole solution $\hat{\boldsymbol{y}}(\tau_1, \tau_2)$ in the entire domain $[0, t_{Final}] \times [0, T_2]$ we have to solve a total of K_1 periodic boundary value problems (4.4), (4.5). Now we solve each one of these boundary value problems using the shooting method based on multirate Runge-Kutta integration.

4.2.3 Shooting Based on Multirate Runge-Kutta Integration

As seen, shooting is a procedure that consists of guessing the initial condition by comparing, and wisely updating, initial estimates after successive time-step integrations (consecutive shooting iterations). Traditionally, this initial estimate updating is achieved with Newton iteration (which is the technique that was chosen for our method), extrapolation methods [21], or, occasionally, with fixed-point iteration, and the successive time-step integrations are performed with standard initial value solvers, like Runge-Kutta methods (the most popular time-step integrators). However, although we are using here the shooting method to find the periodic solution of (4.4), (4.5), we will not make use of any traditional initial-value solver to integrate the system of (4.4) on our consecutive shooting iterations. In its place, we will utilize the modern multirate Runge-Kutta methods. We do so by splitting the set of differential algebraic equations of (4.4) into two subsets,

according to the time rates of change of its components, so that we can apply the MRK algorithms described in Section 3.2.2. Indeed, the system of (4.4) will be partitioned into the following active and latent subsystems,

$$\begin{aligned}\boldsymbol{p}_{\boldsymbol{A}}\left[\hat{\boldsymbol{y}}_{A,i}(\tau_2),\hat{\boldsymbol{y}}_{L,i}(\tau_2)\right]+\frac{\boldsymbol{q}_{\boldsymbol{A}}\left[\hat{\boldsymbol{y}}_{A,i}(\tau_2),\hat{\boldsymbol{y}}_{L,i}(\tau_2)\right]-\boldsymbol{q}_{\boldsymbol{A}}\left[\hat{\boldsymbol{y}}_{A,i-1}(\tau_2),\hat{\boldsymbol{y}}_{L,i-1}(\tau_2)\right]}{h_{1,i}}\\ +\omega(\tau_{1,i})\frac{d\boldsymbol{q}_{\boldsymbol{A}}\left[\hat{\boldsymbol{y}}_{A,i}(\tau_2),\hat{\boldsymbol{y}}_{L,i}(\tau_2)\right]}{d\tau_2}=\hat{\boldsymbol{x}}_i(\tau_2),\end{aligned} \tag{4.6}$$

$$\begin{aligned}\boldsymbol{p}_{\boldsymbol{L}}\left[\hat{\boldsymbol{y}}_{A,i}(\tau_2),\hat{\boldsymbol{y}}_{L,i}(\tau_2)\right]+\frac{\boldsymbol{q}_{\boldsymbol{L}}\left[\hat{\boldsymbol{y}}_{A,i}(\tau_2),\hat{\boldsymbol{y}}_{L,i}(\tau_2)\right]-\boldsymbol{q}_{\boldsymbol{L}}\left[\hat{\boldsymbol{y}}_{A,i-1}(\tau_2),\hat{\boldsymbol{y}}_{L,i-1}(\tau_2)\right]}{h_{1,i}}\\ +\omega(\tau_{1,i})\frac{d\boldsymbol{q}_{\boldsymbol{L}}\left[\hat{\boldsymbol{y}}_{A,i}(\tau_2),\hat{\boldsymbol{y}}_{L,i}(\tau_2)\right]}{d\tau_2}=\hat{\boldsymbol{x}}_i(\tau_2),\end{aligned} \tag{4.7}$$

where

$$\hat{\boldsymbol{y}}_i(\tau_2)=\begin{bmatrix}\hat{\boldsymbol{y}}_{A,i}(\tau_2)\\ \hat{\boldsymbol{y}}_{L,i}(\tau_2)\end{bmatrix},\quad \hat{\boldsymbol{y}}_{A,i}(\tau_2)\in\mathbb{R}^{n_A},\quad \hat{\boldsymbol{y}}_{L,i}(\tau_2)\in\mathbb{R}^{n_L},\quad n_A+n_L=n. \tag{4.8}$$

$\hat{\boldsymbol{y}}_{A,i}(\tau_2)$ is the active (fast-varying) state variable components' vector at the slow time instant $\tau_{1,i}$, and $\hat{\boldsymbol{y}}_{L,i}(\tau_2)$ is the latent (slowly varying) state variable components' vector at the same slow time instant. The active components will be integrated with a small step size h (microstep) while the latent components will be integrated with a much larger step size $H=m\cdot h$ (macrostep). By attributing different time-step sizes to the active and latent state variables within the shooting iterations, significant gains in computation speed will be obtained.

4.2.4 Active-Latent Partitioning Strategy

An algorithm capable of automatically detecting the fast-varying and the slowly varying state variables would be of great utility for a general-purpose simulator. Using embedded Runge-Kutta methods [15], error estimates, usually computed for step-size control and stiffness detection [16], may be used for this automatic classification and the consequent partition of the system into the fast and slow subsystems. Such partitioning strategy is described in detail in [22], [38] and [39], and it is particularly suitable for the transient integration of one-dimensional multirate problems, especially for circuits that have parts which change their active-latent status with time. Although it could also be used here for the partitioning of the differential algebraic system of (4.4), the bivariate nature of the circuit example under study and the particular characteristics of the RF problems considered in this chapter, dictate a different approach, which leads to a simpler and faster algorithm. This technique is explained in the following

For a general RF circuit with dynamic active-latent partition (a circuit in which the partition into active and latent sub-circuits may vary with time), we solve the periodic boundary value

problem of (4.4), (4.5) for each level $\tau_{1,i}$ of the $[0,t_{Final}]\times[0,T_2]$ rectangular domain, using a uni-rate scheme on the first shooting iteration and the multirate scheme on the subsequent shooting iterations. With this approach, we start by considering in (4.4) the same microstep *h* for all system's components. We do so by considering $m=1$ in the multirate Runge-Kutta time-step integrator, so that this method degenerates into a standard Runge-Kutta method. We then split the differential algebraic system according to the variations in its components' time derivatives. Each component that practically evidences no variations in its time derivatives for the entire line $\tau_{1,i}\times[0,T_2]$, i.e., each component that satisfies the condition

$$\max\left(slope_j\right)-\min\left(slope_j\right)<Tol, \tag{4.9}$$

where

$$slope_j=\left[\hat{y}_i\left(\tau_{2,j}+h\right)-\hat{y}_i\left(\tau_{2,j}\right)\right]\Big/h,\quad \tau_{2,j}\in\{0,h,2h,\ldots,T_2-h\}, \tag{4.10}$$

and *Tol* is a small prescribed deviation tolerance, will be treated as latent (slow) on the next shooting iterations. The remaining components will be treated as active (fast). All the subsequent shooting iterations on the $\tau_{1,i}$ time instant will be conducted in a multirate way. In a nonuniform grid, step sizes *h* and *H* may be chosen using any step-size control tool. In a uniform grid, they can be predefined or successively refined to achieve a desired accuracy.

In order to increase the robustness of this partitioning strategy, more than one shooting iteration with the uni-rate scheme could be considered for each level $\tau_{1,i}$. However, it obviously would lead to some efficiency reduction of the method, since its efficiency gain is essentially dependent on the number of latent components and on *m* (the number of microsteps within a macrostep).

In general, and as was just explained, the partition into fast and slow subsystems may dynamically vary with time, throughout the integration process. However, in many RF circuits this subset division is static, i.e., does not change with time. In such cases, it will be useful if the simulator can take advantage of this characteristic. It will avoid some unnecessary computational work. For example, in our RF sample application presented in Section 4.3 the active-latent partition will always remain constant along the simulation process, and so we have decided to adopt the following simpler procedure.

We start by solving (4.4), (4.5) with classical shooting for the first level $\tau_{1,i}$ of the rectangle $[0,t_{Final}]\times[0,T_2]$. As mentioned above, we do so by considering $m=1$ in the multirate Runge-Kutta time-step integrator, when integrating the system of (4.4). Then, we split this differential algebraic system according to the fluctuations of the solution in the τ_2 dimension. Each state variable that practically evidences no fluctuations in this dimension, i.e., each component that satisfies the condition that the corresponding numerical peak-to-peak value stays within a small prescribed deviation tolerance, will be treated as latent on the next K_1-1 levels. The remaining components will be treated as active.

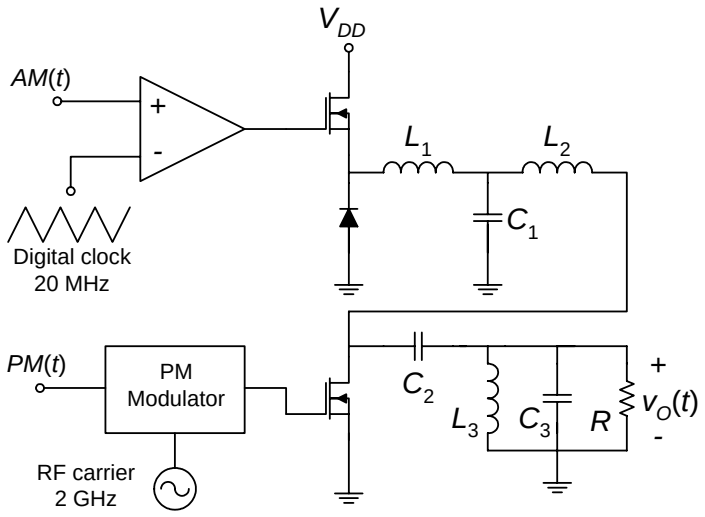

Figure 4.1 Simplified power amplifier schematic used in wireless polar transmitters.

4.3 Experimental Results

4.3.1 Illustrative Application Example

In order to test the performance and the efficiency of the method presented in the previous section, we will now discuss an illustrative application example. The nonlinear circuit of Figure 4.1 is a simplified power amplifier schematic of a wireless polar transmitter. Its most relevant components' values are V_{DD} = 25 V, L_1 = 2 μH , C_1 = 3.2 nF, L_2 = 40 nH, C_2 = 16 pF, L_3 = 0.4 nH, C_3 = 16 pF and R = 50 Ω , and the MOSFETs are represented by the following simplified nonlinear device model:

$$\begin{aligned} i_{DS}\left(v_{GS}, v_{DS}\right) &= \beta \frac{1}{2}\left[v + \ln\left(e^{v} + e^{-v}\right)\right]\tanh\left(\alpha v_{DS}\right), \\ v &= K_T\left(v_{GS} - V_T\right), \end{aligned} \tag{4.11}$$

with $\alpha = 1\ \mathrm{V}^{-1}$, $\beta = 0.25$ A/V, $K_T = 2$ and $V_T = 3$ V. Similarly, the diode current-voltage characteristic is given by

$$i_D\left(v_D\right) = I_S\left(e^{\frac{v_D}{\eta V_{Temp}}} - 1\right), \tag{4.12}$$

where I_S = 1 μA , η = 2 and V_{Temp} = 0.026 V.

This circuit includes two independent baseband excitations, the $AM(t)$ and the $PM(t)$ signals, whose bandwidth is around 2 MHz. The $AM(t)$ signal is over-sampled with a digital clock of f_0 = 20 MHz, to get a desired pulse-width modulation format, while the $PM(t)$ signal modulates the phase of a CW RF carrier of f_C = 2 GHz frequency. In order to get highly efficient power

amplification, the amplitude of the driving voltages of both MOSFETs are set so that the devices are forced to operate in the switching mode, leading this way to a strongly nonlinear problem.

As we can see, in this illustrative circuit we have a mixture of periodic (RF carrier and digital clock) and aperiodic [$AM(t)$ and $PM(t)$] forcing functions, of very distinct time scales. In addition, we will see bellow that beyond this stimuli heterogeneity we have also a combination of heterogeneous state variables (node voltages and branch currents) with widely disparate rates of variation. For instance, while the L_3 inductor current and the C_3 capacitor voltage of the output bandpass filter are very fast (and thus will be detected as active state variables), the L_1 inductor current and the C_1 capacitor voltage of the AM branch low-pass filter are both much slower (and so will be classified as latent state variables).

4.3.2 Numerical Simulation Results

To put in evidence the speedup advantage of the proposed method, we simulated the circuit in MATLAB® with the technique presented in Section 4.2 (warped bivariate envelope transient over a shooting algorithm based on multirate Runge-Kutta, MRK, schemes). We then compared its results with the corresponding warped bivariate envelope transient over classical shooting based on standard Runge-Kutta, RK, schemes of the same order. No comparison was made with any classical time-marching engine (univariate time-step integration), as SPICE, because the bivariate nature of the circuit operation would determine an unbearably large simulation time. Also, no comparison was made with any frequency-domain, or hybrid (combination) solvers, because the highly nonlinear regimes of the circuit would lead to an intolerably large number of harmonics.

Numerical computation times (in seconds) for simulations in the [0, 100 ns] and [0, 500 ns] intervals are presented in Tables 4.1 and 4.2, for explicit MRK and RK schemes of order 1 (forward Euler) and 3 (Bogacki-Shampine [7]), respectively. We processed both the 2 MHz baseband signals and the 20 MHz digital clock in the τ_1 slow time scale. The 2 GHz RF carrier was treated in the τ_2 fast warped time scale. Uniform grids were assumed, in which step length h_1 was chosen according to the time rates of change of the circuit's state variables in the τ_1 dimension and step lengths h_2 and H_2 were chosen according to the rates of variation of the active and latent components (state variables) in the τ_2 dimension. As we can attest, significant speedups were obtained with the proposed new method.

Figures 4.2 and 4.4 show the bivariate solutions for the AM branch transistor source voltage and the C_1 capacitor voltage, on the $[0,100\,\text{ns}]\times[0,T_2]$ and $[0,500\,\text{ns}]\times[0,T_2]$ rectangular domains, respectively. We chose a warped time function $\phi(t)$ so that $T_2 = 1$. These are slowly varying state variables in the one-dimensional time t (see Figures 4.3 and 4.5), which is the reason why there are no fluctuations in the fast warped time τ_2, enabling the use of a large step size in that dimension.

TABLE 4.1

COMPUTATION TIMES (COMPUTER: AMD 1.8 GHz, 700 MB RAM)

EXPLICIT RUNGE-KUTTA SCHEME OF ORDER 1

Simulation time interval	Warped bivariate envelope transient over shooting		Speedup (approx.)
	MRK based (new method)	RK based	
[0, 100 ns]	9 s	127 s	14
[0, 500 ns]	40 s	535 s	13

TABLE 4.2

COMPUTATION TIMES (COMPUTER: AMD 1.8 GHz, 700 MB RAM)

EXPLICIT RUNGE-KUTTA SCHEME OF ORDER 3

Simulation time interval	Warped bivariate envelope transient over shooting		Speedup (approx.)
	MRK based (new method)	RK based	
[0, 100 ns]	24 s	244 s	10
[0, 500 ns]	103 s	1029 s	10

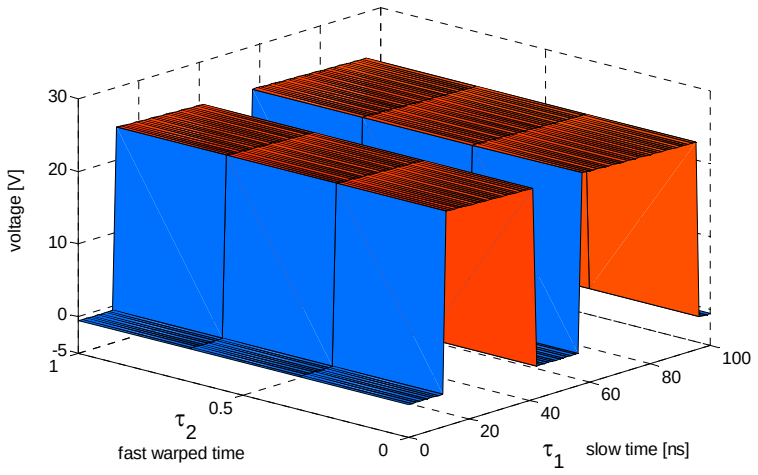

Figure 4.2 Bivariate AM branch transistor source voltage.

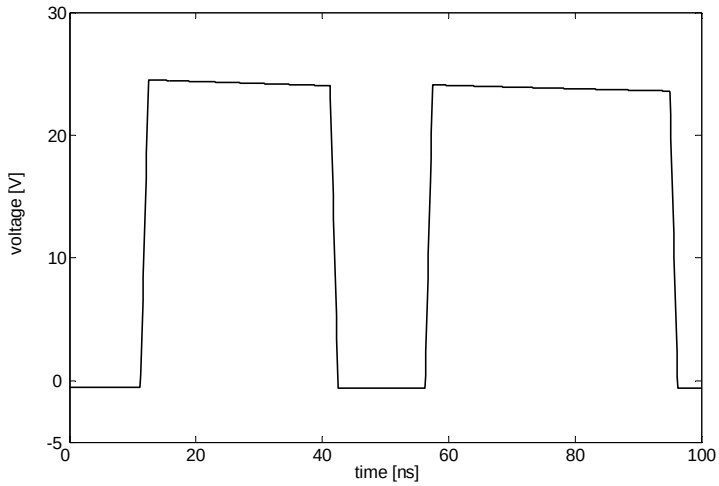

Figure 4.3 Univariate AM branch transistor source voltage in the digital clock time scale.

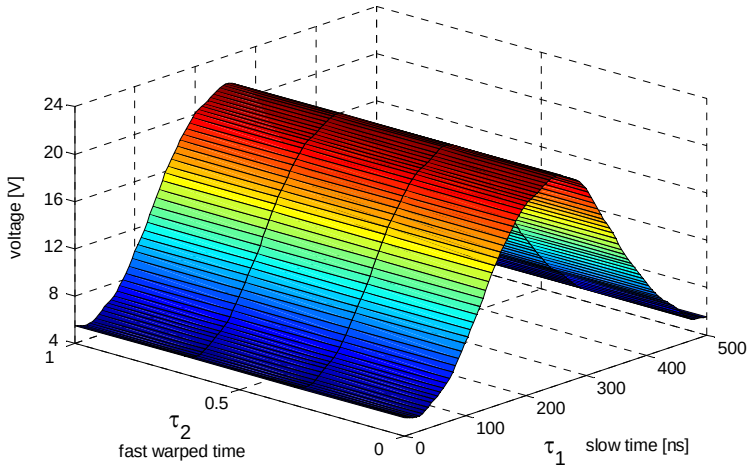

Figure 4.4 Bivariate C_1 capacitor voltage.

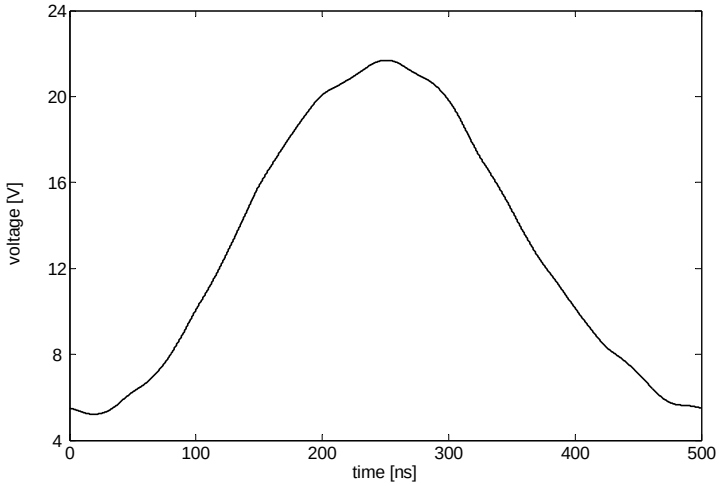

Figure 4.5 Univariate C_1 capacitor voltage in the slow envelope time scale.

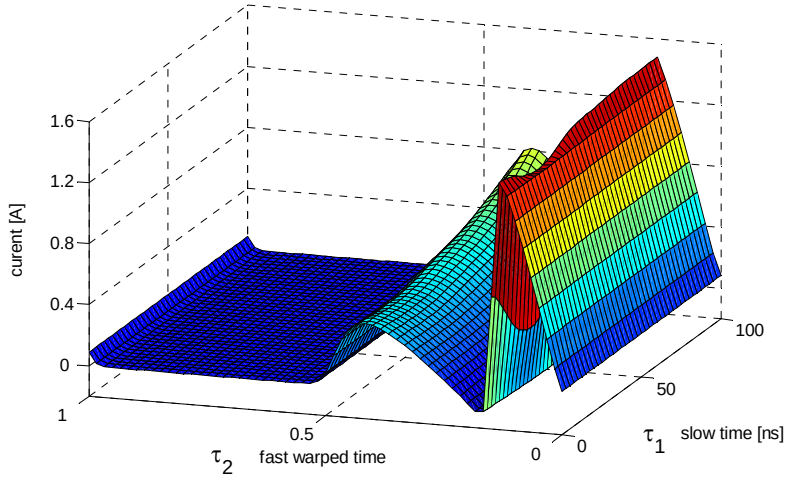

Figure 4.6 Bivariate RF transistor current.

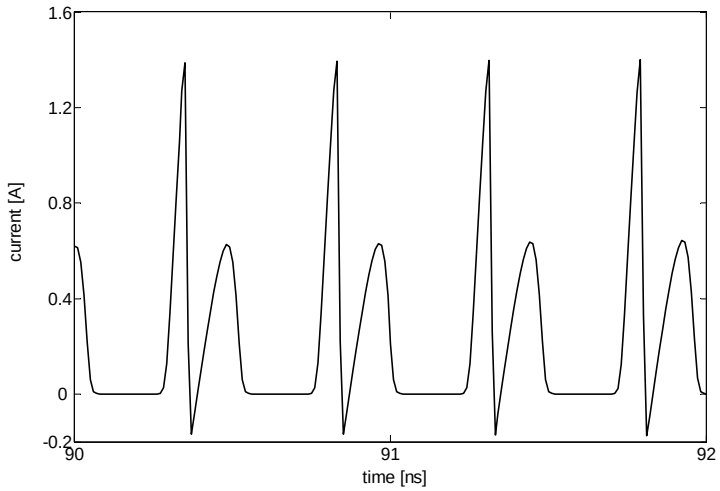

Figure 4.7 Univariate RF transistor current in the fast carrier time scale.

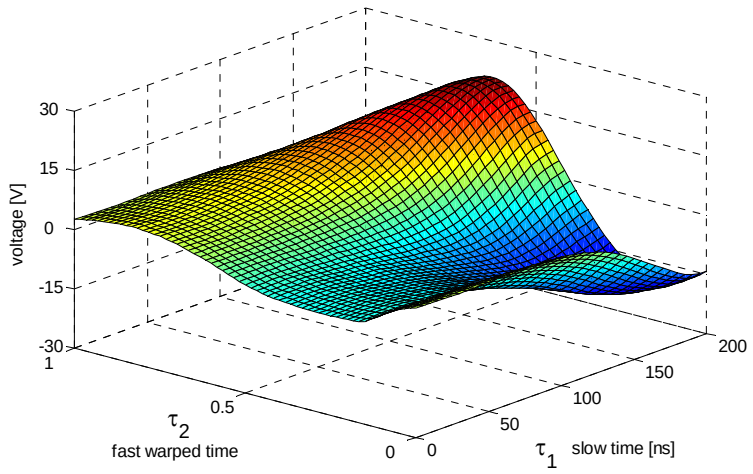

Figure 4.8 Bivariate output voltage.

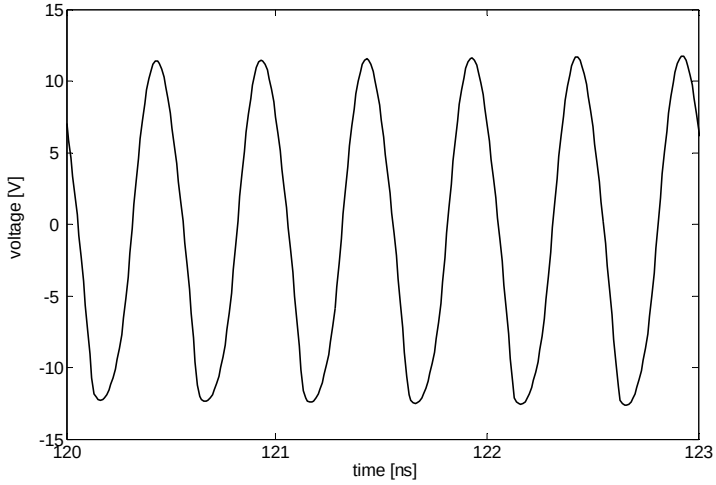

Figure 4.9 Univariate output voltage in the fast carrier time scale.

TABLE 4.3

COMPUTATION TIMES (COMPUTER: AMD 1.8 GHz, 700 MB RAM)

EXPLICIT RUNGE-KUTTA SCHEME OF ORDER 1

Simulation time interval	Conventional bivariate envelope transient over shooting		Speedup (approx.)
	MRK based (new method)	RK based (Commercial tools)	
[0, 100 ns]	13 s	160 s	12
[0, 500 ns]	98 s	1024 s	10

Figures 4.6 and 4.8 show the bivariate solutions for the RF transistor current and the output voltage of the circuit, on the $[0,100\,\text{ns}]\times[0,T_2]$ and $[0,200\,\text{ns}]\times[0,T_2]$ rectangular domains, respectively. Small step sizes were now used in both time dimensions because these are examples of fast-varying state variables, as can be concluded from their time-scaled versions plotted in Figures 4.7 and 4.9.

We have conducted several other simulations under different conditions and different time intervals, but the results were always similar to the ones presented in Tables 4.1 and 4.2. The new multirate Runge-Kutta based method always exhibited significant advantages in speed over its corresponding Runge-Kutta based classical algorithm.

Finally, for comparison, we have also considered the simulation of the circuit with the conventional (unwarped) bivariate envelope transient over shooting based on a multirate Runge-Kutta scheme, versus the corresponding unwarped envelope transient over classical shooting based on a standard Runge-Kutta scheme (the technique used by commercial RF simulators for strongly

nonlinear multirate problems operating in two widely separated time scales). The results of these simulations for the explicit MRK and RK schemes of order 1 (forward Euler) can be seen in Table 4.3. By comparing Tables 4.1 and 4.3 we can attest the efficiency provided by the warped time concept, within the envelope transient over multirate and uni-rate shooting techniques, when handling PM signals.

4.4 Conclusions

In this chapter, a new powerful time-domain simulation method, particularly suitable for heterogeneous and strongly nonlinear RF circuits, has been discussed. This new method demonstrated to be highly efficient because it uses an envelope transient technique over an innovative periodic steady-state (shooting) algorithm based on modern multirate Runge-Kutta schemes. With this innovative technique we managed to first split the one-dimensional time into two distinct time dimensions according to the multirate excitation regimes of the circuit, and then divide the circuit itself into two coupled active and latent sub-circuits composed of only slow and fast-varying state variables, respectively.

Significant reductions of the computational work were achieved, without compromising accuracy, as we simultaneously took advantage of the stimuli time-rate disparities and of the slowness of some state variables. Numerical experiments revealed very promising results, since speedups of one order of magnitude, or more, were obtained for the tested circuit example. In this sense, the presented approach offers an effective new possibility for the numerical simulation of current and upcoming RF circuits.

Chapter 5

An Efficient Multiple-Line Double Multirate Shooting Technique

5.1 Introduction

The high heterogeneity and strong nonlinearity features of some current RF networks brought a new range of challenges to circuit simulation. To cope with this, in the previous chapter we presented a powerful time-domain simulation method that was particularly suitable for such strongly nonlinear heterogeneous circuits. The proposed method revealed a high efficiency that resulted from the use of an envelope transient technique over an innovative shooting algorithm based on modern multirate Runge-Kutta (MRK) numerical integration schemes. Indeed, this gain in efficiency was mainly due to the inclusion of multirate Runge-Kutta algorithms within a 2-D warped framework, as they were conceived to take advantage of the slow variation in time of some state variables of the circuits.

The efficiency of the method reported in the previous chapter was tested in the RF polar transmitter PA illustrated in Figure 4.1, where we had a mixture of periodic (RF carrier and digital clock) and aperiodic [$AM(t)$ and $PM(t)$] forcing functions, of widely separated time scales. The $AM(t)$ and the $PM(t)$ signals were baseband excitations whose bandwidth was about 2 MHz and, while the $AM(t)$ signal was over-sampled with a digital clock of $f_0 = 20$ MHz, to get a desired pulse-width modulation format, the $PM(t)$ signal modulated the phase of a CW RF carrier of $f_C = 2$ GHz. A simplified 2-D formulation was assumed, and so we treated the digital clock and the baseband signals in the same time scale. Although we obtained good simulation speeds for the RF polar transmitter PA illustrative example, the efficiency of the method (which is dependent on the time-scale separation of the two signals) naturally degrades if the disparity between the digital clock and the baseband excitations is increased, as these have to be treated in the same time scale. In such a case, we have no choice than to consider the true problem running in three different time scales instead of running only in two time scales. To put this need in evidence, we will now consider a smaller bandwidth (200 kHz) for both baseband $AM(t)$ and $PM(t)$ signals, which will

dictate a 3-D multirate problem formulation, with a fast time scale (the RF carrier of f_C = 2 GHz), an intermediate time scale (the digital clock of f_0 = 20 MHz) and a slow time scale (the 200 kHz baseband signals). The slow time scale is aperiodic, while the intermediate and the fast time scales are both periodic.

Having the above in mind, in this chapter we will present an analytical formulation and a novel numerical method for simulating, in a very efficient way, strongly nonlinear heterogeneous RF circuits running in three different time scales. The proposed method is based on a 3-D envelope oriented technique over an innovative multiple-line double multirate shooting strategy, operating within a multidimensional warped time framework. In order to reduce the computational workload, and to turn the proposed technique into a robust simulation tool, an antistiffness strategy (which avoids numerical stiffness difficulties) and a versatile multipartitioning strategy (which allows the automatic identification and classification of the circuit's state variables according to their different rates of variation) will be included. Finally, a detailed comparison between the method addressed in this chapter and the one discussed in the previous chapter will show that there is a hidden computational efficiency compromise when the ratio between the slow and the intermediate time scales is changed.

5.2 Innovative Simulation Method

In this section, an extensive and detailed explanation of the proposed simulation method is provided. In Section 5.2.1 the mathematical problem describing the 3-D circuit operation is firstly formulated in a warped partial differential equation framework. Next, Section 5.2.2 describes the adopted envelope transient oriented formulation, which converts the 3-D problem into a set of successive 2-D bi-periodic boundary value problems, in the intermediate and fast time scales. Section 5.2.3 addresses the conventional numerical techniques that may be used to solve such boundary value problems, whereas Section 5.2.5 proposes an innovative technique, which is based on the mathematical scheme described in Section 5.2.4. Section 5.2.6 presents a double multirate strategy that significantly improves the efficiency of the method, while in Section 5.2.7 some numerical stability issues are discussed. Finally, Section 5.2.8 explains an algorithm to automatically classify the circuit's state variables according to their time rates of change.

5.2.1 Multivariate and Warped Time Formulations

Let us consider the generic system of differential algebraic equations of (2.1), describing a general nonlinear RF circuit. Since we are interested now in a case where the excitation $\boldsymbol{x}(t)$ and the state variables $\boldsymbol{y}(t)$ combine diverse type of periodic and aperiodic signals running in three distinct time scales, the system of (2.1) will be solved in a much more efficient way if $\boldsymbol{x}(t)$ and $\boldsymbol{y}(t)$ are rewritten as 3-D time-scale entities, $\hat{\boldsymbol{x}}(t_1,t_2,t_3)$ and $\hat{\boldsymbol{y}}(t_1,t_2,t_3)$. The application of this multivariate

strategy to the system of (2.1) converts it into the following multirate partial differential algebraic equations' system

$$\begin{aligned}&\boldsymbol{p}\left[\hat{\boldsymbol{y}}\left(t_1,t_2,t_3\right)\right]+\frac{\partial \boldsymbol{q}\left[\hat{\boldsymbol{y}}\left(t_1,t_2,t_3\right)\right]}{\partial t_1}\\&+\frac{\partial \boldsymbol{q}\left[\hat{\boldsymbol{y}}\left(t_1,t_2,t_3\right)\right]}{\partial t_2}+\frac{\partial \boldsymbol{q}\left[\hat{\boldsymbol{y}}\left(t_1,t_2,t_3\right)\right]}{\partial t_3}=\hat{\boldsymbol{x}}\left(t_1,t_2,t_3\right),\end{aligned} \tag{5.1}$$

which can be seen as the 3-D version of (3.33).

However, in the polar transmitter PA of Figure 4.1 we have a phase modulated carrier, which is not compact in the straightforward multivariate representation of (5.1). In consequence, similarly to what we have done in the previous chapter, we have to make use again of the concept of warped time. It is so because the multivariate forms of PM signals have many fluctuations, and thus they can not be sampled efficiently on a basic 3-D grid. As explained in detail before, by using this technique within the multivariate formulation, we dynamically rescale the fast time axis to significantly reduce the number of fluctuations of the PM signals. In this case we will adopt the following procedure: for the slowly varying parts of the expressions of $\boldsymbol{x}(t)$ and $\boldsymbol{y}(t)$ (baseband *AM*(*t*) and *PM*(*t*) time scale) t is replaced by $\tau_1 = t$; for the intermediate-varying parts (digital sampling clock and pulse-width modulated time scale) t is replaced by $\tau_2 = t$; finally, for the fast-varying parts (RF sinusoidal and PM carrier time scale), t is replaced by $\tau_3 = \phi(t)$, where $\phi(t)$ is any appropriate rescaling warped time function. In this context, we will have the warped multivariate forms $\hat{\boldsymbol{x}}\left(\tau_1,\tau_2,\tau_3\right)$ and $\hat{\boldsymbol{y}}\left(\tau_1,\tau_2,\tau_3\right)$, and the system of (5.1) will now be converted into the warped multirate partial differential algebraic equations' system

$$\begin{aligned}&\boldsymbol{p}\left[\hat{\boldsymbol{y}}\left(\tau_1,\tau_2,\tau_3\right)\right]+\frac{\partial \boldsymbol{q}\left[\hat{\boldsymbol{y}}\left(\tau_1,\tau_2,\tau_3\right)\right]}{\partial \tau_1}\\&+\frac{\partial \boldsymbol{q}\left[\hat{\boldsymbol{y}}\left(\tau_1,\tau_2,\tau_3\right)\right]}{\partial \tau_2}+\omega\left(\tau_1\right)\frac{\partial \boldsymbol{q}\left[\hat{\boldsymbol{y}}\left(\tau_1,\tau_2,\tau_3\right)\right]}{\partial \tau_3}\\&=\hat{\boldsymbol{x}}\left(\tau_1,\tau_2,\tau_3\right),\end{aligned} \tag{5.2}$$

where $\omega(t) = d\phi(t)/dt$.

In the same way as we mentioned in Section 3.6, it is easy to show that if $\hat{\boldsymbol{x}}\left(\tau_1,\tau_2,\tau_3\right)$ and $\hat{\boldsymbol{y}}\left(\tau_1,\tau_2,\tau_3\right)$ satisfy (5.2), then the univariate forms $\boldsymbol{x}(t) = \hat{\boldsymbol{x}}\left(t,t,\phi(t)\right)$ and $\boldsymbol{y}(t) = \hat{\boldsymbol{y}}\left(t,t,\phi(t)\right)$ satisfy (2.1) [35]. Consequently, the univariate solutions of (2.1) are available on paths of parametric equations $\tau_1 = t$, $\tau_2 = t$, $\tau_3 = \phi(t)$, along the multivariate solutions $\hat{\boldsymbol{y}}\left(\tau_1,\tau_2,\tau_3\right)$ in the τ_1,τ_2,τ_3 space. Since now we will have periodicity in the τ_2 and τ_3 dimensions, and thus an enclosed domain in those time axes, the original univariate solution will be recovered from its multivariate form by setting

$$\boldsymbol{y}(t) = \hat{\boldsymbol{y}}\left(t, t \bmod T_2, \phi(t) \bmod T_3\right), \tag{5.3}$$

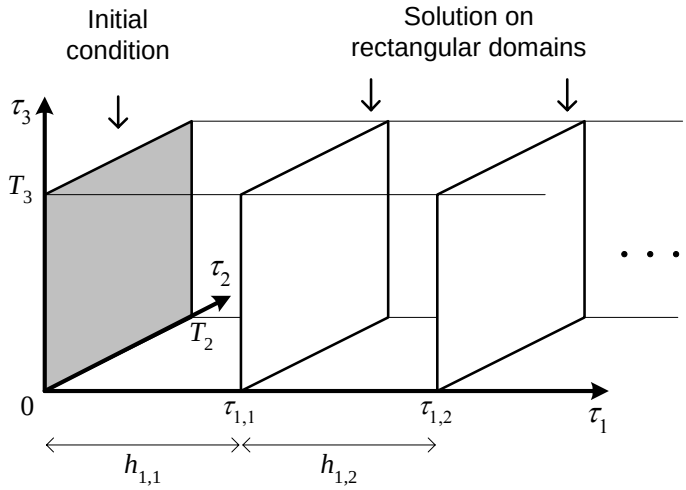

Figure 5.1 Rectangular domains in the 3-D warped space.

where T_2 and T_3 are the period of the excitation and the solution in the τ_2 and τ_3 dimensions, respectively.

5.2.2 3-D Envelope Transient Oriented Technique

Let us consider again the polar transmitter PA presented in Figure 4.1. As stated above, the τ_1, τ_2 and τ_3 dimensions of this circuit will be, respectively, the slow baseband time scale, the digital clock intermediate time scale and the fast carrier warped time scale. Taking this into account we will solve (5.2) exploiting the periodicity of the problem in the τ_2 and τ_3 dimensions. Indeed, by using a 3-D envelope transient oriented technique, we replace each derivative of (5.2) in the τ_1 dimension (the aperiodic baseband slow time scale) with a finite-differences approximation, to obtain, for each time instant $\tau_{1,i}$, the partial differential algebraic system

$$\begin{aligned} &\boldsymbol{p}\left[\hat{\boldsymbol{y}}_i\left(\tau_2,\tau_3\right)\right]+\frac{\boldsymbol{q}\left[\hat{\boldsymbol{y}}_i\left(\tau_2,\tau_3\right)\right]-\boldsymbol{q}\left[\hat{\boldsymbol{y}}_{i-1}\left(\tau_2,\tau_3\right)\right]}{h_{1,i}} \\ &+\frac{\partial \boldsymbol{q}\left[\hat{\boldsymbol{y}}_i\left(\tau_2,\tau_3\right)\right]}{\partial \tau_2}+\omega\left(\tau_{1,i}\right)\frac{\partial \boldsymbol{q}\left[\hat{\boldsymbol{y}}_i\left(\tau_2,\tau_3\right)\right]}{\partial \tau_3}=\hat{\boldsymbol{x}}_i\left(\tau_2,\tau_3\right), \end{aligned} \tag{5.4}$$

where $\hat{\boldsymbol{x}}_i\left(\tau_2,\tau_3\right)=\hat{\boldsymbol{x}}\left(\tau_{1,i},\tau_2,\tau_3\right)$, $\hat{\boldsymbol{y}}_i\left(\tau_2,\tau_3\right)\simeq\hat{\boldsymbol{y}}\left(\tau_{1,i},\tau_2,\tau_3\right)$, and $h_{1,i}=\tau_{1,i}-\tau_{1,i-1}$, with the bi-periodic boundary conditions

$$\begin{aligned} \hat{\boldsymbol{y}}_i\left(0,\tau_3\right)&=\hat{\boldsymbol{y}}_i\left(T_2,\tau_3\right), \\ \hat{\boldsymbol{y}}_i\left(\tau_2,0\right)&=\hat{\boldsymbol{y}}_i\left(\tau_2,T_3\right), \end{aligned} \tag{5.5}$$

on the rectangle $\tau_{1,i}\times\left[0,T_2\right]\times\left[0,T_3\right]$. In other words, we start with some initial condition for $\tau_1=0$ and then solve a set of 2-D boundary value problems with periodic boundary conditions in both τ_2 and τ_3 dimensions. This is illustrated in Figure 5.1.

5.2.3 2-D Bi-Periodic Boundary Value Problems

Let us now focus in the 2-D bi-periodic boundary value problems of (5.4), (5.5), defined on the rectangular regions $[0,T_2]\times[0,T_3]$ for each of the successive slow time instants $\tau_{1,i}$. As seen in Section 3.5.4, the conventional numerical techniques that may be used for solving a bi-periodic boundary value problem defined on a rectangular region of a 2-D space are: 2-D harmonic balance, MFDTD and hierarchical shooting.

The first one, 2-D harmonic balance, should be avoided here because it is not suitable for representing waveforms produced under strongly nonlinear regimes in wideband circuits. In particular, the switching behavior of the AM power-supply modulator of our illustrative application example of Figure 4.1 generates waveforms of very short rise and fall times, which are extremely demanding on the number of harmonics for a convenient frequency-domain representation.

The MFDTD is a technique that, if applied to (5.4), (5.5), consists in defining a time grid in both τ_2 and τ_3 dimensions,

$$0=\tau_{2,0}<\tau_{2,1}<\cdots<\tau_{2,j-1}<\tau_{2,j}<\cdots<\tau_{2,K_2}=T_2,\quad h_{2,j}=\tau_{2,j}-\tau_{2,j-1}, \tag{5.6}$$

$$0=\tau_{3,0}<\tau_{3,1}<\cdots<\tau_{3,k-1}<\tau_{3,k}<\cdots<\tau_{3,K_3}=T_3,\quad h_{3,k}=\tau_{3,k}-\tau_{3,k-1}, \tag{5.7}$$

of the rectangular domain $[0,T_2]\times[0,T_3]$, to then impose a finite-differences discretization of (5.4) in τ_2 and τ_3. As explained, this technique will convert the *n* state variables partial differential algebraic system of (5.4) into a nonlinear system of $n\times K_2\times K_3$ algebraic equations, where K_2+1 and K_3+1 are the number of grid points in the τ_2 and τ_3 dimensions, respectively. In order to solve the nonlinear algebraic system, a $n\times K_2\times K_3$-dimensional Newton-Raphson iterative solver is required, and, consequently, the amount of storage needed will be extremely large. As explained before, this is the main reason that has prevented the use of MFDTD in general-purpose simulators.

Hierarchical shooting is thus the most suitable technique to solve (5.4), (5.5). As stated in Section 3.5.4, the main advantage of hierarchical shooting over MFDTD is that the amount of storage required is much smaller. In this case, hierarchical shooting consists in performing shooting in one dimension, say τ_3, nested in the other dimension, τ_2. This means that, by considering the semi-discretization of the $[0,T_2]\times[0,T_3]$ rectangular domain defined by (5.6), first we have to go through successive shooting iterations for each one of the consecutive vertical lines $\tau_{2,j},\tau_3$ (inner loop), starting from $\tau_{2,0},\tau_3$ until τ_{2,K_2},τ_3. Then, we have to compare and update the initial solution on the left side of the rectangle, according to the solution obtained on the right side, to then repeat the vertical line shooting process all over the domain, until a bi-periodic solution is achieved (outer loop). This is illustrated in Figure 5.2(a).

In the following sub-sections we will propose an innovative multiple-line shooting strategy that solves the (5.4), (5.5) 2-D bi-periodic boundary value problems in a much more efficient way than the hierarchical shooting technique. This multiple-line shooting strategy is based on the mathematical method of lines [62], and, as we will see, it requires only one shooting loop.

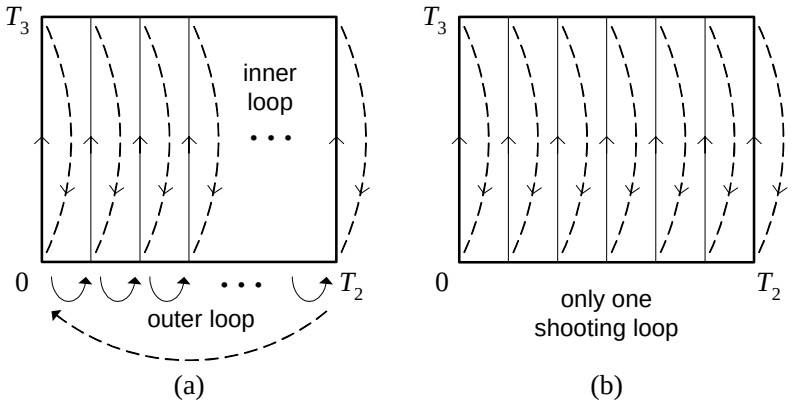

Figure 5.2 Shooting strategies: (a) hierarchical shooting and (b) multiple-line shooting.

Furthermore, it will allow us to take advantage of the latency of some state variables in τ_2, in τ_3, or in both dimensions.

5.2.4 The Method of Lines

The method of lines is a mathematical scheme that can be used for obtaining the solution of bivariate problems described by partial differential equations. By discretizing the corresponding bi-dimensional domains in only one dimension, this method converts the partial differential equations in ordinary differential systems. Then, these can then be time-step integrated with any appropriate initial value solver (e.g. Runge-Kutta).

For explaining the method, let us consider the simple example described in the following. For simplicity, let us suppose that, instead of the bi-periodic boundary value problem of (5.4), (5.5), we have a n state variables initial-boundary-value problem, which is defined on the same $[0,T_2]\times[0,T_3]$ rectangular domain by the partial differential equations' system

$$\frac{\partial \hat{\boldsymbol{y}}(\tau_2,\tau_3)}{\partial \tau_2}+\frac{\partial \hat{\boldsymbol{y}}(\tau_2,\tau_3)}{\partial \tau_3}=\boldsymbol{f}\left[\tau_2,\tau_3,\hat{\boldsymbol{y}}(\tau_2,\tau_3)\right], \tag{5.8}$$

the periodic boundary value condition for τ_2 only

$$\hat{\boldsymbol{y}}(0,\tau_3)=\hat{\boldsymbol{y}}(T_2,\tau_3), \tag{5.9}$$

and the initial condition for time τ_3

$$\hat{\boldsymbol{y}}(\tau_2,0)=\boldsymbol{g}(\tau_2), \tag{5.10}$$

where $\boldsymbol{f}$ and $\boldsymbol{g}$ are known functions. If we discretize the τ_2 time axis according to (5.6), and replace the derivatives of (5.8) in τ_2 with a finite-differences approximation, we obtain a system of $n\times K_2$ ordinary differential equations in τ_3

$$\frac{\hat{\boldsymbol{y}}_j(\tau_3)-\hat{\boldsymbol{y}}_{j-1}(\tau_3)}{h_{2,j}}+\frac{d\hat{\boldsymbol{y}}_j(\tau_3)}{d\tau_3}=\boldsymbol{f}\left[\tau_{2,j},\tau_3,\hat{\boldsymbol{y}}_j(\tau_3)\right], \qquad j=1,\ldots,K_2, \tag{5.11}$$

where $\hat{\boldsymbol{y}}_j(\tau_3)\simeq\hat{\boldsymbol{y}}(\tau_{2,j},\tau_3)$ are the unknowns. Finally, and according to the periodic boundary condition $\hat{\boldsymbol{y}}_0(\tau_3)=\hat{\boldsymbol{y}}_{K_2}(\tau_3)$, the system of (5.11) can be rewritten in the classical initial-value form

$$\begin{aligned}
\frac{d\hat{\boldsymbol{y}}_1(\tau_3)}{d\tau_3}&=\boldsymbol{f}\left[\tau_{2,1},\tau_3,\hat{\boldsymbol{y}}_1(\tau_3)\right]-\frac{\hat{\boldsymbol{y}}_1(\tau_3)-\hat{\boldsymbol{y}}_{K_2}(\tau_3)}{h_{2,j}}\\
\frac{d\hat{\boldsymbol{y}}_2(\tau_3)}{d\tau_3}&=\boldsymbol{f}\left[\tau_{2,2},\tau_3,\hat{\boldsymbol{y}}_2(\tau_3)\right]-\frac{\hat{\boldsymbol{y}}_2(\tau_3)-\hat{\boldsymbol{y}}_1(\tau_3)}{h_{2,j}}\\
&\vdots\\
\frac{d\hat{\boldsymbol{y}}_{K_2}(\tau_3)}{d\tau_3}&=\boldsymbol{f}\left[\tau_{2,K_2},\tau_3,\hat{\boldsymbol{y}}_{K_2}(\tau_3)\right]-\frac{\hat{\boldsymbol{y}}_{K_2}(\tau_3)-\hat{\boldsymbol{y}}_{K_2-1}(\tau_3)}{h_{2,j}}
\end{aligned} \tag{5.12}$$

and then be time-step integrated with an initial value solver.

5.2.5 Multiple-Line Shooting Technique

Let us now return to our problem so that we use the method of lines embedded in a shooting technique, when solving the 2-D bi-periodic boundary value problems of (5.4), (5.5).

Let us consider the system of (5.4) with n state variables, and let us also consider the semi-discretization of the rectangular domain $[0,T_2]\times[0,T_3]$ in the τ_2 dimension defined by (5.6). By using a finite-differences scheme to approximate the derivatives of (5.4) in the τ_2 dimension, we can obtain a set of $n\times K_2$ ordinary differential algebraic equations in τ_3

$$\begin{aligned}
\boldsymbol{p}\left[\hat{\boldsymbol{y}}_{i,j}(\tau_3)\right]+\frac{\boldsymbol{q}\left[\hat{\boldsymbol{y}}_{i,j}(\tau_3)\right]-\boldsymbol{q}\left[\hat{\boldsymbol{y}}_{i-1,j}(\tau_3)\right]}{h_{1,i}}+\frac{\boldsymbol{q}\left[\hat{\boldsymbol{y}}_{i,j}(\tau_3)\right]-\boldsymbol{q}\left[\hat{\boldsymbol{y}}_{i,j-1}(\tau_3)\right]}{h_{2,j}}\\
+\omega(\tau_{1,i})\frac{d\boldsymbol{q}\left[\hat{\boldsymbol{y}}_{i,j}(\tau_3)\right]}{d\tau_3}=\hat{\boldsymbol{x}}_{i,j}(\tau_3),\\
j=1,2,\ldots,K_2,\qquad \hat{\boldsymbol{y}}_{i,0}(\tau_3)=\hat{\boldsymbol{y}}_{i,K_2}(\tau_3),
\end{aligned} \tag{5.13}$$

where $\hat{\boldsymbol{x}}_{i,j}(\tau_3)=\hat{\boldsymbol{x}}(\tau_{1,i},\tau_{2,j},\tau_3)$ and $\hat{\boldsymbol{y}}_{i,j}(\tau_3)\simeq\hat{\boldsymbol{y}}(\tau_{1,i},\tau_{2,j},\tau_3)$. The method of lines applied to the system of (5.4) consists in time-step integrating the whole system of (5.13) with an appropriate initial value solver (e.g. Runge-Kutta). Then, if we want to do shooting, we have to look only at the solution $\hat{\boldsymbol{y}}_{i,j}(T_3)$ on the top of the rectangle $[0,T_2]\times[0,T_3]$, to then wisely update the initial solution on the bottom, $\hat{\boldsymbol{y}}_{i,j}(0)$, until the second condition of (5.5) is satisfied. It must be noted that, by taking into account $\hat{\boldsymbol{y}}_{i,0}=\hat{\boldsymbol{y}}_{i,K_2}$ in (5.13), the first periodic boundary condition of (5.5) will be automatically satisfied. So, contrary to the hierarchical shooting technique, there is only one loop in this multiple-line shooting strategy [please compare Figure 5.2(a) and (b)]. Consequently,

due to the reduced number of shooting iterations required, the final bi-periodic solution of (5.4), (5.5) is achieved faster.

5.2.6 Double Multirate Approach

The polar transmitter PA example presented in Figure 4.1 is a highly heterogeneous nonlinear RF multirate circuit, whose state variables evolve according to different time scales. For that reason, when this circuit is described by the warped multirate system of (5.2) some of its components (state variables) practically evidence no fluctuations in the τ_2 dimension (the digital clock time scale), while others have no fluctuations in the τ_3 dimension (the carrier time scale). The innovative multiple-line shooting technique proposed in this study will allow us to take advantage of this double latency, when solving each one of the (5.4), (5.5) 2-D bi-periodic boundary value problems.

First, since when shooting on $[0,T_2]\times[0,T_3]$ we have to time-step integrate (5.13) in the τ_3 dimension, instead of using standard Runge-Kutta solvers we can use modern multirate Runge-Kutta (MRK) schemes. With these methods, we can apply a large time-step size H_3 (macrostep) to the components that have no fluctuations in the τ_3 dimension and a small step size h_3 (microstep) to the remaining components [please compare Figure 5.3(a) and (b)]. As shown in the previous chapter, this multirate technique significantly reduces the simulation time.

Next, because we have components that evidence no fluctuations in the τ_2 dimension, instead of considering a fine grid in (5.6), we can use a coarse grid with large grid spacing H_2 [please compare Figure 5.3(a) and (c)]. This will considerably reduce the number of equations in (5.13) and will prevent a lot of unnecessary computational work. So, it will further reduce the required simulation time.

Finally, for components that show no fluctuations in τ_2 or τ_3, we can use a coarse grid in both dimensions [please see Figure 5.3(d)].

5.2.7 Antistiffness Strategy

Shooting is an iterative procedure that consists in executing successive time-step integrations with an initial value solver. When these consecutive integrations are performed, stiffness may occur. *Stiffness* [16] is a phenomenon that takes place when numerical stability requirements, rather than those of accuracy, constrain the time-step integration size. In other words, if an initial value solver, with a certain finite region of stability [16] - employed to solve a differential system with some initial conditions - is forced to use a time-step length which is excessively small in relation to the smoothness of the exact solution, the problem is said to be *stiff*.

In order to avoid severely small time steps, implicit schemes [15], [16], [24] (which are more stable but more computationally expensive than their explicit rivals) must be used. Thus, for guaranteeing simulation efficiency, our aim here is not to cope with stiffness, but to prevent its occurrence. To achieve clarity in the explanation of our antistiffness strategy, let us consider the

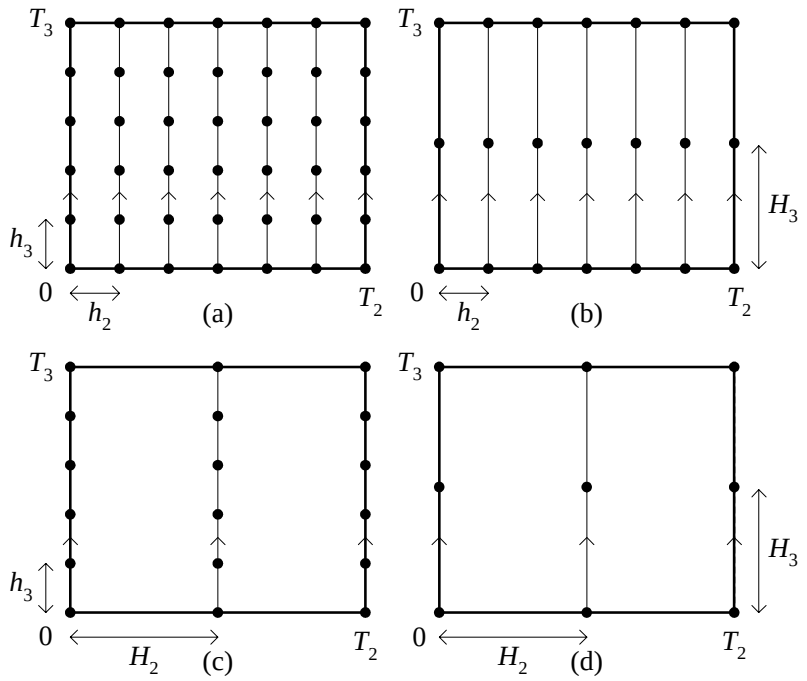

Figure 5.3 Double multirate uniform time grids to be used in the multiple-line shooting technique: (a) microsteps in τ_3 with a fine grid in τ_2, (b) macrosteps in τ_3 with a fine grid in τ_2, (c) microsteps in τ_3 with a coarse grid in τ_2 and (d) macrosteps in τ_3 with a coarse grid in τ_2.

basic n state variables 2-D bi-periodic boundary value problem defined on the enclosed region $[0,T_2]\times[0,T_3]$ of τ_2,τ_3 space by the system of (5.8) and the following periodic boundary value conditions

$$\begin{aligned}\hat{\boldsymbol{y}}(\tau_2,0)&=\hat{\boldsymbol{y}}(\tau_2,T_3),\\ \hat{\boldsymbol{y}}(0,\tau_3)&=\hat{\boldsymbol{y}}(T_2,\tau_3).\end{aligned}\tag{5.14}$$

Suppose that we want to obtain the bi-periodic numerical solution to this problem, using the multiple-line shooting technique described above. Obviously, there are two possible distinct ways to do it: we can semi-discretize the problem in τ_2 and use the method of lines to time-step integrate it in τ_3, or, conversely, we can semi-discretize the problem in τ_3 and time-step integrate it in τ_2. Apparently, there is no difference between these two choices, if we consider the same number of grid points, K, for both τ_2 and τ_3 dimensions on $[0,T_2]\times[0,T_3]$. In fact, they seem to lead to the same computational work, i.e., the same efficiency. However, this is not true if the τ_2 and τ_3 time scales are widely separated. Actually, in such situations there is a huge difference between the two choices. Since τ_2 is the slowest time scale and τ_3 is the fastest, the former choice will lead us to a nonstiff problem, while the latter will lead us to a stiff problem [please see Figure 5.4(a) and (b)].

A measure of stiffness of a differential system is the ratio $\left|\mathrm{Re}\,\bar{\lambda}\right|/\left|\mathrm{Re}\,\underline{\lambda}\right|$, where $\bar{\lambda}$ and $\underline{\lambda}$ are the eigenvalues of the corresponding Jacobian matrix, with the largest and the smallest real part absolute values, respectively. If this stiffness ratio is small (typically less than 20) then the problem

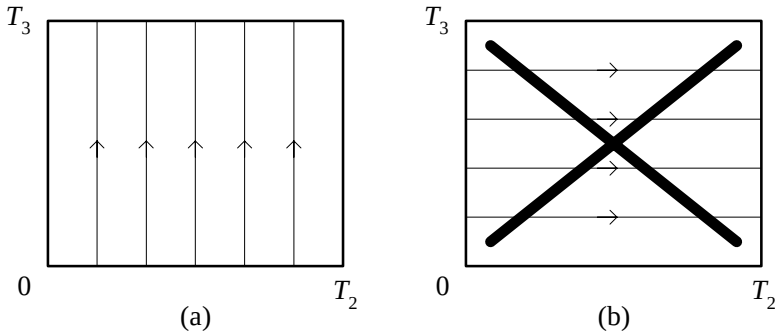

Figure 5.4 Antistiffness strategy: (a) right choice (b) wrong choice.

is said to be *nonstiff*. Stiffness arises when this ratio is large. In this case, when shooting with the method of lines for solving the basic illustrative 2-D bi-periodic boundary value problem defined by (5.8) and (5.14), we have to integrate a system of the form of (5.12). The Jacobian matrix of such system will have the block structure

$$\boldsymbol{J} = \begin{bmatrix} \boldsymbol{D}_1 & & & \boldsymbol{L} \\ \boldsymbol{L} & \boldsymbol{D}_2 & & \\ & \ddots & \ddots & \\ & & \boldsymbol{L} & \boldsymbol{D}_K \end{bmatrix} \tag{5.15}$$

where the blocks $\boldsymbol{D}_i$ and $\boldsymbol{L}$ are themselves $n \times n$ matrices. If we discretize the problem in τ_2 and time-step integrate it in τ_3 (first choice), then we will have

$$\boldsymbol{D}_i = \frac{d\boldsymbol{f}_i}{d\hat{\boldsymbol{y}}_i} - \frac{\boldsymbol{I}}{h_2}, \qquad \boldsymbol{L} = \frac{\boldsymbol{I}}{h_2}, \tag{5.16}$$

with $\boldsymbol{I}$ the $n \times n$ identity matrix. Otherwise, if we discretize the problem in τ_3 and time-step integrate it in τ_2 (second choice), we will have

$$\boldsymbol{D}_i = \frac{d\boldsymbol{f}_i}{d\hat{\boldsymbol{y}}_i} - \frac{\boldsymbol{I}}{h_3}, \qquad \boldsymbol{L} = \frac{\boldsymbol{I}}{h_3}. \tag{5.17}$$

Now, we must note that if, for simplicity, a uniform grid of K points is assumed for both the τ_2 and τ_3 dimensions, since τ_2 is the slowest time scale and τ_3 is the fastest, the value of the step length $h_2 = T_2/K$ will be much larger than $h_3 = T_3/K$. This will imply that, independently of $\boldsymbol{f}$ in (5.8), the Jacobian matrix (5.15) is such that the stiffness ratio will be much smaller in the first choice than in the second. For instance, numerical experiments obtained when performing the simulation of the polar transmitter PA of Figure 4.1 revealed stiffness ratios lesser than one order of magnitude for the first choice (discretization in τ_2 and time-step integration in τ_3), and of more than two or three orders of magnitude for the second choice (discretization in τ_3 and time-step integration in τ_2). This means that numerical stability requirements will severely constrain the time-step integration size if we opt for the second alternative (stiff problem). That is, $h_2 = T_2/K$

will be dramatically large to be considered as the appropriate time-step size, unless an implicit scheme with a large stability region [16], [24] (more stable but also more expensive) is used to perform the successive time-step integrations.

In conclusion, if we want to avoid stiff scenarios and strong numerical instability when solving a 2-D bi-periodic boundary value problem with the multiple-line shooting technique, first, we must semi-discretize the rectangular region in the slowest time dimension to then perform time-step integration in the faster time axis.

5.2.8 Multipartitioning Strategy

A time-domain simulation package using the innovative multiple-line double multirate shooting technique presented in this chapter would not be useful if an algorithm able to automatically classify the circuit's state variables (according to their time-rates of change) was not included. In fact, this classification is imperative because we want to split the circuit into several sub-circuits, to benefit from the multirate strategies presented above. In the same way as we have proposed for the method discussed in the previous chapter, we will now suggest a circuit partitioning strategy with two distinct variants. The former is conceived for RF circuits with dynamic subset division (circuits in which the partition into sub-circuits may vary with time), and the later is tailored for RF circuits with static subset division (circuits in which the partition does not change along the simulation process). These strategy variants are described in detail the following.

For a general RF circuit with dynamic active-latent partition, we solve the 2-D bi-periodic boundary value problem (5.4), (5.5) defined on the rectangle $[0,T_2]\times[0,T_3]$ at each slow time instant $\tau_{1,i}$, using a purely uni-rate scheme on the first multiple-line shooting iteration and a double multirate scheme on the subsequent iterations. With this methodology we start by considering the same small time-step lengths h_2 and h_3 for all system's components, i.e., we start by treating all the n circuit's state variables in the same way. We do so by considering $H_3 = h_3$ in the multirate Runge-Kutta integrator (so that this method degenerates into a standard uni-rate Runge-Kutta method), and by considering the same fine grid (5.6), i.e., the same number of shooting lines for all system's components. We then split the system in several subsystems according to the fluctuations of its components in τ_2 and according to the variations of its time derivatives in τ_3. Components that practically evidence no fluctuations in the τ_2 dimension, i.e., components that satisfy the condition that the corresponding numerical peak-to-peak value stays within a small prescribed deviation tolerance are classified as "latent in τ_2". These are represented with a coarse grid in (5.6), i.e., we utilize only a few shooting lines on the subsequent shooting iterations. The remaining components are classified as "active in τ_2", which means that we consider a fine grid in (5.6). Components that practically evidence no variations in their τ_3 time derivatives are classified as "latent in τ_3" and will be integrated with a large macrostep H_3 on the next shooting iterations. In opposition, components that exhibit variations in their derivatives are classified as "active in τ_3"

and are integrated with a microstep h_3. According to these 2-D partitioning criteria we have a total of four possible classifications, which indicates that the warped multirate system of (5.2) can be seen as the following four subsystems set,

$$\begin{aligned}
&\boldsymbol{p}_{AA}\left[\hat{\boldsymbol{y}}\right]+\frac{\partial \boldsymbol{q}_{AA}\left[\hat{\boldsymbol{y}}\right]}{\partial \tau_1}+\frac{\partial \boldsymbol{q}_{AA}\left[\hat{\boldsymbol{y}}\right]}{\partial \tau_2}+\omega\left(\tau_1\right)\frac{\partial \boldsymbol{q}_{AA}\left[\hat{\boldsymbol{y}}\right]}{\partial \tau_3}=\hat{\boldsymbol{x}}\\
&\boldsymbol{p}_{AL}\left[\hat{\boldsymbol{y}}\right]+\frac{\partial \boldsymbol{q}_{AL}\left[\hat{\boldsymbol{y}}\right]}{\partial \tau_1}+\frac{\partial \boldsymbol{q}_{AL}\left[\hat{\boldsymbol{y}}\right]}{\partial \tau_2}+\omega\left(\tau_1\right)\frac{\partial \boldsymbol{q}_{AL}\left[\hat{\boldsymbol{y}}\right]}{\partial \tau_3}=\hat{\boldsymbol{x}}\\
&\boldsymbol{p}_{LA}\left[\hat{\boldsymbol{y}}\right]+\frac{\partial \boldsymbol{q}_{LA}\left[\hat{\boldsymbol{y}}\right]}{\partial \tau_1}+\frac{\partial \boldsymbol{q}_{LA}\left[\hat{\boldsymbol{y}}\right]}{\partial \tau_2}+\omega\left(\tau_1\right)\frac{\partial \boldsymbol{q}_{LA}\left[\hat{\boldsymbol{y}}\right]}{\partial \tau_3}=\hat{\boldsymbol{x}}\\
&\boldsymbol{p}_{LL}\left[\hat{\boldsymbol{y}}\right]+\frac{\partial \boldsymbol{q}_{LL}\left[\hat{\boldsymbol{y}}\right]}{\partial \tau_1}+\frac{\partial \boldsymbol{q}_{LL}\left[\hat{\boldsymbol{y}}\right]}{\partial \tau_2}+\omega\left(\tau_1\right)\frac{\partial \boldsymbol{q}_{LL}\left[\hat{\boldsymbol{y}}\right]}{\partial \tau_3}=\hat{\boldsymbol{x}}
\end{aligned} \tag{5.18}$$

in which $\hat{\boldsymbol{x}}=\hat{\boldsymbol{x}}\left(\tau_1,\tau_2,\tau_3\right)$ and

$$\hat{\boldsymbol{y}}=\hat{\boldsymbol{y}}\left(\tau_1,\tau_2,\tau_3\right)=\begin{bmatrix}\hat{\boldsymbol{y}}_{AA}\left(\tau_1,\tau_2,\tau_3\right)\\ \hat{\boldsymbol{y}}_{AL}\left(\tau_1,\tau_2,\tau_3\right)\\ \hat{\boldsymbol{y}}_{LA}\left(\tau_1,\tau_2,\tau_3\right)\\ \hat{\boldsymbol{y}}_{LL}\left(\tau_1,\tau_2,\tau_3\right)\end{bmatrix} \tag{5.19}$$

where $\hat{\boldsymbol{y}}_{AA}$, $\hat{\boldsymbol{y}}_{AL}$, $\hat{\boldsymbol{y}}_{LA}$ and $\hat{\boldsymbol{y}}_{LL}$, denote, respectively, the state variable components' vectors that are active in both τ_2 and τ_3, active in τ_2 and latent in τ_3, latent in τ_2 and active in τ_3, and latent in both dimensions.

As stated in the previous chapter, since many RF circuits have a static subset partition (as is the case of our illustrative application example), it is possible and also convenient to adopt a simpler approach than the one presented above. It will avoid some redundant computational work. Taking this into account we have decided to adopt the following procedure.

We start by computing the solution of the 2-D bi-periodic boundary value problem (5.4), (5.5) for the first slow time instant $\tau_{1,1}$ in a purely uni-rate manner. That is, we start by considering a fine grid in both the τ_2 and τ_3 dimensions for all circuit's state variables, which obviously means that we start by treating all the components of (5.4) in the same way. We then split the circuit into sub-circuits, according to the same criteria presented above, and finally we proceed in a double multirate way for all the remaining slow time instants $\tau_{1,i}$.

5.3 Experimental Results

We will now test the performance and the efficiency of the method proposed in the previous section, through its application to the RF polar transmitter PA presented in Figure 4.1. The most relevant components' values of this heterogeneous nonlinear multirate circuit were already described in Section 4.3.1. As seen, in order to get highly efficient power amplification, the

TABLE 5.1

COMPUTATION TIMES (COMPUTER: AMD 1.8 GHz, 700 MB RAM)

RF POLAR TRANSMITTER PA BASEBAND SIGNALS = 200 kHz SINE WAVES

Simulation time interval	3-D warped envelope transient over shooting		2-D warped envelope transient over shooting with MRK
	Multiple-line double multirate shooting (new method)	Hierarchical shooting with MRK	
[0, 0.5 μs]	4 s	26 s	32 s
[0, 5.0 μs]	29 s	212 s	225 s

amplitude of the driving voltages of both MOSFETs are set so that the devices are forced to operate in switching mode, leading this way to a strongly nonlinear problem.

As mentioned in Section 5.1, we have now a combination of four independent excitations running in three different time scales: the slow baseband time scale, the digital clock intermediate time scale and the fast carrier time scale. In our experiments, we first considered two simple hypothetical cases, of 200 kHz and 2 MHz purely sinusoidal regimes, for both $AM(t)$ and $PM(t)$ baseband excitations. Then, in order to test the proposed method in a more realistic wireless communications scenario, we simulated the circuit with a EDGE signal.

5.3.1 Numerical Results for Simulations with Baseband Sinusoidal Regimes

The RF polar transmitter PA was simulated in MATLAB® with the proposed novel numerical method (3-D warped envelope transient over multiple-line double multirate shooting). Then, we compared its results with the corresponding 3-D warped envelope transient over hierarchical shooting and with the method proposed in the previous chapter (2-D warped envelope transient over shooting), treating the digital clock and the baseband signals in the same time scale. No comparison was made with any classical time-marching engine (univariate time-step integration), as SPICE, because the 3-D nature of the circuit operation would determine an extremely large simulation time. Also, no comparison with any frequency-domain, or hybrid solvers was performed, because the highly nonlinear regimes of the circuit would lead to an intolerably large number of harmonics.

Numerical computation times (in seconds) for simulations with 200 kHz sine waves for both baseband $AM(t)$ and $PM(t)$ signals are presented in Table 5.1. A comparison between the simulation times achieved in the three tested methods clearly reveals the computational efficiency of the now proposed method. Uniform grids were assumed for simplicity in all the three methods. In the 3-D warped envelope transient over shooting methods, each cycle of the slow 200 kHz sine

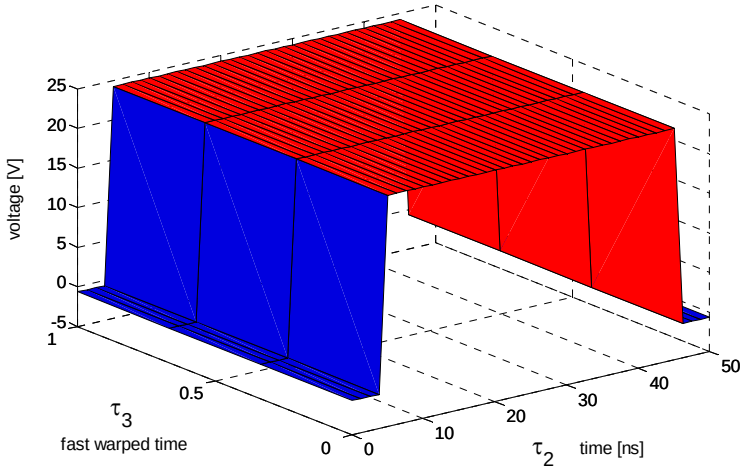

Figure 5.5 Bivariate AM branch MOSFET source voltage.

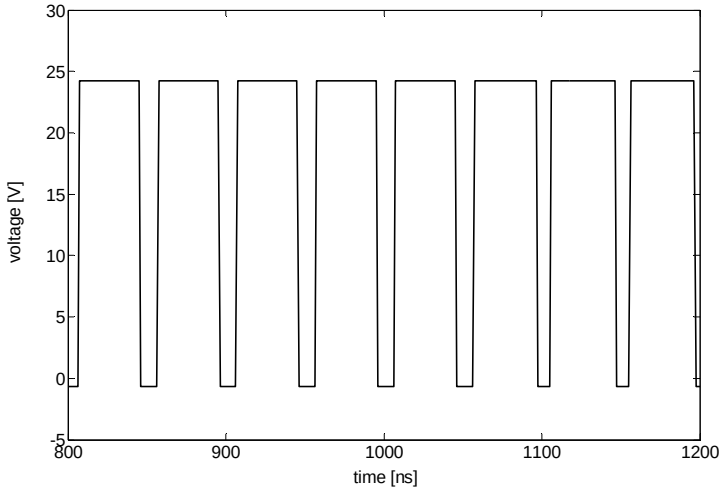

Figure 5.6 Univariate AM branch MOSFET source voltage in the digital clock time scale.

waves was sampled at 40 points, which has led to a τ_1 time-step integration size of $h_1 = 125\,\text{ns}$. Also, each cycle of the 20 MHz digital clock was sampled at 40 points, i.e., a step length of $h_2 = 1.25\,\text{ns}$ was considered in the τ_2 fine grid. Finally, in the τ_3 fine grid (fast warped time scale), 60 points were used per carrier cycle.

Figure 5.5 depicts the solution for the AM branch transistor source voltage on $[0,T_2]\times[0,T_3]$, with $\tau_1 = 1\mu\text{s}$. T_2 is the 50 ns digital clock period and we chose a warped time function $\phi(t)$ so that $T_3 = 1$. As we can see, there are no fluctuations in the τ_3 dimension, which allowed us to use a large time-step integration size in that dimension. The univariate version of this state variable is plotted in Figure 5.6, for the [800, 1200 ns] interval. Figure 5.7 shows the solution for the RF transistor drain voltage on $[0,T_2]\times[0,T_3]$, with $\tau_1 = 1\mu\text{s}$. Now, no fluctuations can be observed in the τ_2 dimension, which allowed us to use a coarse grid with a large grid spacing in τ_2, i.e., only a

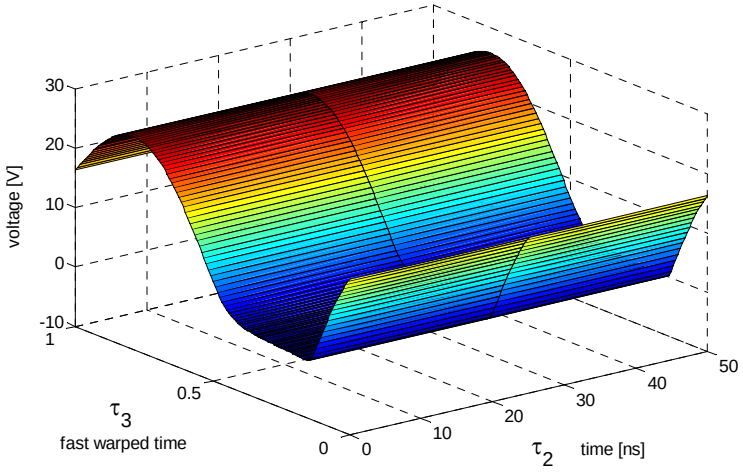

Figure 5.7 Bivariate drain voltage of the MOSFET RF switching-mode amplifier.

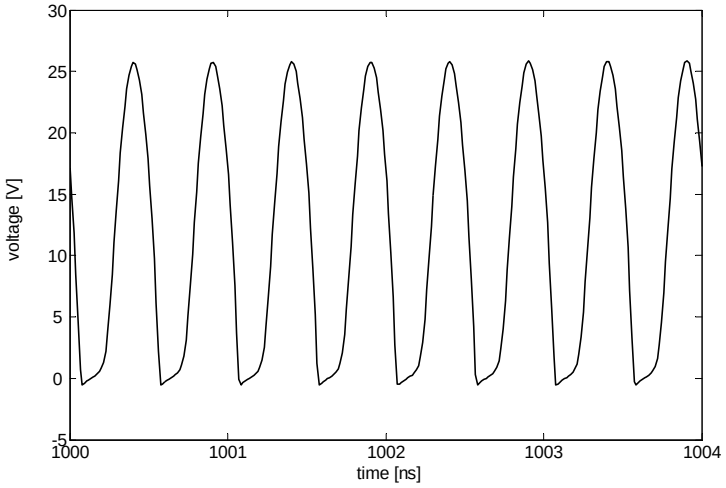

Figure 5.8 Univariate RF PA MOSFET drain voltage in the fast carrier time scale.

few shooting lines. The corresponding time scaled univariate version is plotted in Figure 5.8, for the [1000, 1004 ns] interval. Finally, Figure 5.9 depicts the time scaled univariate version of the output voltage of the circuit, for the same [1000, 1004 ns] time interval.

Additionally, for comparison, we have simulated the circuit considering an higher frequency (2 MHz sine waves) for both *AM*(*t*) and *PM*(*t*) baseband excitations. The corresponding computation times are presented in Table 5.2. As above, uniform grids were assumed, with the same number of grid points per cycle. Since, in the 3-D methods, each cycle of the 2 MHz sine waves is sampled at 40 points, the τ_1 time-step integration size is reduced from $h_1 = 125$ ns to $h_1 = 12.5$ ns, and the ratio h_1/h_2 is reduced from 100 to 10.

By comparing Tables 5.1 and 5.2, we realize that the efficiency of the proposed new method degrades if we decrease the disparity between the slow time scale (baseband excitations) and the

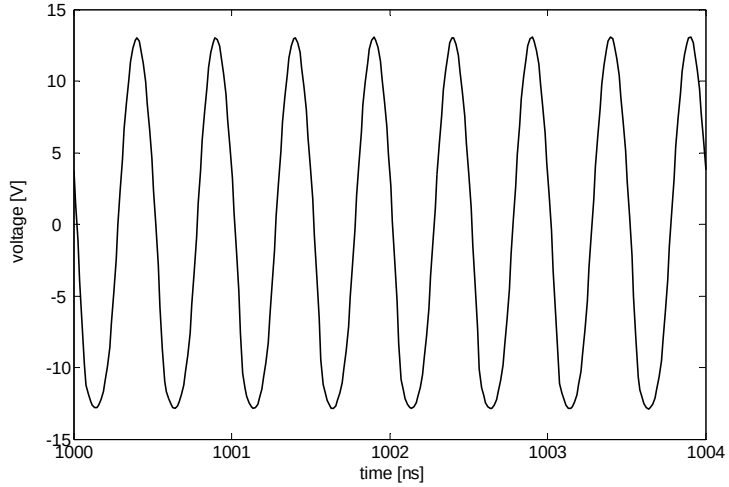

Figure 5.9 Univariate output voltage in the fast carrier time scale.

TABLE 5.2

COMPUTATION TIMES (COMPUTER: AMD 1.8 GHz, 700 MB RAM)

RF POLAR TRANSMITTER PA BASEBAND SIGNALS = 2 MHz SINE WAVES

Simulation time interval	3-D warped envelope transient over shooting		2-D warped envelope transient over shooting with MRK
	Multiple-line double multirate shooting (new method)	Hierarchical shooting with MRK	
[0, 0.5 μs]	35 s	173 s	33 s
[0, 5.0 μs]	352 s	1622 s	266 s

intermediate time scale (20 MHz digital clock). Conversely, the efficiency of the method proposed in the previous chapter degrades when we raise this time-scale disparity.

5.3.2 Numerical Results for Simulations with Baseband EDGE Signals

For testing the proposed method in a realistic wireless communications scenario, we have also considered the simulation of the RF polar transmitter PA subject to the baseband EDGE signals [magnitude, $AM(t)$, and phase, $PM(t)$] depicted in Figures 5.10 and 5.11, and with a carrier frequency of f_C = 1.9 GHz. The magnitude and phase EDGE waveforms were obtained converting to polar coordinates the corresponding in-phase and quadrature signals generated with a R&S SMU200A[1] vector signal generator. Once again, uniform grids were assumed for simplicity, in which the selection of $h_1 = 125\,\text{ns}$ was enough to represent both EDGE excitations accurately in

[1] [Online]. Available: http://www2.rohde-schwarz.com/product/smu200a.html

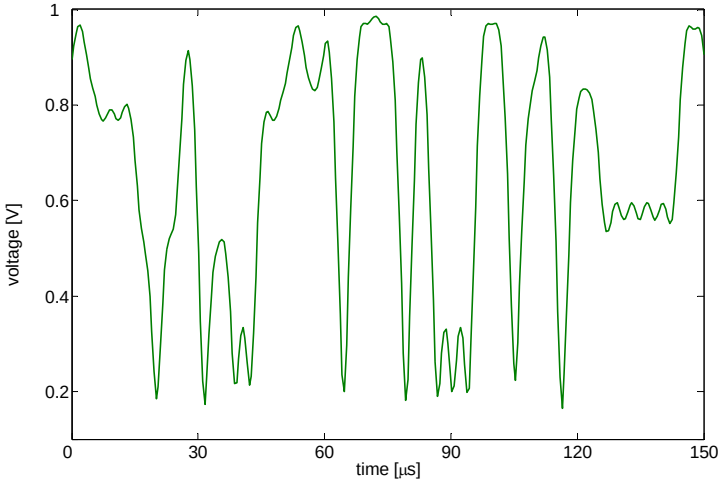

Figure 5.10 Magnitude $AM(t)$ of the EDGE test signal.

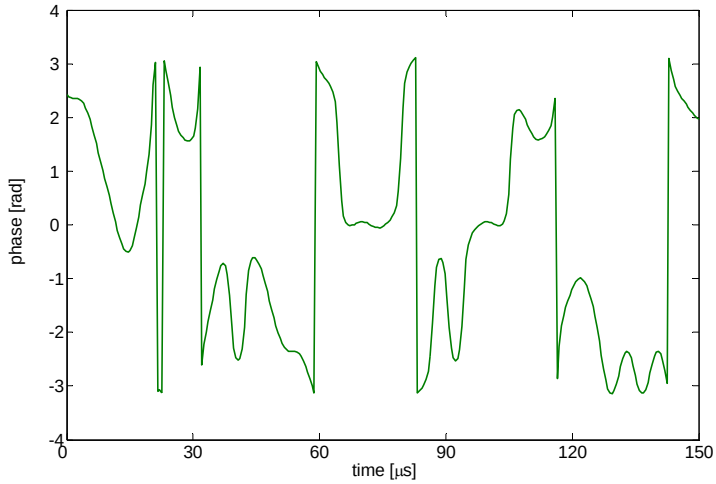

Figure 5.11 Phase $PM(t)$ of the EDGE test signal.

the 3-D methods. Numerical computation times (in seconds) for simulations in the [0, 20 μs] and [0, 150 μs] intervals are presented in Table 5.3. These attest again the computational efficiencies provided by the method under discussion in this chapter, as it exhibits significant speed gains over the other methods.

5.4 Conclusions

An innovative, and very efficient, time-domain simulation method has been developed and tested in this chapter. This technique is particularly suitable for highly heterogeneous nonlinear RF circuits running in three disparate time scales, and introduces a new multiple-line double multirate shooting technique within a 3-D warped time framework. Significant reductions of the

TABLE 5.3

COMPUTATION TIMES (COMPUTER: AMD 1.8 GHz, 700 MB RAM)

RF POLAR TRANSMITTER PA BASEBAND SIGNALS = EDGE TEST SIGNALS

Simulation time interval	3-D warped envelope transient over shooting		2-D warped envelope transient over shooting with MRK
	Multiple-line double multirate shooting (new method)	Hierarchical shooting with MRK	
[0, 20 μs]	115 s	703 s	785 s
[0, 150 μs]	882 s	5270 s	5810 s

computational work were achieved, without compromising accuracy, as the method was conceived to take advantage of the circuits' heterogeneity and stimuli time-rate disparities.

The speedup advantage of the method, when compared to the method previously presented in Chapter 4, depends on the discrepancy between the slow, the intermediate and the fast time scales. As seen in the case of the illustrative polar transmitter example, this speedup is achieved when the time-scale separation (step size ratio) between the baseband signals and the digital clock is increased from 10 to 100. In general, for a generic application running in three time scales, we expect that time-scale disparities of two orders of magnitude and above will always confer significant gains in simulation speed to the method described in this chapter.

Chapter 6

Two Innovative Time-Domain Simulation Techniques

6.1 Introduction

In Chapter 4 we have presented a powerful time-domain simulation method particularly suitable for strongly nonlinear heterogeneous RF circuits, not only including diverse type of stimuli, as also exhibiting slow (latent) and fast-varying (active) state variables. We have exploited the subset circuit latency by using multirate Runge-Kutta schemes within a 2-D framework, which integrated the slow state variables with a larger step length than the one used for the fast ones. Since the efficiency of such method was dependent on the active-latent time-scale separation, and degraded when we had a problem running in multiple time scales instead of running only in two time scales, in Chapter 5 we have proposed an innovative multiple-line double multirate shooting technique within a 3-D warped time framework, which has demonstrated to be very efficient for simulating RF circuits operating in three distinct time scales (slow, intermediate and fast).

Another interesting class of multirate problems will be discussed in this chapter. Let us suppose that, contrary to what we had previously considered in Chapters 4 and 5, we have now nonlinear RF circuits in which all the corresponding state variables are fast. For concreteness, let us suppose that all the circuits' signals fluctuate at the frequency dictated by the fast-varying RF carrier. As a result, and since we do not have slow (latent) signals, it seems that multirate Runge-Kutta schemes could no longer be used. However, as we will see in the following, this is not inevitably true.

Let us suppose that we have two aperiodic baseband signals, $e_1(t)$ and $e_2(t)$, modulating the amplitude of a high frequency RF carrier $\sin(2\pi f_C t)$. If $e_1(t)$ and $e_2(t)$ present significant disparate rates of change, then we will have two modulated signals,

$$\begin{aligned} x_1(t) &= e_1(t)\sin(2\pi f_C t), \\ x_2(t) &= e_2(t)\sin(2\pi f_C t), \end{aligned} \tag{6.1}$$

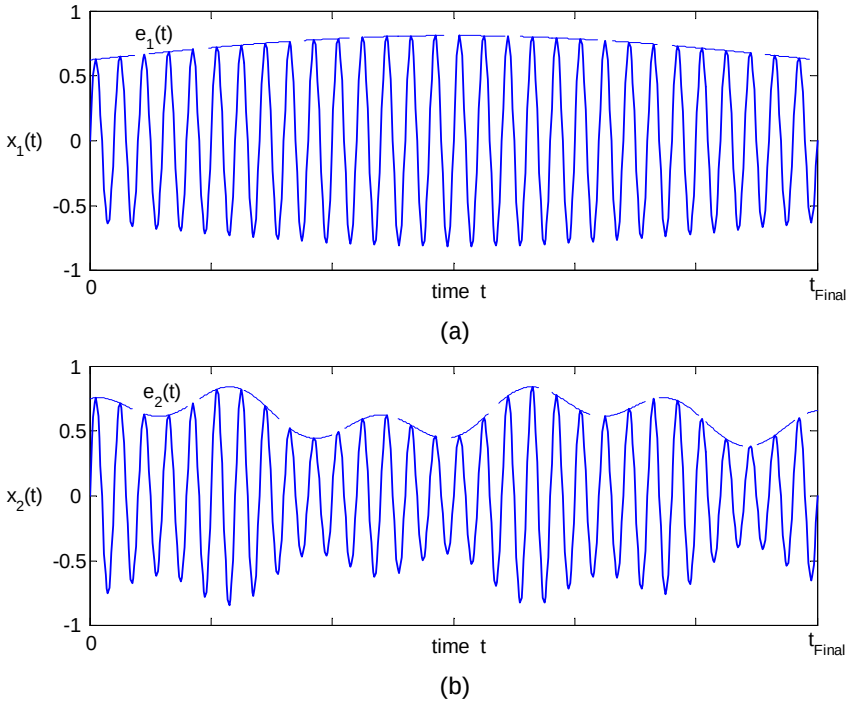

Figure 6.1 Envelope modulated signals: (a) $x_1(t)$ and (b) $x_2(t)$.

whose envelopes evolve according to different time scales. This is illustrated in Figure 6.1(a) and (b) for some $[0, t_{Final}]$ time interval.

For instance, let us momentarily suppose that $f_C = 2\,\text{GHz}$ and that the bandwidths of $e_1(t)$ and $e_2(t)$ are 200 kHz and 20 MHz, respectively. Although this discrepancy woud lead us to a problem running in three time scales, since $e_1(t)$ and $e_2(t)$ are both aperiodic we must mix them in the same time dimension when formulating the problem in the multivariate time space. This was explained in detail in Section 3.5. Consequently, instead of a 3-D formulation of the problem we must consider a 2-D framework, where $x_1(t)$ and $x_2(t)$ are rewritten as the bivariate entities

$$\begin{aligned} \hat{x}_1(t_1,t_2) &= e_1(t_1)\sin(2\pi f_C t_2), \\ \hat{x}_2(t_1,t_2) &= e_2(t_1)\sin(2\pi f_C t_2), \end{aligned} \tag{6.2}$$

where t_1 is the slow envelope time dimension and t_2 is the fast carrier time dimension.

Figure 6.2(a) and (b) depict the plots of $\hat{x}_1(t_1,t_2)$ and $\hat{x}_2(t_1,t_2)$ on the rectangle $[0,t_{Final}]\times[0,T_2]$. These are the bivariate forms of the modulated signals shown in Figure 6.1(a) and (b), where $T_2 = 1/f_C$ is the carrier period. Obviously, $\hat{x}_1(t_1,t_2)$ is much smoother in the t_1 dimension than $\hat{x}_2(t_1,t_2)$, allowing thus a numerical representation with fewer samples. So, when using numerical schemes for solving problems with this kind of stimulus, we can use a large time-step size H_1 on components that are smooth in the t_1 dimension (smaller bandwidth) and a small time-step size h_1 on components that are not so smooth (larger bandwidth). Please compare Figure 6.2(a) and (b). In this sense, although we may have RF circuits in which all the stimuli and all the

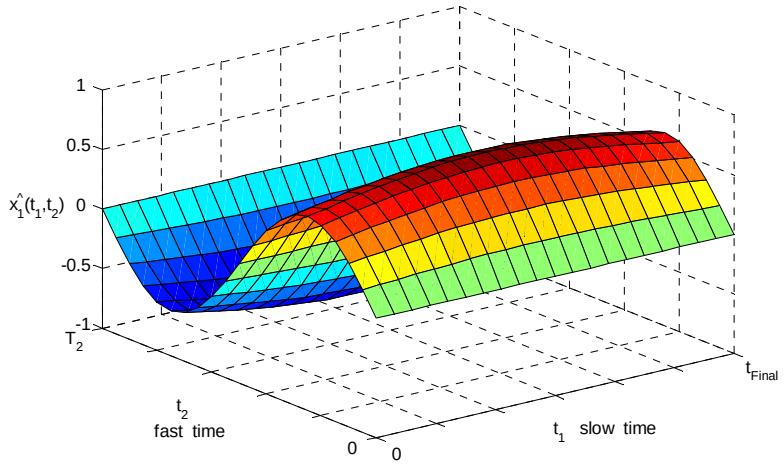

(a)

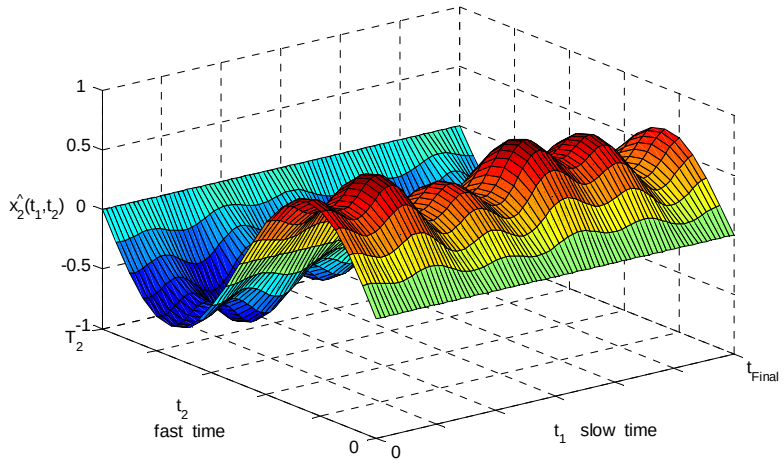

(b)

Figure 6.2 Bivariate forms of the envelope modulated signals: (a) $\hat{x}_1$ and (b) $\hat{x}_2$.

state variables are fast, we can define an active-latent concept based on the envelope analysis of the waveforms, i.e., supported on the examination of the smoothness of the corresponding bivariate forms in the t_1 slow time scale.

We must note that the spectral representation of the envelope modulated signals $x_1(t)$ and $x_2(t)$ defined by (6.1) is of the form of the ones sketched in Figure 6.3, where we have two different bandwidth spectra centred in the same carrier frequency f_C. So, we must observe that, obviously, the $x_1(t)$ spectrum type could be obtained if we apply to $x_2(t)$ a bandpass filter with a narrow passband centred in f_C. Therefore, the scenario just described of multirate circuits operating in one periodic fast time scale and two distinct aperiodic slow time scales may possibly occur, for example, in RF circuits containing narrow bandpass filters. In effect, in such case,

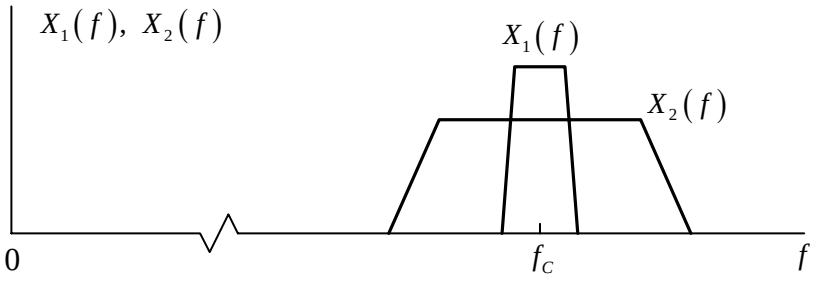

Figure 6.3 Frequency-domain representation of two envelope modulated signals.

signals' bandwidth may be considerably reduced at the output of the filters, as they produce high frequency waveforms with very slowly changing envelopes.

The main difference between the kind of 2-D problems examined in this chapter and the ones discussed in Chapter 4 (where a 2-D formulation was also adopted), is that instead of performing time-step integration with different step sizes for the fast dimension, we have now to consider different grid sizes in the slow time dimension. Thus, the active-latent partition of the circuits will no longer be performed according to the fluctuations of their state variables in t_2. In its place, we will have a circuit partitioning strategy based on the smoothness of the state variable components in the t_1 slow time scale. Components that are extremely smooth in t_1 will be treated as latent. Components that evidence significant fluctuations in t_1 will be treated as active.

In order to simulate this kind of problems efficiently, in this chapter we will propose and test two distinct innovative time-domain simulation techniques. These techniques are based on the mathematical method of lines presented in Chapter 5, and on the envelope transient over shooting technique. They are described in detail in the following sections.

6.2 Method of Lines MRK

6.2.1 Theoretical Formulation

Let us start by considering and rewriting here the generic unwarped bivariate formulation described by the partial differential algebraic system of (3.31), i.e.,

$$\boldsymbol{p}\left[\hat{\boldsymbol{y}}(t_1,t_2)\right]+\frac{\partial \boldsymbol{q}\left[\hat{\boldsymbol{y}}(t_1,t_2)\right]}{\partial t_1}+\frac{\partial \boldsymbol{q}\left[\hat{\boldsymbol{y}}(t_1,t_2)\right]}{\partial t_2}=\hat{\boldsymbol{x}}(t_1,t_2), \tag{6.3}$$

characterizing the 2-D behaviour of a nonlinear multirate RF circuit with n state variables, now operating in one periodic fast time scale (the t_2 dimension) and two aperiodic slow time scales (mixed in t_1). Let us also consider the semi-discretization of the rectangular domain $[0,t_{Final}]\times[0,T_2]$ in t_2 defined by the grid (3.44), i.e.,

$$0=t_{2,0}<t_{2,1}<\cdots<t_{2,j-1}<t_{2,j}<\cdots<t_{2,K_2}=T_2, \qquad h_{2,j}=t_{2,j}-t_{2,j-1}. \tag{6.4}$$

If we use a finite-differences scheme to approximate the derivatives of (6.3) in t_2, we can obtain a set of $n \times K_2$ ordinary differential algebraic equations in t_1

$$\begin{gathered} \boldsymbol{p}\left[\hat{\boldsymbol{y}}_j(t_1)\right] + \frac{d\boldsymbol{q}\left[\hat{\boldsymbol{y}}_j(t_1)\right]}{dt_1} + \frac{\boldsymbol{q}\left[\hat{\boldsymbol{y}}_j(t_1)\right] - \boldsymbol{q}\left[\hat{\boldsymbol{y}}_{j-1}(t_1)\right]}{h_{2,j}} = \hat{\boldsymbol{x}}_j(t_1), \\ j = 1, \ldots, K_2, \qquad \hat{\boldsymbol{y}}_0(t_1) = \hat{\boldsymbol{y}}_{K_2}(t_1), \end{gathered} \tag{6.5}$$

where $\hat{\boldsymbol{y}}_j(t_1) \simeq \hat{\boldsymbol{y}}(t_1, t_{2,j})$ and $\hat{\boldsymbol{x}}_j(t_1) = \hat{\boldsymbol{x}}(t_1, t_{2,j})$. This whole system can be time-step integrated with an appropriate initial value solver, which means that we can use the method of lines to obtain the solution of (6.3). The periodic boundary value condition $\hat{\boldsymbol{y}}_0(t_1) = \hat{\boldsymbol{y}}_{K_2}(t_1)$ will ensure the periodicity of the solution in the t_2 dimension.

The reason we have chosen the method of lines to solve (6.3) is because we want to benefit from the existence of two different rates of variation in the t_1 slow envelope time scale. In fact, we will do so by time-step integrating (6.5) with multirate Runge-Kutta methods. For that, we split the partial differential algebraic system of (6.3) into coupled active and latent subsystems

$$\begin{gathered} \boldsymbol{p}_A\left[\hat{\boldsymbol{y}}_A(t_1,t_2), \hat{\boldsymbol{y}}_L(t_1,t_2)\right] + \frac{\partial \boldsymbol{q}_A\left[\hat{\boldsymbol{y}}_A(t_1,t_2), \hat{\boldsymbol{y}}_L(t_1,t_2)\right]}{\partial t_1} \\ + \frac{\partial \boldsymbol{q}_A\left[\hat{\boldsymbol{y}}_A(t_1,t_2), \hat{\boldsymbol{y}}_L(t_1,t_2)\right]}{\partial t_2} = \hat{\boldsymbol{x}}(t_1,t_2), \end{gathered} \tag{6.6}$$

$$\begin{gathered} \boldsymbol{p}_L\left[\hat{\boldsymbol{y}}_A(t_1,t_2), \hat{\boldsymbol{y}}_L(t_1,t_2)\right] + \frac{\partial \boldsymbol{q}_L\left[\hat{\boldsymbol{y}}_A(t_1,t_2), \hat{\boldsymbol{y}}_L(t_1,t_2)\right]}{\partial t_1} \\ + \frac{\partial \boldsymbol{q}_L\left[\hat{\boldsymbol{y}}_A(t_1,t_2), \hat{\boldsymbol{y}}_L(t_1,t_2)\right]}{\partial t_2} = \hat{\boldsymbol{x}}(t_1,t_2), \end{gathered} \tag{6.7}$$

with

$$\hat{\boldsymbol{y}}(t_1,t_2) = \begin{bmatrix} \hat{\boldsymbol{y}}_A(t_1,t_2) \\ \hat{\boldsymbol{y}}_L(t_1,t_2) \end{bmatrix}, \quad \hat{\boldsymbol{y}}_A \in \mathbb{R}^{n_A}, \quad \hat{\boldsymbol{y}}_L \in \mathbb{R}^{n_L}, \quad n_A + n_L = n, \tag{6.8}$$

according to the rates of variation of its components in the slow time t_1. That is to say, we split the $n \times K_2$ ordinary differential algebraic equations' system of (6.5) into the following $n_A \times K_2$ equations and $n_L \times K_2$ equations active and latent subsystems

$$\begin{gathered} \boldsymbol{p}_A\left[\hat{\boldsymbol{y}}_{A,j}(t_1), \hat{\boldsymbol{y}}_{L,j}(t_1)\right] + \frac{d\boldsymbol{q}_A\left[\hat{\boldsymbol{y}}_{A,j}(t_1), \hat{\boldsymbol{y}}_{L,j}(t_1)\right]}{dt_1} \\ + \frac{\boldsymbol{q}_A\left[\hat{\boldsymbol{y}}_{A,j}(t_1), \hat{\boldsymbol{y}}_{L,j}(t_1)\right] - \boldsymbol{q}_A\left[\hat{\boldsymbol{y}}_{A,j-1}(t_1), \hat{\boldsymbol{y}}_{L,j-1}(t_1)\right]}{h_{2,j}} = \hat{\boldsymbol{x}}_j(t_1), \end{gathered} \tag{6.9}$$

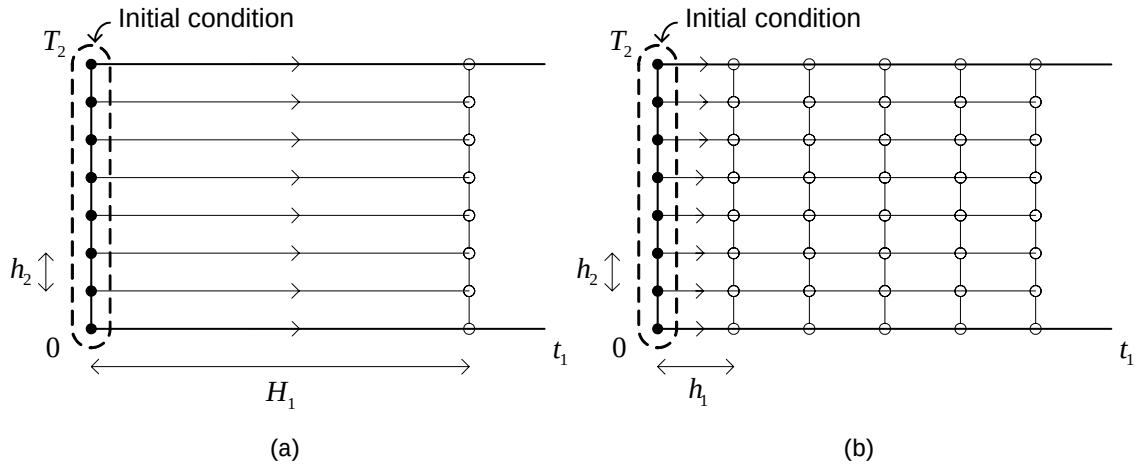

Figure 6.4 Method of lines with MRK: (a) latent components and (b) active components.

$$\begin{aligned} &\boldsymbol{p}_L\left[\hat{\boldsymbol{y}}_{A,j}(t_1),\hat{\boldsymbol{y}}_{L,j}(t_1)\right]+\frac{d\boldsymbol{q}_L\left[\hat{\boldsymbol{y}}_{A,j}(t_1),\hat{\boldsymbol{y}}_{L,j}(t_1)\right]}{dt_1} \\ &+\frac{\boldsymbol{q}_L\left[\hat{\boldsymbol{y}}_{A,j}(t_1),\hat{\boldsymbol{y}}_{L,j}(t_1)\right]-\boldsymbol{q}_L\left[\hat{\boldsymbol{y}}_{A,j-1}(t_1),\hat{\boldsymbol{y}}_{L,j-1}(t_1)\right]}{h_{2,j}}=\hat{\boldsymbol{x}}_j(t_1), \\ &j=1,\ldots,K_2,\quad \hat{\boldsymbol{y}}_{A,0}(t_1)=\hat{\boldsymbol{y}}_{A,K_2}(t_1),\quad \hat{\boldsymbol{y}}_{L,0}(t_1)=\hat{\boldsymbol{y}}_{L,K_2}(t_1). \end{aligned} \tag{6.10}$$

This way, active components will be integrated with a small step size h_1 (microstep), whereas latent components will be integrated with a large time-step size H_1 (macrostep). This is illustrated in Figure 6.4.

6.2.2 Active-Latent Partitioning Strategy

In order to split the circuit into active and latent sub-circuits, an automatic classification of the circuit's state variables (according to their rates of change in time t_1) must be performed. By using MRK methods based in embedded RK formulas [15], local error estimates usually evaluated for step-size control may be utilized for carrying out this automatic state-variable classification and subsequent circuit partition. Such partitioning technique is described in detail in [22], [38] and [39]. It is suitable for general RF circuits with dynamic subset partition (circuits in which the partition may vary with time) and RF circuits with static subset partition (circuits in which the subset partition does not change along the simulation process). In the first case, every partitioning implementation details (local error evaluations, selection of new step sizes, partitioning into active and latent components) must be performed at the end of each macrostep H_1. In the second case, these partitioning implementation details may be performed only on the first compound step. Additionally, in this case, we may also adopt a different and simpler approach: we may start by time-step integrating (6.5) in a uni-rate way for several time steps, using a standard RK scheme as the method of lines initial value solver; next we split the differential system according to the

fluctuations of the solution in t_1; and then we switch to a MRK scheme to proceed with the time-step integration of (6.9), (6.10) in a multirate way.

6.2.3 Stiffness Occurrence

As stated above, we have chosen the method of lines based on MRK schemes because we want to benefit from the existence of two different rates of variation in the t_1 slow envelope time scale. Our intention is to reduce the computational work required for obtaining the solution of (6.3). However, we must take into account that we are semi-discretizing the problem in the fast time dimension, to then time-step integrate it in the slow time dimension. As seen in Chapter 5, this strategy will lead us to a stiff problem. This means that explicit schemes can no longer be utilized. In fact, numerical stability requirements will now demand for implicit schemes, as they are much more stable. As a result, MRK methods based on implicit RK schemes for both active and latent parts will be required.

As explained in Section 5.2.7, the occurrence of stiffness means that we are dealing with differential systems whose Jacobian matrices present large stiffness ratios $\left|\mathrm{Re}\,\bar{\lambda}\right| / \left|\mathrm{Re}\,\underline{\lambda}\right|$. However, we have to face an extra difficulty. We have to deal also with large Lipschitz constants [15]. As we will see in the following, large Lipschitz constants will inhibit us to use the cheap fixed-point iterative solver, when computing the Runge-Kutta slopes in the implicit MRK time-step integrators. Consequently, we have to compute these slopes with another iterative solver, e.g., Newton-Raphson. In addition, every time we try to improve the accuracy of the solution in the fast time t_2, by increasing the number of grid lines K_2, the stiffness restrictive scenario becomes even worse.

In order to provide some explanations about these stiffness difficulties, let us consider, and rewrite here, the (2.16) classical form of a generic initial value problem

$$\frac{d\boldsymbol{y}(t)}{dt} = \boldsymbol{f}(t,\boldsymbol{y}), \quad \boldsymbol{y}(t_0) = \boldsymbol{y}_0, \quad t_0 \le t \le t_{Final}, \quad \boldsymbol{y}(t) \in \mathbb{R}^n. \tag{6.11}$$

Theorem 6.1: Cauchy-Lipschitz. Let $\boldsymbol{f}(t,\boldsymbol{y})$ be defined in $D \subset [t_0, t_{Final}] \times \mathbb{R}^n$, $\boldsymbol{f} : D \to \mathbb{R}^n$, and continuous with respect to t. Let there exist a constant L such that

$$\left\| \boldsymbol{f}(t,\boldsymbol{y}) - \boldsymbol{f}(t,\tilde{\boldsymbol{y}}) \right\| \le L \left\| \boldsymbol{y} - \tilde{\boldsymbol{y}} \right\| \tag{6.12}$$

holds for any $(t,\boldsymbol{y}), (t,\tilde{\boldsymbol{y}}) \in D$. Then, for any $\boldsymbol{y}_0 \in \mathbb{R}^n$ there exists a unique solution $\boldsymbol{y}(t)$ of the problem (6.11).

Proof: The proof of this theorem can be seen in [15], where the requirement (6.12) is known as the *Lipschitz condition*, and L is known as the *Lipschitz constant*.

Now, let us suppose that we want to numerically time-step integrate (6.11) with a standard Runge-Kutta scheme. So, for convenience, let us rewrite here the definition of a Runge-Kutta

method, previously presented in Chapter 2. As seen, a standard *s*-stage RK method expressed by its Butcher tableau $(\boldsymbol{b},\boldsymbol{A},\boldsymbol{c})$, for integrating all the components of $\boldsymbol{y}$ in (6.11) with the same time-step size *h*, is defined as:

$$\boldsymbol{y}_1 = \boldsymbol{y}_0 + h\sum_{i=1}^{s} b_i \boldsymbol{k}_i, \tag{6.13}$$

$$\boldsymbol{k}_i = \boldsymbol{f}\left(t_0 + c_i h, \boldsymbol{y}_0 + h\sum_{j=1}^{s} a_{ij}\boldsymbol{k}_j\right), \quad i = 1,2,\ldots,s. \tag{6.14}$$

In case of explicit RK schemes we have $a_{ij} = 0$ for $j \geq i$ and the RK slopes $\boldsymbol{k}_i$ in (6.14) may be evaluated successively. However, if (6.11) is a stiff problem, explicit schemes will not perform well, unless a tremendously small time-step size *h* is used. Thus, implicit RK schemes are required instead. In such cases $a_{ij} \neq 0$ for $j \geq i$, which means that all the RK slopes $\boldsymbol{k}_i$ have to be determined simultaneously, i.e., we have to solve a nonlinear system of $n \times s$ algebraic equations when computing the $\boldsymbol{k}_i$. Obviously, the nonlinear system of (6.14) have to be solved iteratively. A cheap way to do so consists in making use of the fixed-point iterative solver, which, in this case, would simply result in

$$\boldsymbol{k}_i^{[r+1]} = \boldsymbol{f}\left(t_0 + c_i h, \boldsymbol{y}_0 + h\sum_{j=1}^{s} a_{ij}\boldsymbol{k}_j^{[r]}\right), \quad i = 1,2,\ldots,s. \tag{6.15}$$

However, when large Lipschitz constants *L* are involved, the iterative convergence to the solution of (6.14) can not be achieved with the fixed-point iteration technique of (6.15). This can be clarified via the following theorem.

Theorem 6.2: Let $\boldsymbol{f}(t,\boldsymbol{y})$ be continuous and Lipschitz with constant *L* in a neighbourhood of the initial value $\boldsymbol{y}_0$. If

$$h < \frac{1}{L \max_i \sum_j |a_{ij}|} \tag{6.16}$$

there exists a unique solution of (6.14), which can be obtained by fixed-point iteration.

Proof: The proof of this theorem can be seen in [15].

According to the theorem, when *L* is too large the step size limit (6.16) becomes dramatically restrictive. As a result, the implicit RK scheme becomes completely useless if we try to solve (6.14) with fixed-point iteration. Hence, other iterative solvers must be used to compute the $\boldsymbol{k}_i$ slopes (e.g., Newton's method). Obviously, as mentioned above, we will time-step integrate the system of (6.5) with MRK methods and not with classical RK methods. However, this stiffness restrictive scenario is not better, or becomes even worse, when MRK methods are used [23], [38].

Finally, it must be stated that, although we are proposing here the use of MRK schemes within the method of lines with the intention of taking profit from the existence of two different rates of variation in the t_1 slow envelope time scale, due to the stiffness of the problems we really do not expect to obtain significant improvements with the method proposed in this section. This will be confirmed with the numerical results obtained for the simulation of the illustrative example presented in Section 6.4.

6.3 Mixed Method

6.3.1 Method of Lines MRK Merged with Envelope Transient over Shooting

The stiffness difficulties just discussed in the previous section advise the substitution of the pure method of lines MRK technique by an alternative stratagem. Thus, in order to try to get some computational work reduction while evaluating the numerical solution of the 2-D problems under discussion in this chapter, we will now propose a slightly different technique.

For achieving an intuitive explanation of the method proposed in this section, let us consider again the generic unwarped bivariate formulation of (6.3). Let us suppose that we would like to numerically solve this 2-D problem with the envelope transient over shooting technique. In order to do that, we should consider the semi-discretization of the rectangle $\left[0,t_{Final}\right]\times\left[0,T_2\right]$ in the slow time t_1, defined by the grid (3.40), i.e.,

$$0=t_{1,0}<t_{1,1}<\cdots<t_{1,i-1}<t_{1,i}<\cdots<t_{1,K_1}=T_{Final},\qquad h_{1,i}=t_{1,i}-t_{1,i-1}, \tag{6.17}$$

and replace the derivatives of (6.3) in t_1 with a finite-differences approximation (e.g., the backward Euler rule), to obtain, for each level $t_{1,i}$, the periodic boundary value problem of (3.41), i.e.,

$$\begin{gathered}\boldsymbol{p}\left[\hat{\boldsymbol{y}}_i\left(t_2\right)\right]+\frac{\boldsymbol{q}\left[\hat{\boldsymbol{y}}_i\left(t_2\right)\right]-\boldsymbol{q}\left[\hat{\boldsymbol{y}}_{i-1}\left(t_2\right)\right]}{h_{1,i}}+\frac{d\boldsymbol{q}\left[\hat{\boldsymbol{y}}_i\left(t_2\right)\right]}{dt_2}=\hat{\boldsymbol{x}}_i\left(t_{1,i},t_2\right),\\ \hat{\boldsymbol{y}}_i\left(0\right)=\hat{\boldsymbol{y}}_i\left(T_2\right),\end{gathered} \tag{6.18}$$

which is numerically solved with the shooting method. With this strategy, we would not have the stiffness restrictive scenario reported in the previous section. It is so because the problem is semi-discretized in the t_1 slow time dimension and the time step-integrations are performed in the t_2 fast time scale. However, since we have to use the same time-step size $h_{1,i}$ for all the components in (6.18), we could not take advantage of the envelopes' disparity in the t_1 aperiodic slow time scale. Thus, we will now propose a mixed method that combines both the envelope transient over shooting technique and the method of lines MRK.

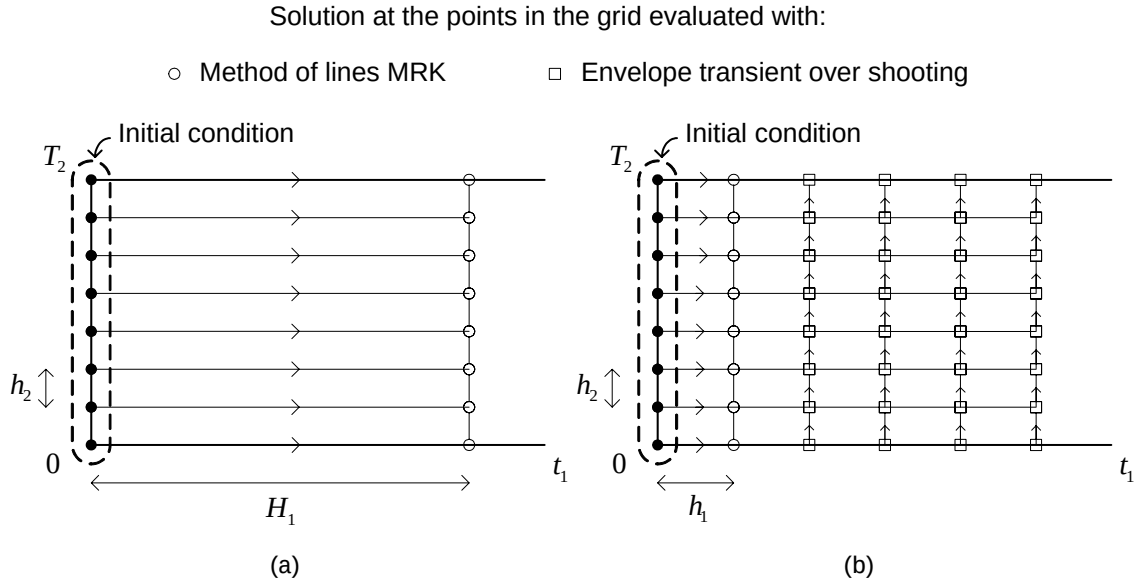

Figure 6.5 Mixed method: (a) latent components and (b) active components.

The proposed mixed method operates in the following way: for the successive rectangular regions $[t_0, t_0 + H_1] \times [0, T_2]$ in the $[0, t_{Final}] \times [0, T_2]$ domain, it starts by making use of the method of lines with MRK to perform a compound step in (6.9), (6.10), i.e., to evaluate the solution of (6.3) at the coarse grid instants $(t_0 + H_1, t_{2,j})$ for the latent components, and at the fine grid instants $(t_0 + h_1, t_{2,j})$ for the active components. Then, the values of the active components at the remaining grid instants $(t_0 + \lambda h_1, t_{2,j})$, $\lambda = 2, \ldots, m$, where m is the number of microsteps within a macrostep, will be computed by applying the envelope transient over shooting technique to the active subsystem of (6.6). The key idea of this mixed method is to avoid the stiffness difficulties that emerged when we evaluated the active components at the fine grid instants (microsteps) $t_0 + \lambda h_1$, $\lambda = 2, \ldots, m$, with the solely method of lines MRK technique. The implementation of this mixed method is illustrated in Figure 6.5, and some of its relevant technical details are presented in the following.

6.3.2 Technical Details of Implementation

In the pure envelope transient over shooting technique we have to solve a set of boundary value problems with periodic boundary conditions in the fast time t_2. Each one of these boundary value problems is of the form of (6.18), where the derivatives of (6.3) in the t_1 slow time scale are approximated by the backward Euler rule scheme. Now we will also make use of the backward Euler rule (which is an order 1 scheme), to discretize the t_1 time axis when applying the envelope transient over shooting technique to evaluate the solution of the active subsystem of (6.6) at the fine grid instants $t_0 + \lambda h_1$. For that reason, we have decided to use an implicit MRK scheme also based on the backward Euler method (the one stage order 1 implicit RK method), for both active

and latent subsystems. This MRK scheme will perform the method of lines compound step integration in (6.9), (6.10), and it is defined as follows.

Definition 6.1: MRK based on the backward Euler method. Let us consider the generic initial value problem of (6.11) partitioned into the coupled active and latent subsystems

$$\begin{aligned} \frac{d\boldsymbol{y}_A(t)}{dt} &= \boldsymbol{f}_A(t, \boldsymbol{y}_A, \boldsymbol{y}_L), \quad \boldsymbol{y}_A(t_0) = \boldsymbol{y}_{A,0}, \\ \frac{d\boldsymbol{y}_L(t)}{dt} &= \boldsymbol{f}_L(t, \boldsymbol{y}_A, \boldsymbol{y}_L), \quad \boldsymbol{y}_L(t_0) = \boldsymbol{y}_{L,0}, \end{aligned} \tag{6.19}$$

with

$$\boldsymbol{y} = \begin{bmatrix} \boldsymbol{y}_A \\ \boldsymbol{y}_L \end{bmatrix}, \quad \boldsymbol{y}_A \in \mathbb{R}^{n_A}, \quad \boldsymbol{y}_L \in \mathbb{R}^{n_L}, \quad n_A + n_L = n. \tag{6.20}$$

The implicit MRK scheme of order 1 based on the backward Euler method, for obtaining the numerical solution of the partitioned system of (6.19), by time-step integrating the active components with a microstep *h* and the latent components with a macrostep *H*, is defined as:

$$\boldsymbol{y}_{A,\lambda+1} = \boldsymbol{y}_{A,\lambda} + h\boldsymbol{k}_A^{\lambda}, \quad \lambda = 0,1,\ldots.m-1, \tag{6.21}$$

$$\boldsymbol{k}_A^{\lambda} = \boldsymbol{f}_A\left(t_0 + (\lambda+1)h, \boldsymbol{y}_{A,\lambda} + h\boldsymbol{k}_A^{\lambda}, \boldsymbol{y}_{L,0} + (\lambda+1)h\boldsymbol{k}_L\right), \tag{6.22}$$

$$\boldsymbol{y}_{L,1} = \boldsymbol{y}_{L,0} + H\boldsymbol{k}_L, \tag{6.23}$$

$$\boldsymbol{k}_L = \boldsymbol{f}_L\left(t_0 + H, \boldsymbol{y}_{A,0} + H\boldsymbol{k}_A^0, \boldsymbol{y}_{L,0} + H\boldsymbol{k}_L\right). \tag{6.24}$$

As stated above, since we will make use of this MRK scheme to evaluate the solution only on each compound step (only on the first microstep h_1 for the active components and on the macrostep H_1 for the latent components), we simply need to compute the $\boldsymbol{k}_A^0$ and $\boldsymbol{k}_L$ slopes. We do not have to compute the remaining $\boldsymbol{k}_A^{\lambda}$ active slopes. The $\boldsymbol{k}_A^0$ and $\boldsymbol{k}_L$ slopes have to be determined iteratively, by simultaneously solving the following subsystem of n_A nonlinear algebraic equations

$$\boldsymbol{k}_A^0 = \boldsymbol{f}_A\left(t_0 + h, \boldsymbol{y}_{A,0} + h\boldsymbol{k}_A^0, \boldsymbol{y}_{L,0} + h\boldsymbol{k}_L\right), \tag{6.25}$$

and the subsystem of n_L nonlinear algebraic equations of (6.24). Due to the stiffness difficulties reported in the previous section and the large Lipschitz constants involved, (6.24), (6.25) will be solved with the Newton-Raphson iterative solver, which in this case results in

$$\begin{bmatrix} \boldsymbol{k}_A^{0[r]} - \boldsymbol{f}_A\left(t_0+h, \boldsymbol{y}_{A,0}+h\boldsymbol{k}_A^{0[r]}, \boldsymbol{y}_{L,0}+h\boldsymbol{k}_L{}^{[r]}\right) \\ \boldsymbol{k}_L{}^{[r]} - \boldsymbol{f}_L\left(t_0+H, \boldsymbol{y}_{A,0}+H\boldsymbol{k}_A^{0[r]}, \boldsymbol{y}_{L,0}+H\boldsymbol{k}_L{}^{[r]}\right) \end{bmatrix}$$
$$+\begin{bmatrix} I - h\left[\frac{d\boldsymbol{f}_A}{d\boldsymbol{y}_A}\right]_{t=t_0+h}^{[r]} & h\left[\frac{d\boldsymbol{f}_A}{d\boldsymbol{y}_L}\right]_{t=t_0+h}^{[r]} \\ H\left[\frac{d\boldsymbol{f}_L}{d\boldsymbol{y}_A}\right]_{t=t_0+H}^{[r]} & I - H\left[\frac{d\boldsymbol{f}_L}{d\boldsymbol{y}_L}\right]_{t=t_0+H}^{[r]} \end{bmatrix} \begin{bmatrix} \boldsymbol{k}_A^{0[r+1]} - \boldsymbol{k}_A^{0[r]} \\ \boldsymbol{k}_L{}^{[r+1]} - \boldsymbol{k}_L{}^{[r]} \end{bmatrix} = 0, \tag{6.26}$$

where I is the $n \times n$ identity matrix.

Returning to the mixed method presented in this section, we must recall that the (6.21)-(6.24) MRK algorithm will be applied to perform a compound step in the (6.9), (6.10) partitioned differential algebraic system. So, this will turn (6.24) and (6.25) into subsystems of $n_A \times K_2$ and $n_L \times K_2$ nonlinear algebraic equations, respectively. As a consequence, we will have to solve a total of $n \times K_2$ linear equations on each iteration r in (6.26).

As described and illustrated above, after performing each compound step with the method of lines, the values for the active components at the remaining fine grid instants $\left(t_0+\lambda h_1, t_{2,j}\right)$, $\lambda = 2,\ldots,m,$ will be evaluated by applying the envelope transient over shooting technique to the active subsystem of (6.6). This means that we have to consider the discretization of the t_1 slow time scale defined by

$$t_0 + 2h_1 = t_{1,2} < \cdots < t_{1,\lambda} = t_0 + \lambda h_1 < \cdots < t_{1,m} = t_0 + H_1, \tag{6.27}$$

and replace the derivatives of (6.6) in t_1 with a finite-differences approximation, to obtain for each level $t_{1,\lambda}$ the boundary value problem

$$\boldsymbol{p}_A\left[\hat{\boldsymbol{y}}_{A,\lambda}\left(t_2\right), \hat{\boldsymbol{y}}_{L,\lambda}\left(t_2\right)\right] + \frac{\boldsymbol{q}_A\left[\hat{\boldsymbol{y}}_{A,\lambda}\left(t_2\right), \hat{\boldsymbol{y}}_{L,\lambda}\left(t_2\right)\right] - \boldsymbol{q}_A\left[\hat{\boldsymbol{y}}_{A,\lambda-1}\left(t_2\right), \hat{\boldsymbol{y}}_{L,\lambda-1}\left(t_2\right)\right]}{h_1}$$
$$+\frac{d\boldsymbol{q}_A\left[\hat{\boldsymbol{y}}_{A,\lambda}\left(t_2\right), \hat{\boldsymbol{y}}_{L,\lambda}\left(t_2\right)\right]}{dt_2} = \hat{\boldsymbol{x}}_\lambda\left(t_2\right), \tag{6.28}$$

with the periodic boundary condition

$$\hat{\boldsymbol{y}}_{A,\lambda}\left(0\right) = \hat{\boldsymbol{y}}_{A,\lambda}\left(T_2\right), \tag{6.29}$$

where $\hat{\boldsymbol{y}}_{A,\lambda}\left(t_2\right) \simeq \hat{\boldsymbol{y}}_A\left(t_{1,\lambda}, t_2\right)$, $\hat{\boldsymbol{y}}_{L,\lambda}\left(t_2\right) \simeq \hat{\boldsymbol{y}}_L\left(t_{1,\lambda}, t_2\right)$ and $\hat{\boldsymbol{x}}_\lambda\left(t_2\right) = \hat{\boldsymbol{x}}\left(t_{1,\lambda}, t_2\right)$. In order to evaluate the unknowns, $\hat{\boldsymbol{y}}_{A,\lambda}\left(t_2\right)$, each boundary value problem (6.28), (6.29) will be numerically solved with the shooting method, where the values of the latent components $\hat{\boldsymbol{y}}_{L,\lambda}\left(t_{2,j}\right)$ at the fine grid instants $\left(t_0+\lambda h_1, t_{2,j}\right)$ are obtained by interpolating the corresponding values at the coarse grid instants $\left(t_0, t_{2,j}\right)$ and $\left(t_0+H_1, t_{2,j}\right)$, previously computed with the method of lines MRK.

6.3.3 Active-Latent Partitioning Strategy

For a general RF circuit with dynamic subset partition, the active-latent partitioning strategy proposed in Section 6.2.2 for the pure method of lines MRK technique may also be used in the now proposed mixed method. By using MRK methods based in embedded RK formulas, when performing each compound step with the method of lines, we will be able to identify which are the active and which are the latent circuit's state variables. As mentioned, all the details of this partitioning strategy can be seen in [22], [38], or [39].

For a RF circuit with static subset partition, we can adopt the above strategy, where the partitioning implementation details are performed only on the first method of lines compound step. Alternatively, since there is no need to continuously classify the circuit's state variables, we may also adopt a different approach. This approach consists in starting to solve (6.3) in a uni-rate way (by using a pure RK method of lines technique, or, alternatively, a sole envelope transient over shooting technique), to then split (6.3) into (6.6), (6.7) according to the fluctuations of the state variables in the t_1 slow time dimension, and finally proceed in a multirate way, by evaluating the numerical solution of (6.6), (6.7) with the mixed method proposed in this section.

6.4 Experimental Results

6.4.1 Illustrative Application Example

In order to test the performance and the efficiency of the methods proposed in Sections 6.2 and 6.3, we will now discuss an illustrative application example. The heterogeneous circuit depicted in Figure 6.6 is a simplified power amplifier schematic of a wireless polar transmitter, constituting an alternative topology to the RF polar transmitter PA previously presented in Chapter 4. The most relevant components' values of this highly nonlinear multirate RF circuit are $V_{DD} = 25$ V, $L_3 = 400$ nH, $C_B = 16$ pF, $L_0 = 0.39$ pH, $C_0 = 16$ nF, $L_1 = 416$ pH, $C_1 = 16$ pF, $L_2 = 386$ pH, $C_2 = 15.6$ pF and $R = 50\ \Omega$, and the MOSFET is represented by the (4.11) simplified nonlinear device model.

In the same way as in the polar transmitter PA discussed in Chapters 4 and 5, in this circuit we have two independent baseband excitations, the $AM(t)$ and the $PM(t)$ signals, whose bandwidth is around 2 MHz. The $AM(t)$ signal is over-sampled with a digital clock of 50 MHz to get a desired pulse-width modulation format and the $PM(t)$ signal modulates the phase of a sinusoidal RF carrier of $f_C = 2$ GHz frequency. Also, in order to get highly efficient power amplification, the amplitude of the MOSFET driving voltage is set in a way that this device is forced to operate in switching mode. Additionally, a narrow bandpass filter is included, which provides the reconstruction of the $AM(t)$ signal as the envelope of the $v_O(t)$ output voltage.

With the exception of the baseband AM path (which was considered as ideal and so was not simulated at the circuit level), all the state variables of this circuit are very fast, i.e., evidence

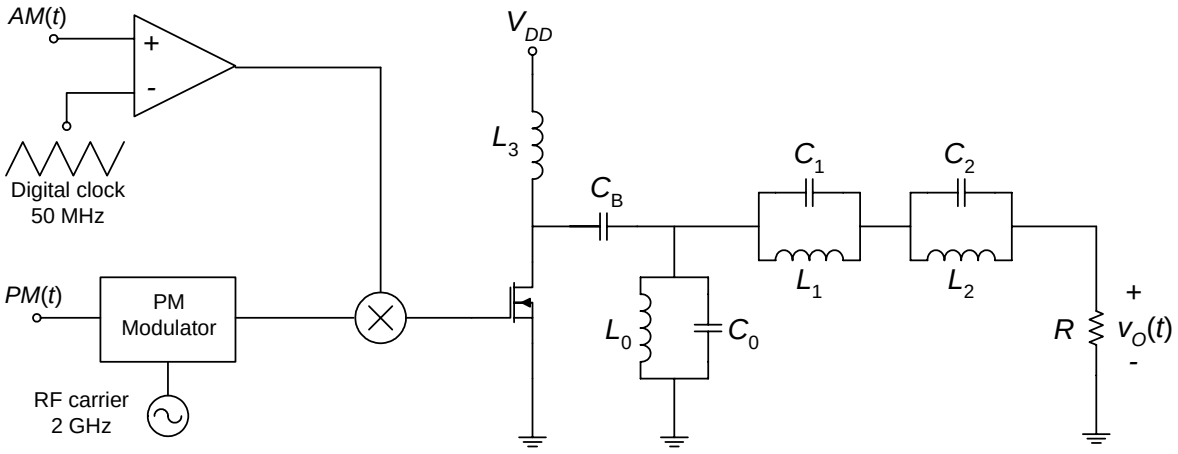

Figure 6.6 Simplified power amplifier schematic of a wireless polar transmitter.

fluctuations of 2 GHz frequency. However, it must be noted that, in spite of their common high speed characteristic, these state variables present envelopes with distinct time rates of change. For instance, while in the MOSFET gate voltage we have fast rectangular envelopes dictated by the AM branch PWM signals of 50 MHz fundamental frequency, at the output of the circuit we have slowly varying (smooth) envelopes of 2 MHz frequency.

Finally, it must be noted that due to the existence of PM signals in this sample application, we were forced once again to make use of the warped time concept within the bivariate formulation discussed along this chapter.

6.4.2 Numerical Simulation Results

The RF polar transmitter PA of Figure 6.6 was simulated in MATLAB® with the method proposed in Section 6.2 (the method of lines based on MRK schemes) and with the method proposed in Section 6.3 (the mixed method). Then, we compared both results with a purely envelope transient over shooting reference method (the technique used by commercial RF simulators for the time-domain simulation of strongly nonlinear 2-D multirate problems). In the same way as in Chapters 4 and 5, no comparison was made with any classical time-marching engine (univariate time-step integration), because the multivariate nature of the circuit operation would determine an unbearably large simulation time. Also, no comparison with any frequency-domain, or hybrid solvers, was performed, because the highly nonlinear regimes of the circuit would lead to an intolerably large quantity of harmonic components.

Numerical computation times (in seconds) for simulations in the [0, 20 ns] and [0, 100 ns] intervals are presented in Table 6.1. Uniform grids were assumed for simplicity in all cases: step size h_2 was chosen according to the rates of variation of the components in the t_2 fast time scale; step lengths h_1 and H_1 were chosen according to the time evolution rates of the active and latent

TABLE 6.1

COMPUTATION TIMES (COMPUTER: AMD 1.8 GHz, 700 MB RAM)

Simulation time interval	Proposed methods:		Reference method:
	Method of lines with MRK	Mixed method	Envelope transient over shooting
[0, 20 ns]	15 s	11 s	11 s
[0, 100 ns]	99 s	65 s	66 s

components, respectively, in the t_1 slow time scale. The (6.21)-(6.24) implicit MRK algorithm was used to perform the time-step integration in the pure method of lines technique and in the compound step integration of the mixed method. An explicit RK method of order 3 (Bogacki-Shampine [7]) was used to perform all the shooting iterations in both the mixed method and the pure envelope transient over shooting reference method.

By analyzing the computation times shown in Table 6.1 we can appreciate that no promising results were obtained with the simulation methods proposed in this chapter. As can be seen, no speedup advantages were achieved with any of the methods when we compared them with the reference method (envelope transient over shooting). In fact, while with the mixed method we have obtained approximately the same computation times, with the method of lines MRK the scenario becomes even worse, since increased computation times were obtained.

Finally, it must be stated that we have conducted several other simulations under different conditions (different initial conditions, different grid sizes, different time intervals), but the results obtained were always similar to the ones presented in Table 6.1. No substantial improvements were achieved in any case.

6.5 Conclusions

This chapter has been dedicated to the discussion of two innovative time-domain simulation techniques. The proposed methods are based on the mathematical method of lines and on the envelope transient over shooting technique, and operate within a bivariate framework of an aperiodic slow time scale and a periodic fast time scale. Both methods were especially conceived for simulating RF circuits whose state variables are all fluctuating in the fast carrier time scale, but, in opposition, are presenting different rates of variation in the slow envelope time dimension.

Although an alternative concept of subset circuit latency has been exploited, tests performed in an illustrative application example reveal, however, that no significant reductions of the computational work were achieved with the methods. The main reason for this inefficiency is the stiffness difficulties that arise from the semi-discretization of the problems in the fast time dimension and their time-step integration in the slow time dimension. Consequently, we are forced

to conclude that, despite both innovative methods may benefit from the existence of different rates of variation in the slow envelope time scale (by using a MRK scheme within the method of lines), the stiffness restrictive scenario will always severely constrain the efficiency of the methods.

Chapter 7

An Efficient Mixed Frequency-Time Simulation Method

7.1 Introduction

This chapter is dedicated to the discussion of an innovative mixed frequency-time method especially conceived for the efficient simulation of moderately nonlinear multirate RF circuits running in an aperiodic slow time scale and a periodic fast time scale. As seen in Chapter 3, a classical example of practical interest involving such time evolution characteristics refers to circuits driven by envelope modulated signals, in which the baseband signal (the information) is aperiodic and has a spectral content of much lower frequency than the periodic carrier. As discussed in Sections 3.4.2 and 3.5.4, if the waveforms produced by the circuit are not excessively demanding on the number of harmonics for a convenient frequency-domain representation, these typical multirate RF problems can be efficiently simulated with the envelope transient harmonic balance (ETHB) techniques. The ETHB handles the envelope in time-domain (time-step integration for determining the response to the slowly varying envelope) and the carrier in frequency-domain (HB for computing the steady-state response to the carrier).

Although the ETHB techniques can take advantage of the stimulus time-rate disparity and of the inexistence of highly nonlinear regimes, they do not perform any distinction between nodes or blocks within the circuit, that is to say, they treat all the circuit's state variables in the same way. Thus, if the circuit evidences some heterogeneity, ETHB simulation engines cannot benefit from such aspect.

In order to provide an illustrative explanation of the issues under discussion in this chapter, let us start by considering an RF circuit in which some of its state variables (node voltages and branch currents) are fast carrier envelope modulated waveforms, while the remaining state variables are slowly varying aperiodic signals. For concreteness, let us suppose that the signals

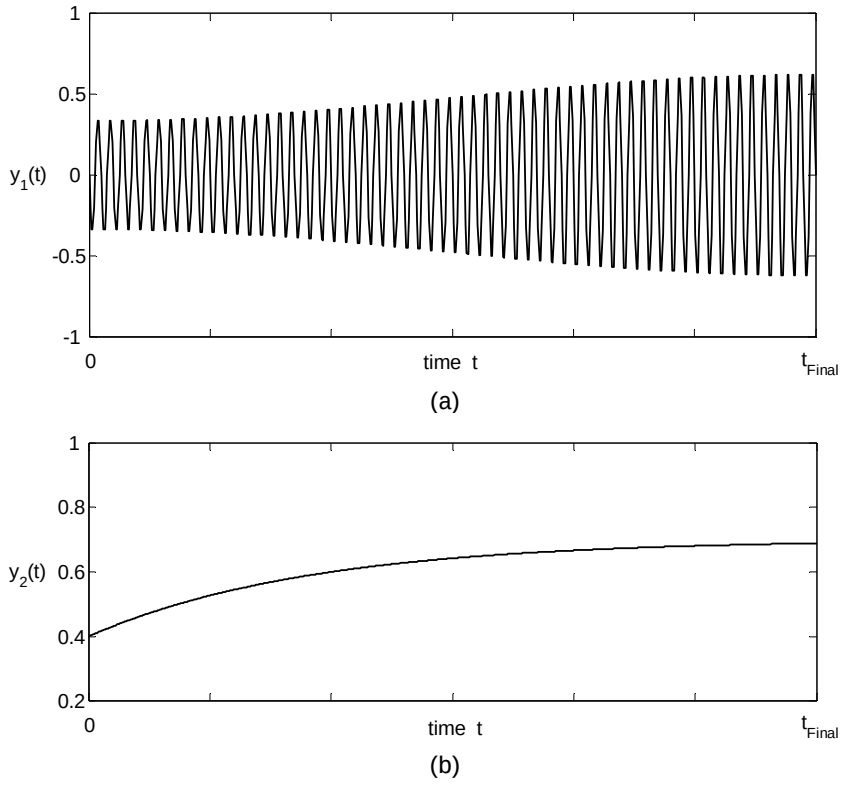

Figure 7.1 Two distinct state variables: (a) a fast carrier envelope modulated waveform, $y_1(t)$ (b) a slowly varying aperiodic baseband signal, $y_2(t)$.

$$\begin{aligned} y_1(t) &= \sum_{k=-K}^{K} Y_k(t) e^{jk2\pi f_C t}, \\ y_2(t) &= e(t), \end{aligned} \tag{7.1}$$

plotted in Figure 7.1(a) and (b), are two distinct state variables in different parts of the circuit. $Y_k(t)$ represents the Fourier coefficients of $y_1(t)$, which are slowly varying in the baseband time scale, f_C is the carrier frequency and $e(t)$ is a slowly varying aperiodic baseband function. The latency revealed by $y_2(t)$ indicates that this variable belongs to a circuit block where there are no fluctuations dictated by the fast carrier. Consequently, due to its slowness it can be represented efficiently with much less sample points than $y_1(t)$. On the other hand, since it does not evidence any periodicity, it can not be processed with harmonic balance. On the contrary, if the number of harmonics *K* is not too large, the fast carrier oscillation components of $y_1(t)$ can be efficiently computed in the frequency-domain. Consequently, since we are confronted with signals having completely different characteristics within the same problem, it is easy to conclude that distinct numerical strategies will be probably required for the evaluation of $y_1(t)$ and $y_2(t)$ if we want to simulate circuits having such signal format disparities in an efficient way.

Taking the above into account, in this chapter we will propose an innovative multirate ETHB method that is tailored to take advantage of this signal heterogeneity, i.e., that will benefit from the time-domain latency of some state variables in the circuits. As we will see in the next sections, because we will treat the aperiodic slowly varying state variables only in time domain, the proposed method can be seen as a hybrid scheme combining multitime ETHB [42], [43], [59], based on the MPDAE formulation, with a purely time-marching engine. By exploiting the subset circuit latency significant computation and memory savings will be achieved, which will lead to considerable reductions in the required simulation times. Simulation tests will be performed with an illustrative circuit example.

7.2 Innovative Simulation Method

7.2.1 Time-Domain Latency within the MPDAE Formulation

In view of the fact that multitime ETHB operates in a bi-dimensional framework, let us now consider the bivariate forms of $y_1(t)$ and $y_2(t)$, denoted by $\hat{y}_1(t_1,t_2)$ and $\hat{y}_2(t_1,t_2)$, and defined as

$$\begin{aligned} \hat{y}_1(t_1,t_2) &= \sum_{k=-K}^{K} Y_k(t_1) e^{jk2\pi f_C t_2}, \\ \hat{y}_2(t_1,t_2) &= e(t_1), \end{aligned} \tag{7.2}$$

where t_1 and t_2 are, respectively, the slow envelope time dimension and the fast carrier time dimension. Figure 7.2(a) and (b) depict the plots of these bivariate entities on the $[0,t_{Final}]\times[0,T_2]$ rectangular domain, where $T_2 = 1/f_C$ is the carrier period. As we can see, $\hat{y}_2(t_1,t_2)$ has no fluctuations in the t_2 fast time axis. In fact, it is so because $y_2(t)$ does not oscillate at the carrier frequency. Consequently, for each slow time instant $t_{1,i}$ defined on the grid

$$0 = t_{1,0} < t_{1,1} < \cdots < t_{1,i-1} < t_{1,i} < \cdots < t_{1,K_1} = t_{Final}, \qquad h_{1,i} = t_{1,i} - t_{1,i-1}, \tag{7.3}$$

while $\hat{y}_1(t_{1,i},t_2)$ is a waveform that has to be represented by a certain quantity $k=-K,\ldots,K$ of harmonic components, $\hat{y}_2(t_{1,i},t_2)$ is merely a constant (DC) signal that can be simply represented by the $k=0$ DC component. Therefore, there is not any necessity to perform the conversion between time and frequency domains for $\hat{y}_2(t_{1,i},t_2)$, which means that this state variable can be processed in a purely time-domain scheme.

7.2.2 Multitime ETHB

In order to provide an illustrative explanation of the method proposed in this chapter, we shall now study in more detail the multitime ETHB technique reported in Section 3.5.4. For achieving clarity in our explanation, let us once again consider the bivariate formulation described by the multitime

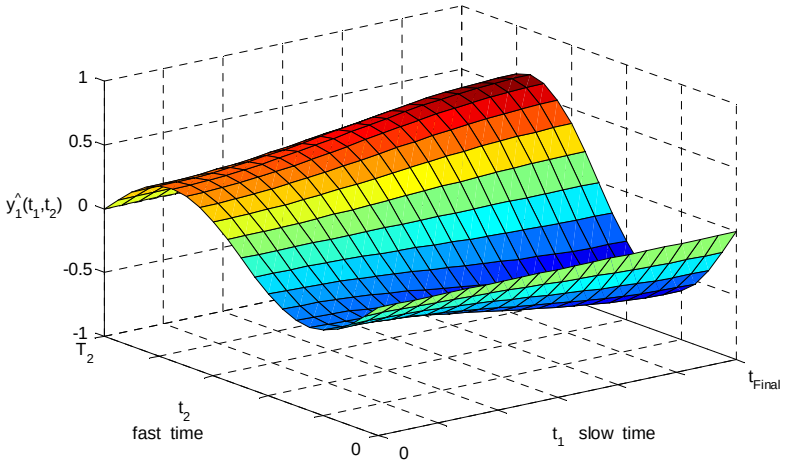

(a)

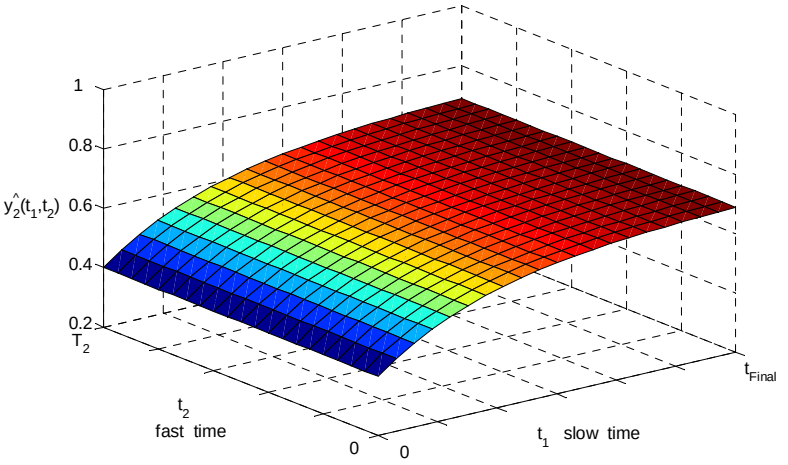

(b)

Figure 7.2 Bivariate forms of the state variables: (a) $\hat{y}_1$ and (b) $\hat{y}_2$.

partial differential algebraic system of (3.31), together with the condition expressing the periodic regime in the t_2 dimension,

$$\begin{gathered}\boldsymbol{p}\left[\hat{\boldsymbol{y}}(t_1,t_2)\right]+\frac{\partial \boldsymbol{q}\left[\hat{\boldsymbol{y}}(t_1,t_2)\right]}{\partial t_1}+\frac{\partial \boldsymbol{q}\left[\hat{\boldsymbol{y}}(t_1,t_2)\right]}{\partial t_2}=\hat{\boldsymbol{x}}(t_1,t_2),\\ \hat{\boldsymbol{y}}(t_1,0)=\hat{\boldsymbol{y}}(t_1,T_2),\end{gathered} \tag{7.4}$$

characterizing here the 2-D behaviour of a moderately nonlinear multirate RF circuit with *n* state variables, operating in an aperiodic slow time scale and a periodic fast carrier time scale. Let us also consider the semi-discretization of the rectangular domain $[0,t_{Final}]\times[0,T_2]$ in the t_1 slow time dimension defined by (7.3). As seen in the previous chapters, if we use a finite-differences scheme to approximate the derivatives of (7.4) in t_1, we obtain for each slow time instant $t_{1,i}$ a boundary value problem with periodic boundary conditions in the fast time t_2. If we use again the backward

Euler rule to replace the derivatives in t_1, we obtain the differential algebraic equations' system of (3.41), or (6.18), i.e.,

$$\begin{gathered}\boldsymbol{p}\left[\hat{\boldsymbol{y}}_i\left(t_2\right)\right]+\frac{\boldsymbol{q}\left[\hat{\boldsymbol{y}}_i\left(t_2\right)\right]-\boldsymbol{q}\left[\hat{\boldsymbol{y}}_{i-1}\left(t_2\right)\right]}{h_{1,i}}+\frac{d\boldsymbol{q}\left[\hat{\boldsymbol{y}}_i\left(t_2\right)\right]}{dt_2}=\hat{\boldsymbol{x}}_i\left(t_{1,i},t_2\right), \\ \hat{\boldsymbol{y}}_i\left(0\right)=\hat{\boldsymbol{y}}_i\left(T_2\right).\end{gathered} \tag{7.5}$$

In order to obtain the whole solution $\hat{\boldsymbol{y}}\left(t_1,t_2\right)$ in the entire rectangular domain $\left[0,t_{Final}\right]\times\left[0,T_2\right]$, a total of K_1 boundary value problems have to be solved. We have seen in Chapter 3 that with multitime ETHB the solution of each boundary value problem of (7.5) is evaluated by harmonic balance. The corresponding HB system for each slow time instant $t_{1,i}$ is the $n\times\left(2K+1\right)$ algebraic equations set given by (3.42), i.e.,

$$\mathbf{P}\left[\hat{\mathbf{Y}}\left(t_{1,i}\right)\right]+\frac{\mathbf{Q}\left[\hat{\mathbf{Y}}\left(t_{1,i}\right)\right]-\mathbf{Q}\left[\hat{\mathbf{Y}}\left(t_{1,i-1}\right)\right]}{h_{1,i}}+j\boldsymbol{\Omega}\mathbf{Q}\left[\hat{\mathbf{Y}}\left(t_{1,i}\right)\right]=\hat{\mathbf{X}}\left(t_{1,i}\right), \tag{7.6}$$

where $\hat{\mathbf{X}}\left(t_{1,i}\right)$ and $\hat{\mathbf{Y}}\left(t_{1,i}\right)$ are the vectors containing the Fourier coefficients of the excitation sources and of the solution (the state variables), respectively, at $t_1=t_{1,i}$. $\mathbf{P}\left(\bullet\right)$ and $\mathbf{Q}\left(\bullet\right)$ are unknown functions and $j\boldsymbol{\Omega}$ is the diagonal matrix (2.45), i.e.,

$$j\boldsymbol{\Omega}=\operatorname{diag}\left(\underbrace{-jK\omega_0,\ldots,jK\omega_0}_{v=1},\underbrace{-jK\omega_0,\ldots,jK\omega_0}_{v=2},\ldots,\underbrace{-jK\omega_0,\ldots,jK\omega_0}_{v=n}\right), \tag{7.7}$$

with $\omega_0=2\pi f_C$ (the carrier frequency). The $\hat{\mathbf{Y}}\left(t_{1,i}\right)$ vector can be expressed as

$$\hat{\mathbf{Y}}\left(t_{1,i}\right)=\left[\hat{\mathbf{Y}}_1\left(t_{1,i}\right)^T,\hat{\mathbf{Y}}_2\left(t_{1,i}\right)^T,\ldots,\hat{\mathbf{Y}}_n\left(t_{1,i}\right)^T\right]^T, \tag{7.8}$$

where each one of the state variable frequency components, $\hat{\mathbf{Y}}_v\left(t_{1,i}\right)$, $v=1,\ldots,n$, is a $\left(2K+1\right)\times1$ vector defined as

$$\hat{\mathbf{Y}}_v\left(t_{1,i}\right)=\left[Y_{v,-K}\left(t_{1,i}\right),\ldots,Y_{v,0}\left(t_{1,i}\right),\ldots,Y_{v,K}\left(t_{1,i}\right)\right]^T. \tag{7.9}$$

As seen in Chapter 2, since $p\left(\cdot\right)$ and $q\left(\cdot\right)$ are in general nonlinear functions, one possible way to compute $\mathbf{P}\left(\bullet\right)$ and $\mathbf{Q}\left(\bullet\right)$ in (7.6) consists in evaluating $p\left(\cdot\right)$ and $q\left(\cdot\right)$ in the time domain and then calculate its Fourier coefficients. The HB system of (7.6) can be rewritten as

$$\mathbf{F}\left[\hat{\mathbf{Y}}\left(t_{1,i}\right)\right]=\mathbf{P}\left[\hat{\mathbf{Y}}\left(t_{1,i}\right)\right]+\frac{\mathbf{Q}\left[\hat{\mathbf{Y}}\left(t_{1,i}\right)\right]-\mathbf{Q}\left[\hat{\mathbf{Y}}\left(t_{1,i-1}\right)\right]}{h_{1,i}}+j\boldsymbol{\Omega}\mathbf{Q}\left[\hat{\mathbf{Y}}\left(t_{1,i}\right)\right]-\hat{\mathbf{X}}\left(t_{1,i}\right)=0, \tag{7.10}$$

or, in its simplified form, as

$$\mathbf{F}\left[\hat{\mathbf{Y}}\left(t_{1,i}\right)\right]=0, \tag{7.11}$$

in which $\mathbf{F}\left[\hat{\mathbf{Y}}\left(t_{1,i}\right)\right]$ is known as the error function at $t_1 = t_{1,i}$. In order to solve the nonlinear algebraic system of (7.11) a Newton-Raphson iterative solver is usually used. In this case, the Newton-Raphson algorithm conducts us to

$$\mathbf{F}\left[\hat{\mathbf{Y}}^{[r]}\left(t_{1,i}\right)\right] + \left.\frac{d\mathbf{F}\left[\hat{\mathbf{Y}}\left(t_{1,i}\right)\right]}{d\hat{\mathbf{Y}}\left(t_{1,i}\right)}\right|_{\hat{\mathbf{Y}}\left(t_{1,i}\right)=\hat{\mathbf{Y}}^{[r]}\left(t_{1,i}\right)} \left[\hat{\mathbf{Y}}^{[r+1]}\left(t_{1,i}\right) - \hat{\mathbf{Y}}^{[r]}\left(t_{1,i}\right)\right] = 0, \tag{7.12}$$

which means that at each iteration r we have to solve a linear system of $n\times\left(2K+1\right)$ equations to compute the new estimate $\hat{\mathbf{Y}}^{[r+1]}\left(t_{1,i}\right)$. Consecutive Newton iterations will be computed until a desired accuracy is achieved, i.e., until $\left\|\mathbf{F}\left[\hat{\mathbf{Y}}\left(t_{1,i}\right)\right]\right\| < tol$, where *tol* is the allowed error ceiling.

As stated in Chapter 2, the system of (7.12) is typically a sparse linear system and several methods can be used to solve it, such as direct solvers, sparse solvers, or iterative solvers. But for very large systems iterative solvers are usually preferred, and there is a general consensus that the GMRES [61] iterative technique is the preferred one for harmonic balance analysis. The system of (7.12) involves the derivative of the vector $\mathbf{F}\left[\hat{\mathbf{Y}}\left(t_{1,i}\right)\right]$, with respect to the vector $\hat{\mathbf{Y}}\left(t_{1,i}\right)$. The result is a matrix, the so-called Jacobian of $\mathbf{F}\left[\hat{\mathbf{Y}}\left(t_{1,i}\right)\right]$,

$$\mathbf{J}\left[\hat{\mathbf{Y}}\left(t_{1,i}\right)\right] = \frac{d\mathbf{F}\left[\hat{\mathbf{Y}}\left(t_{1,i}\right)\right]}{d\hat{\mathbf{Y}}\left(t_{1,i}\right)} = \begin{bmatrix} \dfrac{d\mathbf{F}_1\left[\hat{\mathbf{Y}}\left(t_{1,i}\right)\right]}{d\hat{\mathbf{Y}}_1\left(t_{1,i}\right)} & \dfrac{d\mathbf{F}_1\left[\hat{\mathbf{Y}}\left(t_{1,i}\right)\right]}{d\hat{\mathbf{Y}}_2\left(t_{1,i}\right)} & \cdots & \dfrac{d\mathbf{F}_1\left[\hat{\mathbf{Y}}\left(t_{1,i}\right)\right]}{d\hat{\mathbf{Y}}_n\left(t_{1,i}\right)} \\ \dfrac{d\mathbf{F}_2\left[\hat{\mathbf{Y}}\left(t_{1,i}\right)\right]}{d\hat{\mathbf{Y}}_1\left(t_{1,i}\right)} & \dfrac{d\mathbf{F}_2\left[\hat{\mathbf{Y}}\left(t_{1,i}\right)\right]}{d\hat{\mathbf{Y}}_2\left(t_{1,i}\right)} & \cdots & \dfrac{d\mathbf{F}_2\left[\hat{\mathbf{Y}}\left(t_{1,i}\right)\right]}{d\hat{\mathbf{Y}}_n\left(t_{1,i}\right)} \\ \cdots & \cdots & \cdots & \cdots \\ \dfrac{d\mathbf{F}_n\left[\hat{\mathbf{Y}}\left(t_{1,i}\right)\right]}{d\hat{\mathbf{Y}}_1\left(t_{1,i}\right)} & \dfrac{d\mathbf{F}_n\left[\hat{\mathbf{Y}}\left(t_{1,i}\right)\right]}{d\hat{\mathbf{Y}}_2\left(t_{1,i}\right)} & \cdots & \dfrac{d\mathbf{F}_n\left[\hat{\mathbf{Y}}\left(t_{1,i}\right)\right]}{d\hat{\mathbf{Y}}_n\left(t_{1,i}\right)} \end{bmatrix} \tag{7.13}$$

which has a block structure, consisting of an $n\times n$ matrix of square submatrices (blocks), each one with dimension $\left(2K+1\right)$. Each block contains information about the harmonic components corresponding to the sensitivity of changes in a component of the error function $\mathbf{F}\left[\hat{\mathbf{Y}}\left(t_{1,i}\right)\right]$, resulting from changes in a specific state variable. The general block of row m and column l can be expressed as

$$\frac{d\mathbf{F}_m\left[\hat{\mathbf{Y}}\left(t_{1,i}\right)\right]}{d\hat{\mathbf{Y}}_l\left(t_{1,i}\right)} = \frac{d\mathbf{P}_m\left[\hat{\mathbf{Y}}\left(t_{1,i}\right)\right]}{d\hat{\mathbf{Y}}_l\left(t_{1,i}\right)} + \frac{1}{h_{1.i}}\frac{d\mathbf{Q}_m\left[\hat{\mathbf{Y}}\left(t_{1,i}\right)\right]}{d\hat{\mathbf{Y}}_l\left(t_{1,i}\right)} + j\Omega\frac{d\mathbf{Q}_m\left[\hat{\mathbf{Y}}\left(t_{1,i}\right)\right]}{d\hat{\mathbf{Y}}_l\left(t_{1,i}\right)}, \tag{7.14}$$

where $j\Omega$ is the diagonal matrix $j\Omega = \mathrm{diag}\left(-jK\omega_0,\ldots,0,\ldots,jK\omega_0\right)$ and $d\mathbf{P}_m\left[\hat{\mathbf{Y}}\left(t_{1,i}\right)\right]\Big/d\hat{\mathbf{Y}}_l\left(t_{1,i}\right)$ and $d\mathbf{Q}_m\left[\hat{\mathbf{Y}}\left(t_{1,i}\right)\right]\Big/d\hat{\mathbf{Y}}_l\left(t_{1,i}\right)$ denote, respectively, the conversion matrices (Toeplitz) [44] of the vectors containing the Fourier coefficients of $dp_m\left[\hat{y}\left(t_{1,i},t_2\right)\right]\Big/d\hat{y}_l\left(t_{1,i},t_2\right)$ and $dq_m\left[\hat{y}\left(t_{1,i},t_2\right)\right]\Big/d\hat{y}_l\left(t_{1,i},t_2\right)$.

7.2.3 Multirate Multitime ETHB

As stated and illustrated above, bivariate forms of latent state variables have no undulations in the t_2 fast time scale. As seen, for each slow time instant $t_{1,i}$ they are merely constant (DC) node voltages or branch currents, which indicate that they can be completely represented only by the corresponding $k=0$ order Fourier coefficients. So, while active state variables have to be represented by a set of $(2K+1)$ harmonic components arranged in vectors of the form of (7.9), latent state variables can be represented as scalar quantities, i.e.,

$$\hat{\mathbf{Y}}_v\left(t_{1,i}\right)=Y_{v,0}\left(t_{1,i}\right)=\hat{y}_v\left(t_{1,i}\right). \tag{7.15}$$

Taking this into account, it is easy to conclude that the size of the $\hat{\mathbf{Y}}\left(t_{1,i}\right)$ vector defined by (7.8) can be considerably reduced, as also the total number of equations in the HB system of (7.10). An additional and important detail is that there is no longer obligation to perform the conversion between time and frequency domains for the latent state variables expressed in the form of (7.15), as well as for the components of $\mathbf{F}\left[\hat{\mathbf{Y}}\left(t_{1,i}\right)\right]$ corresponding to latent blocks of the circuit. Since the $k=0$ order Fourier coefficient $Y_{v,0}\left(t_{1,i}\right)$ is exactly the same as the constant t_2 time value $\hat{y}_v\left(t_{1,i}\right)$, the use of the discrete Fourier transform (DFT) and the inverse discrete Fourier transform (IDFT) – or their fast algorithms, i.e., the fast Fourier transform (FFT) and the inverse fast Fourier transform (IFFT) – will be required only for components in the HB system of (7.10) having dependence on active state variables.

In what the Jacobian matrix (7.13) is concerned, significant matrix size reductions will be achieved, too. In effect, by taking into consideration this multirate characteristic (the subset circuit latency), some of the blocks of (7.13) will be merely 1×1 scalar elements, that contain DC information on the sensitivity of changes in components of $\mathbf{F}\left[\hat{\mathbf{Y}}\left(t_{1,i}\right)\right]$ resulting from changes in latent components of $\hat{\mathbf{Y}}\left(t_{1,i}\right)$. For instance, if the m^{th} component of (7.5) is exclusively dependent on latent state variables and $\hat{y}_l\left(t_{1,i}\right)$ is itself a latent state variable, then the block of row m and column l will simply be given by

$$\frac{d\mathbf{F}_m\left[\hat{\mathbf{Y}}\left(t_{1,i}\right)\right]}{d\hat{\mathbf{Y}}_l\left(t_{1,i}\right)}=\frac{dp_m\left[\hat{y}\left(t_{1,i}\right)\right]}{d\hat{y}_l\left(t_{1,i}\right)}+\frac{1}{h_{1,i}}\frac{dq_m\left[\hat{y}\left(t_{1,i}\right)\right]}{d\hat{y}_l\left(t_{1,i}\right)}. \tag{7.16}$$

The 1×1 (scalar) Jacobian matrix block of (7.16) can be viewed as a special case of the general $(2K+1)\times(2K+1)$ block of (7.14), if we assume $K=0$ as the maximum harmonic order. In fact, since $df_m\left[\hat{y}\left(t_{1,i},t_2\right)\right]/d\hat{y}_l\left(t_{1,i},t_2\right)=df_m\left[\hat{y}\left(t_{1,i}\right)\right]/d\hat{y}_l\left(t_{1,i}\right)$ is a basic constant function presenting no fluctuations in the t_2 fast time scale, there will be no necessity to convert the right hand side terms of (7.16) into the frequency domain. On the other hand, the third term of (7.14) will be simply discarded.

From the above considerations we are able to expect that significant computation and memory savings may be achieved when finding the solution of the HB system of (7.10). Indeed, with the

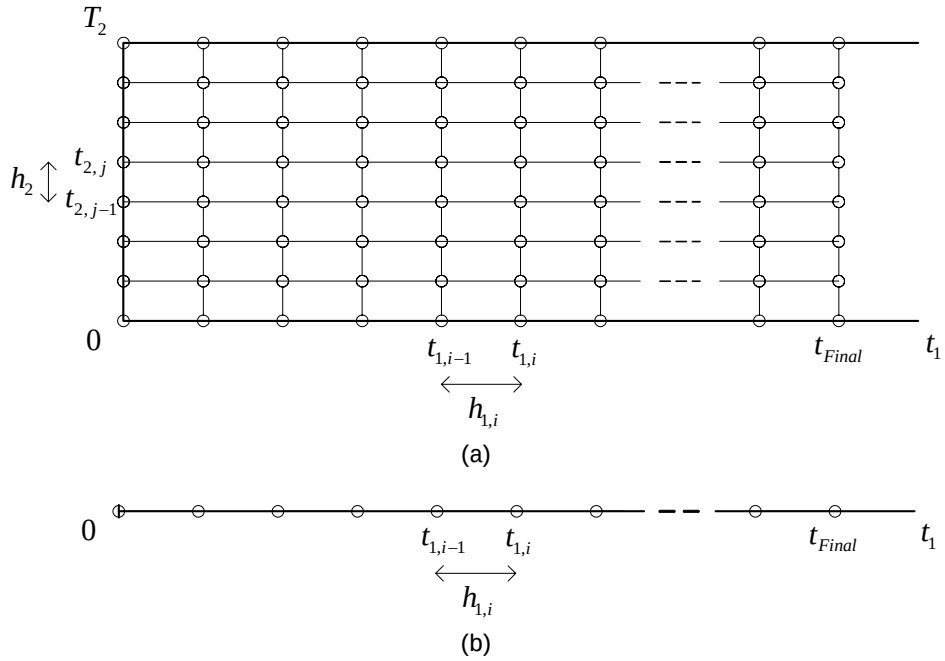

Figure 7.3 Bivariate and univariate grids: (a) active state variables and (b) latent state variables.

state variable $\hat{\mathbf{Y}}\left(t_{1,i}\right)$ and the error function $\mathbf{F}\left[\hat{\mathbf{Y}}\left(t_{1,i}\right)\right]$ vector size reductions, as also the resulting Jacobian $\mathbf{J}\left[\hat{\mathbf{Y}}\left(t_{1,i}\right)\right]$ matrix size reduction, we can avoid dealing with large linear systems in the iterations of (7.12). Thus, a less computationally expensive Newton-Raphson iterative solver will be required.

A final remark that refers to the disparity between active and latent blocks of a circuit, regards the number of time samples used for representing the corresponding state variables. As suggested above, the number of sample points required for the active and the latent parts will be obviously different. In fact, according to the adopted harmonic truncation at least $N=\left(2K+1\right)$ sample points per slow time instant $t_{1,i}$ will be needed for computing the active state variables' waveforms in the t_2 dimension. In contrast, only one time sample will be required for representing the latent state variables at each time instant $t_{1,i}$. So, what we are actually doing with this proposed multirate multitime ETHB method is to process the active state variables in a bi-dimensional mixed frequency-time domain scheme – where the envelope is processed in the t_1 slow time scale, while the steady-state response to the carrier is processed in the frequency-domain – and the latent state variables in a purely one-dimensional time-domain engine. That is, bivariate forms of the active state variables are discretized in both the t_1 and t_2 dimensions of the $\left[0,t_{Final}\right]\times\left[0,T_2\right]$ rectangular domain, according to (7.3) and to the following uniform grid,

$$0=t_{2,0}<t_{2,1}<\cdots<t_{2,j-1}<t_{2,j}<\cdots<t_{2,K_2}=T_2,\qquad h_2=t_{2,j}-t_{2,j-1}=T_2/K_2, \tag{7.17}$$

where $K_2\geq 2K+1$ is the total number of sample points used per slow time instant $t_{1,i}$. On an opposite scenario, latent state variables are treated as purely univariate t_1 slow time dependent

entities, being evaluated only on the one-dimensional grid defined by (7.3). This is illustrated in Figure 7.3(a) and (b).

7.2.4 Circuit Partitioning Strategy

In order to put into practice a multitime ETHB simulator capable to benefit from the multirate approach presented above, a partitioning strategy allowing automatic classification of the circuit's state variables (as active or latent) must be included in the simulation package. Similarly to what we have proposed for the methods discussed in the previous chapters, we will now present a circuit partitioning strategy with two distinct variants, which will split the circuit into active and latent sub-circuits according to the time rates of change of its state variables. The former is conceived for RF circuits with dynamic subset division (circuits in which the partition into active and latent sub-circuits may vary with time), and the later is tailored for RF circuits with static subset division (circuits in which the partition does not change along the simulation process). These strategy variants are described in detail the following.

For a general RF circuit with dynamic active-latent partition, we iteratively solve the periodic boundary value problem of (7.5) at each slow time instant $t_{1,i}$ using the "uni-rate" multitime ETHB engine [42], [43], [59] on the first iteration of (7.12), and the multirate multitime ETHB method on the subsequent iterations. With this methodology we start by considering all the circuit's state variables as active, that is, we start by representing all the state variables in the frequency domain as a set of $(2K+1)$ harmonic components. Thus, in way to obtain the solution of the HB system of (7.10) a single Newton iteration (7.12) is carried out to achieve $\hat{\mathbf{Y}}^{[1]}(t_{1,i})$. Each one of its state variable Fourier coefficients vector, $\hat{\mathbf{Y}}_v^{[1]}(t_{1,i})$, is then examined. With the exception of the $k=0$ order (DC component), state variables whose Fourier coefficients' absolute values are all practically zero (stay under a very small prescribed error tolerance) will be classified as latent. The remaining state variables will be classified as active. After this state variable classification, which will temporarily divide the circuit into active and latent sub-circuits, we automatically switch to the multirate multitime ETHB scheme (benefiting from all the advantages described above) to perform the subsequent numerical iterations that will conduct to the solution of (7.5).

We would like to point out that more than one iteration with the "uni-rate" multitime ETHB engine may be required to be executed before switching to the multirate multitime ETHB technique. This will increase the robustness of the above partitioning strategy. However, it obviously will conduct to some efficiency reduction of the method. We may also note that the state variable classification described above could be defined in time domain, too. For instance, when we perform inverse Fourier transformation of $\hat{\mathbf{Y}}^{[1]}(t_{1,i})$, to get its time domain equivalent, $\hat{y}^{[1]}(t_{1,i},t_2)$, the latent state variables will be those that practically evidence no fluctuations in the fast time t_2.

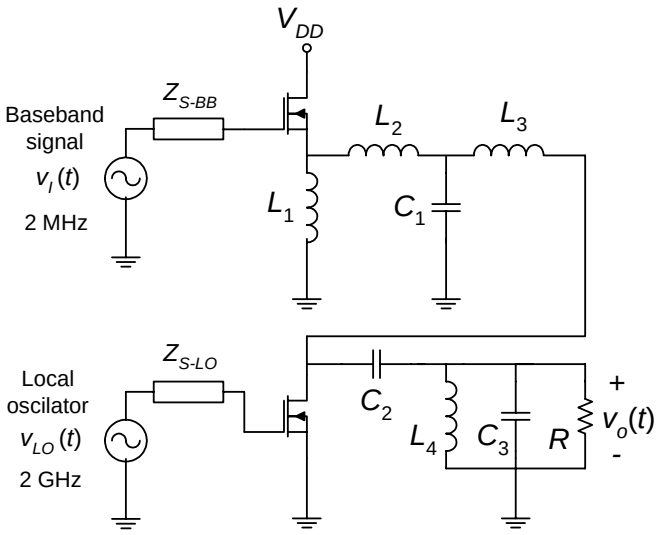

Figure 7.4 Simplified resistive FET mixer used in wireless transmitters.

Since many RF circuits have a static subset partition (as is the case of our RF sample application presented in Section 7.3), it will be helpful if we can profit from this feature. That is, a more suitable circuit partitioning strategy than the one presented above will certainly reduce the computational effort. In this case we have decided to proceed as follows. We start by computing the solution of the periodic boundary value problem of (7.5) for the first slow time instant $t_{1,1}$ using exclusively the "uni-rate" multitime ETHB engine. Then, we split the circuit into active and latent sub-circuits, according to the fluctuations of the state variables $\hat{y}_v\left(t_{1,1},t_2\right)$ in the t_2 fast time scale. Those which do not evidence oscillations in t_2 will be classified as latent. The remaining will be classified as active. This classification will provide a permanently active-latent sub-circuit division, and based on it we will proceed computing the solution of the problem for the remaining $t_{1,i}=t_{1,2},\ldots,t_{1,K_1}$ slow time instants with the new proposed multirate multitime ETHB technique.

7.3 Experimental Results

7.3.1 Application Example

With the purpose of testing the capabilities of the method proposed in this chapter, we will now discuss an illustrative application example. The nonlinear circuit of Figure 7.4 is a simplified resistive FET mixer schematic of a wireless transmitter [26]. This circuit includes two independent excitations of very separated time scales: the baseband input signal, $v_I(t)$, whose bandwidth is around 2 MHz, and the RF carrier of f_C = 2 GHz frequency. We must note that beyond the mix of periodic (RF carrier) and aperiodic (baseband input signal) forcing functions of very distinct time scales, in this nonlinear circuit we have also a combination of heterogeneous state variables with

widely disparate rates of variation. In fact, for instance, while the L_4 inductor current and the C_3 capacitor voltage of the output bandpass filter are very fast (they oscillate at a rhythm dictated by the RF carrier, and thus will be detected as active state variables), the L_1 inductor current and the C_1 capacitor voltage are both much slower (and thus will be detected as latent state variables). The most relevant components' values of this circuit are $V_{DD} = 5$ V, $L_1 = 40$ μH, $L_2 = 20$ nH, $L_3 = 20$ nH, $L_4 = 0.4$ nH, $C_1 = 0.5$ nF, $C_2 = 16$ pF, $C_3 = 16$ pF and $R = 50$ Ω, and the MOSFETs are represented by the simplified nonlinear device model of (4.11), with $\alpha = 1\ \mathrm{V}^{-1}$, $\beta = 0.025$ A/V, $K_T = 2$ and $V_T = 1$ V. The amplitude of the driving voltages of both MOSFETs were set so that the devices operate in moderately nonlinear regimes.

7.3.2 Numerical Simulation Results

The resistive FET mixer of Figure 7.4 was simulated in MATLAB® with the proposed innovative multirate multitime ETHB technique versus the corresponding "uni-rate" multitime ETHB engine [42], [43], [59]. A simple 2 MHz purely sinusoidal regime was considered for the baseband excitation. Since frequency-domain methods are much more efficient than their time-domain rivals when simulating weakly nonlinear circuits, no comparison was made with any purely time-domain engine, such as envelope transient over shooting, envelope transient over FDTD, or one-dimensional time-step integration (SPICE-like simulation). Actually, as stated above in this chapter, and mentioned in Chapter 3, ETHB is in effect the most suitable traditional technique for solving moderately nonlinear circuits involving envelope modulated signals, which is the reason why it is commonly used by commercial RF tools to simulate this kind of problems in a very efficient way.

Figures 7.5 and 7.6 show the bivariate solutions on the $[0, 0.5\,\mu\mathrm{s}]\times[0, 0.5\,\mathrm{ns}]$ rectangular domain, for the RF transistor drain voltage and the output voltage of the circuit, respectively. These are examples of fast-varying (active) state variables in the circuit, which is the reason why they were computed in the bi-dimensional t_1, t_2 framework. Plots of the one-dimensional versions of these state variables, recovered from their corresponding multivariate forms by setting $y_v(t) = \hat{y}_v(t, t \bmod T_2)$, are depicted in Figures 7.7 and 7.8, for the [0, 40 ns] time interval.

Figures 7.9 and 7.10 depict the univariate solutions in the [0, 0.5 μs] time interval, for the baseband transistor source voltage and the L_1 inductor current. Now, these are slowly varying (latent) state variables in the circuit, and thus they were evaluated in a purely one-dimensional time-domain scheme.

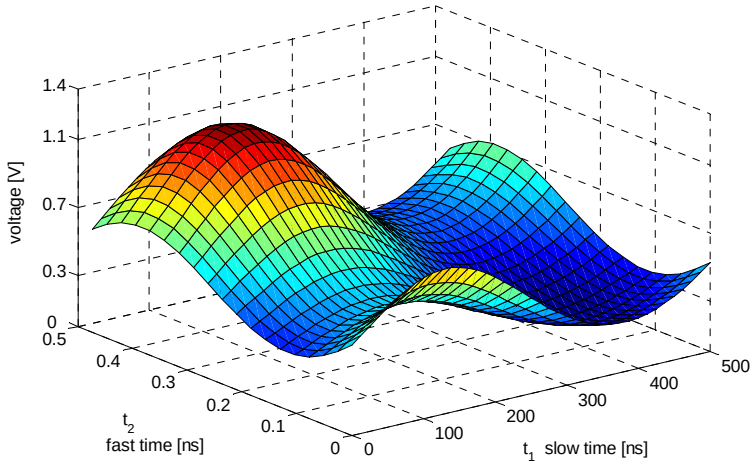

Figure 7.5 Bivariate RF transistor drain voltage.

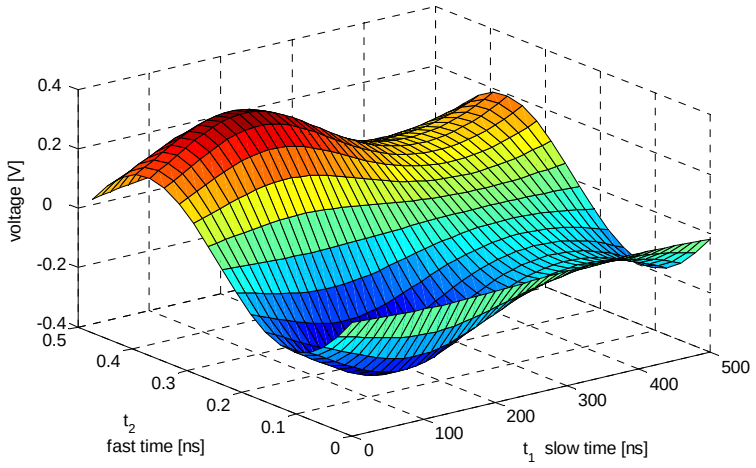

Figure 7.6 Bivariate output voltage.

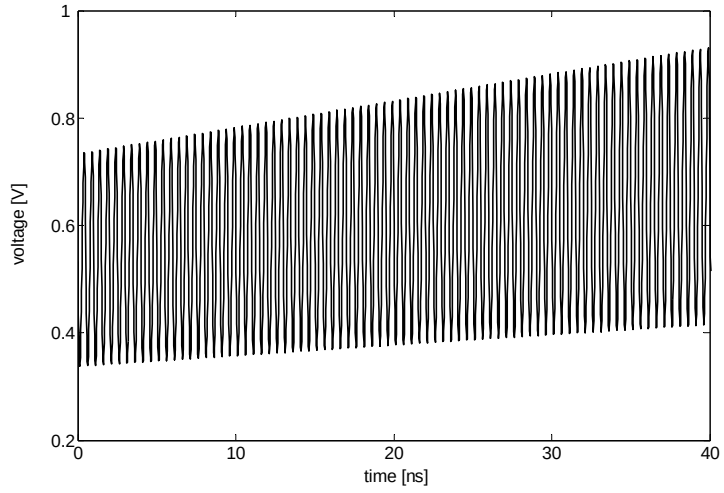

Figure 7.7 Univariate RF transistor drain voltage.

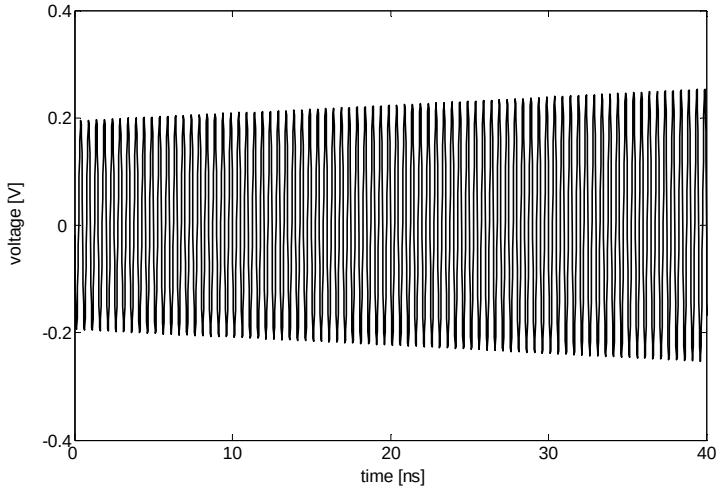

Figure 7.8 Univariate output voltage.

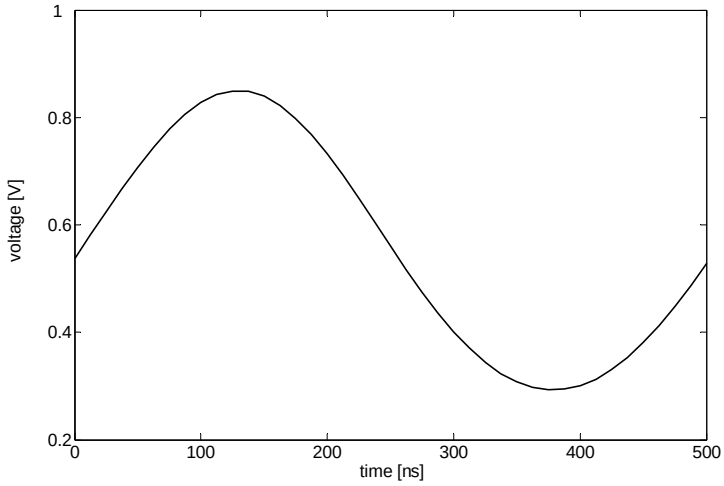

Figure 7.9 Univariate baseband transistor source voltage.

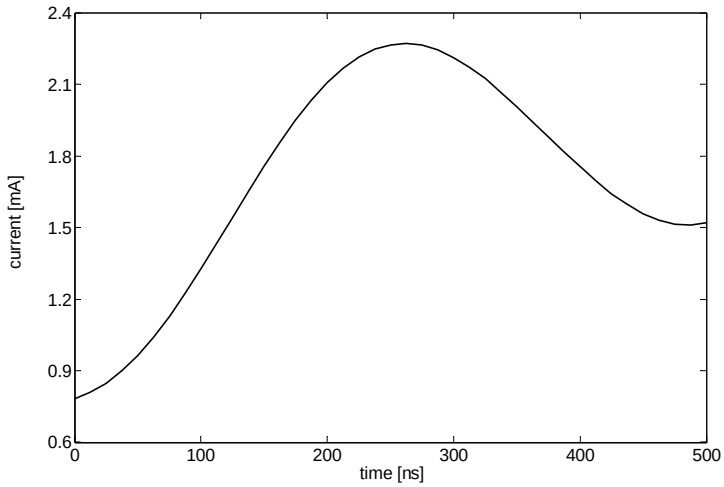

Figure 7.10 Univariate L_1 inductor current.

TABLE 7.1

COMPUTATION TIMES WITH K = 7 (COMPUTER: AMD 1.8 GHz, 700 MB RAM)

Simulation time interval	Multirate multitime ETHB (new method)	"Uni-rate" multitime ETHB	Speedup (approx.)
[0, 0.5 μs]	1.9 s	3.3 s	1.7
[0, 5.0 μs]	15.5 s	28.5 s	1.8

TABLE 7.2

COMPUTATION TIMES WITH K = 9 (COMPUTER: AMD 1.8 GHz, 700 MB RAM)

Simulation time interval	Multirate multitime ETHB (new method)	"Uni-rate" multitime ETHB	Speedup (approx.)
[0, 0.5 μs]	2.1 s	4.6 s	2.2
[0, 5.0 μs]	19.3 s	42.5 s	2.2

Numerical computation times (in seconds) for simulations in the [0, 0.5 μs] and [0, 5.0 μs] intervals are presented in Tables 7.1 and 7.2. A uniform grid was assumed for simplicity in the t_1 slow time scale, in which we have chosen $h_1 = 12.5$ ns as the step size in that dimension. In what the t_2 fast carrier time scale is concerned, two slightly distinct sampling rates were considered: in our first experiments, reported in Table 7.1, we considered $K = 7$ as the maximum harmonic order for the HB evaluations ($2K+1=15$ sample points were used); then, in order to achieve an improved solution with some higher accuracy, $K = 9$, that is, $2K+1=19$ sample points were assumed in the experiments reported in Table 7.2.

As we can see, speedups of approximately 2 times were obtained for the simulation of our illustrative circuit example with the new method. By comparing Tables 7.1 and 7.2 we can also attest the expected occurrence of a small speedup increase, when we raise the order of the harmonic truncation from $K = 7$ to $K = 9$.

Several other simulations under different conditions (different initial conditions, different grid sizes, diverse baseband signals and diverse time intervals) were conducted, and the results in terms of speedup were always similar to the ones presented in Tables 7.1 and 7.2.

Although speedups of 2 times may not seem very promising or satisfactory, it must be noted that the number of active and latent state variables in the resistive FET mixer depicted in Figure 7.4 is approximately the same. This is, indeed, an illustrative example of very small size. Thus, if we take into account the characteristics of the multirate multitime ETHB method proposed in this chapter, we can easily anticipate that considerably increased speedups in simulation time will be

obtained when computing the solution of RF networks having latent subsets much bigger than their active ones.

7.4 Conclusions

In this chapter, an innovative mixed frequency-time method, especially conceived for the efficient simulation of moderately nonlinear multirate RF circuits, has been presented and tested in an illustrative application example. The method is tailored for circuits running in an aperiodic slow time scale and a periodic fast time scale, within a disparate scenario of slowly varying (latent) and fast-varying (active) state variables. It can be seen as a hybrid scheme that combines multitime ETHB based on the MPDAE formulation with a purely time-marching engine, in which active state variables are processed in a bivariate mixed frequency-time domain, whereas latent state variables are treated in a purely one-dimensional time-domain approach. By exploiting the subset circuit latency, i.e., by taking advantage of the fact that there is no necessity to perform the conversion between time and frequency domains for the latent state variables, significant computation and memory savings may be achieved, without compromising accuracy. As the efficiency of the method is strongly dependent on the relation between the number of latent and the number of active state variables, it is reasonable to expect that it will perform very well when simulating RF networks containing a large number of latent blocks.

Chapter 8
Conclusions and Future Work

8.1 Conclusions

The work developed in this thesis was very challenging. However, it also revealed very gratifying. First, because the objectives stated in Chapter 1 were fulfilled. Second, because the achievements of this work were recognized by the scientific and technical community, through the papers already published in some major peer reviewed international conferences and journals. Significant gains in computation speed were achieved with three powerful innovative numerical methods that were proposed for the efficient simulation of nonlinear heterogeneous RF circuits. Two of them operate in a purely time-domain framework and a third operates in a mixed frequency-time domain approach. Although some individual conclusions have already been reported at the end of Chapters 4, 5, 6 and 7, we will now summarize in the following the most important results of this work.

One of the most relevant innovative techniques proposed in this work is the inclusion of modern multirate Runge-Kutta methods within multivariate frameworks defined in warped time domains. In their genesis, MRK methods were conceived for the time-step integration of univariate initial value problems and until now they were only utilized to compute the transient response of electronic circuits. Here they were applied to the modulated periodic steady-state response within a time-domain envelope following method (the envelope transient over shooting method) working in a warped time domain. So, beyond the decoupling of the components of the signals into different time dimensions, and the accommodation of PM signals, this strategy allowed us to benefit from the different rates of variation of slowly varying (latent) and fast-varying (active) currents and voltages (state variables) in the circuit. As seen in Chapter 4, this time-domain technique revealed very efficient for the simulation of highly heterogeneous and strongly nonlinear RF circuits operating in two distinct time scales.

Another important innovative strategy presented in this thesis is the use of the method of lines for creating a new form of 2-D shooting. We named this new form as multiple-line double

multirate shooting, and it has demonstrated to be much more efficient than the well-known hierarchical shooting. The key to the success of this new form of 2-D shooting relies on the need for only one shooting loop, and on the multipartitioning of the circuit into sub-circuits, to benefit from the use of multirate schemes. With this innovative shooting technique is was possible to conceive a 3-D envelope oriented method tailored to take advantage of the circuits' heterogeneity and stimuli time-rate disparities. Such numerical method was discussed in Chapter 5 and revealed particularly suitable for the efficient time-domain simulation of strongly nonlinear mixed digital, baseband and RF circuits operating in three disparate time scales.

A significant aspect that has to be taken into consideration whenever time-step integration engines are used is the possible occurrence of numerical stiffness. This phenomenon causes serious difficulties in the performance of the methods and so, if possible, it must be avoided. Otherwise, it may severely constrain the efficiency of the numerical simulation algorithms. This is what happened with the methods proposed in Chapter 6, where it was not yet possible to prevent the occurrence of a stiffness restrictive scenario.

An additional and significant innovative technique presented in this thesis is the mixed frequency-time method addressed in Chapter 7, named as multirate multitime ETHB. This method, especially conceived for the efficient simulation of moderately nonlinear multirate RF circuits, is a hybrid scheme that splits the circuits into different parts, in which some are treated in a purely time-domain way, while others are treated in a mixed frequency-time manner with the ETHB engine. Taking into account the popularity of frequency-domain solvers, as HB, or mixed frequency-time engines, as ETHB, in the microwave community, we believe that this method has a very promising potential.

Finally, it must be noted that a key aspect to the success of the numerical methods proposed in this thesis was the automatic multipartitioning of the circuits into sub-circuits according to the time rates of change of their state variables. Due to the heterogeneity of the circuits under analysis, and the consequent disparity between signals in their different parts, this turned out to be a crucial detail.

8.2 Future Work

To conclude the present thesis this section summarizes some opportunities for future research work. A few areas that are of interest will be presented in the following.

An important area where further work is needed is the analysis of circuits containing multi aperiodic regimes. As seen, all the methods discussed in this thesis handled periodic and aperiodic regimes of widely separated rates of change, and they all operate within multidimensional time (or warped time) frameworks. However, when two, or more, aperiodic time scales were present, these time scales had to be mixed in the same time dimension. Such situation occurred in both of the

methods proposed in Chapter 6, where the two distinct envelope time scales had to be treated in the same aperiodic slow time dimension. In effect, we had already shown in Chapter 3 that the powerful multivariate strategy based on the MPDAE (or WaMPDAE) formulation becomes useless when multirate signals do not evidence any periodicity in their components. Thus, if we have for example a circuit whose state variables evolve according to distinct aperiodic regimes of widely separated rates of change, and the fastest regime is present in all the circuit's state variables, then we have no choice than to use a classic uni-rate SPICE-like engine to compute its solution in the one-dimensional time. Indeed, in such case, it is not even possible to use a MRK scheme for performing the time-step integration of the DAE system describing the circuit's operation. Similar difficulties arise when one, or more, periodic regimes are also added to the circuit. For instance, if an RF carrier of 2 GHz frequency, affected by low frequency phase noise of 100 kHz bandwidth, is modulated by a 2 MHz baseband information signal in some RF circuit, it is not possible to adopt a 3-D formulation for the simulation of that circuit. It is so because the two aperiodic entities (the 100 kHz phase noise and the 2 MHz baseband signal) have to be mixed in the same time dimension. Consequently, although such case involves three distinct rates of change, a 2-D formulation must be assumed. Taking this into account, it is straightforward to conclude that an interesting issue to explore in the future will be the exploitation of efficient numerical algorithms for the simulation of RF circuits containing two, or more, distinct aperiodic regimes of widely separated rates of change. A computer-aided design tool especially conceived for that purpose is still missing.

Another area where further research may be of interest is the simulation of circuits containing nonlinear devices for which quasi-static models are not accurate enough. Although the quasi-static approximation performs very well for several semiconductor devices, and allows us to devise equivalent circuits for such devices using only lumped linear and nonlinear elements, there are, however, some situations where this assumption may not be adequate. Charge carrier transit time (time delays), or thermal effects in solid-state devices are examples of possible causes of the quasi-static approximation's inaccuracies.

Finally, a potentially interesting subject to be investigated in the future is the possible inclusion of memristors in upcoming RF circuits, that is to say, the impact of such potential technological revolution in the circuit simulation industry. The memristor, or memory resistor the "missing electronic circuit element", first appeared in 1971 with a paper published by Professor Leon Chua [11], from the University of California, Berkeley, adding this way a fourth basic circuit element to the electrical circuit theory. However, only thirty-seven years later, in 2008, a group of scientists from HP Labs has finally built real working memristors, whose most interesting characteristic is that they remember the amount of charge that flows through them. Since researchers believe that this discovery can lead to a new breed of both analog and digital devices, some adjustments in the

numerical algorithms may possibly be required in such case, to improve the efficiency of the simulation tools.

References

[1] Asai, H., and H. Makino, "Frequency Domain Latency and Relaxation-Based Harmonic Analysis of Nonlinear Circuits," *Proc. 34th Midwest Symposium on Circuits and Systems*, Monterey, CA, May 1991, pp. 202-205.

[2] Asai, H., "Relaxation-Based Simulation of Nonlinear Circuits in the Frequency Domain," *Proc. IEEE International Symposium on Circuits and Systems*, Singapore, Jun. 1991, pp. 2745-2748.

[3] Asbeck, P., L. Larson, and I. Galton, "Synergistic Design of DSP and Power Amplifiers for Wireless Communications," *IEEE Transactions on Microwave Theory and Techniques*, vol. 49, no. 11, Nov. 2001, pp. 2163-2169.

[4] Asbeck, P., et al., "Envelope Elimination and Restoration Technology for High Efficiency Base Station Applications," *WMB Workshop on High Efficiency Amplifiers*, presented at International Microwave Symposium 2006.

[5] Bartel, A., "Multirate ROW Methods of Mixed Type for Circuit Simulation," *Scientific Computing in Electrical Engineering*, Lecture Notes in Computational Science and Engineering, Springer, 2001, pp. 241-249.

[6] Bartel, A., M. Günther, and A. Kværnø, "Multirate Methods in Electrical Circuit Simulation," *Progress in Industrial Mathematics at ECMI 2000*, Springer, 2002, pp. 258-265.

[7] Bogacki, P., and L. Shampine, "A 3(2) Pair of Runge-Kutta Formulas," *Applied Mathematics Letters*, 2:1-9, 1989.

[8] Brachtendorf, H., G. Welsch, R. Laur and A. Bunse-Gerstner, "Numerical Steady-State Analysis of Electronic Circuits Driven by Multi-Tone Signals," *Electrical Engineering*, vol. 79, no. 2, 1996, pp. 103-112.

[9] Carvalho, N. B., and J. C. Pedro, "Novel Artificial Frequency Mapping Techniques for Multi-Tone Simulation of Mixers," *Proc. IEEE MTT-S International Microwave Symposium Digest*, Phoenix, May 2001, pp. 455-458.

[10] Christoffersen, C., and J. Alexander, "An Adaptive Time Step Control Algorithm for Nonlinear Time Domain Envelope Transient," *Proc. Canadian Conference on Electrical and Computer Engineering*, Ontario, May 2004, pp. 883-886.

[11] Chua, L., "Memristor - The Missing Circuit Element," *IEEE Transactions on Circuit Theory*, vol. 18, no. 5, Sep. 1971, pp. 507-519.

[12] Günther, M., and P. Rentrop, "Multirate ROW Methods and Latency of Electric Circuits," *Applied Numerical Mathematics*, vol. 13, Issue 1-3, Sep. 1993, pp. 83-102.

[13] Günther, M. and P. Rentrop, "Partitioning and Multirate Strategies in Latent Electric Circuits," *International Series of Numerical Mathematics*, vol. 117, 1994, pp. 33-60.

[14] Günther, M., A. Kværnø and P. Rentrop, "Multirate Partitioned Runge-Kutta Methods," *BIT*, vol. 41, no. 3, Jun. 2001, pp. 504-514.

[15] Hairer, E., S. Nørsett and G. Wanner, *Solving Ordinary Differential Equations I: Nonstiff Problems*, Berlin: Springer-Verlag, 1987.

[16] Hairer, E., and G. Wanner, *Solving Ordinary Differential Equations II: Stiff and Differential Algebraic Problems*, Berlin: Springer-Verlag, 1991.

[17] Janicot, V., "A Novel Time-Frequency Method for the Simulation/Verification of Mixed Analog and RF Communication Systems," *Proc. IEEE Radio and Wireless Conference*, Boston, Aug. 2001, pp. 133-136.

[18] Kimball, D., et al., "High-Efficiency Envelope-Tracking W-CDMA Base-Station Amplifier Using GaN HFETs," *IEEE Transactions on Microwave Theory and Techniques*, vol. 54, no. 11, Nov. 2006, pp. 3848-3856.

[19] Kress, R., *Numerical Analysis*, Graduate Texts in Mathematics 181, Springer-Verlag, New York, 1998.

[20] Kundert, K., G. Sorkin and A. Sangiovanni-Vincentelli, "Applying Harmonic Balance to Almost Periodic Circuits," *IEEE Transactions on Microwave Theory and Techniques*, vol. 36, no. 2, Feb. 1988, pp. 366-378.

[21] Kundert, K., J. White and A. Sangiovanni-Vincentelli, *Steady-State Methods for Simulating Analog and Microwave Circuits*, Norwell, MA: Kluwer Academic Publishers, 1990.

[22] Kværnø, A., and P. Rentrop, "Low Order Multirate Runge-Kutta Methods in Electric Circuit Simulation," *IWRMM Universität Karlsruhe*, Preprint No.99/1, 1999.

[23] Kværnø, A., "Stability of multirate Runge-Kutta schemes," *International Journal of Differential Equations and Applications*, no. 1A, 2000, pp. 97-105.

[24] Lambert, J. D., *Numerical Methods for Ordinary Differential Systems: The Initial Value Problem*, John Wiley & Sons, West Sussex, 1991.

[25] Larson, L., et al., "Digital Predistortion Techniques for Linearized Power Amplifiers," in *Proc. Asia-Pacific Microwave Conference*, Yokohama, Dec. 2006, pp. 1048-1051.

[26] Maas, S. A., "A GaAs MESFET Mixer with Very Low Intermodulation," *IEEE Transactions on Microwave Theory and Techniques*, vol. 35, no. 4, Apr. 1987, pp. 425-429.

[27] Maas, S. A., *Nonlinear Microwave and RF Circuits*, Second Edition, Norwood, MA: Artech House, 2003.

[28] Makino, H., and H. Asai, "Acceleration Techniques for the Circuit Simulation in the Frequency Domain," *Proc. IEEE International Symposium on Circuits and Systems*, San Diego, CA, May 1992, pp. 903-906.

[29] Mayaram, K., D. Lee, D. Rich and J. Roychowdhury, "Computer-Aided Circuit Analysis Tools for RFIC Simulation: Algorithms, Features, and Limitations," *IEEE Transactions on Circuits and Systems II: Analog and Digital Signal Processing*, vol. 47, no. 4, Apr. 2000, pp. 274-286.

[30] Mei, T., J. Roychowdhury, T. Coffey, S. Hutchinson, and D. Day, "Robust, Stable Time-Domain Methods for Solving MPDEs of Fast/Slow Systems," *IEEE Transactions on Computer-Aided Design of Integrated Circuits and Systems*, vol. 24, no. 2, Feb. 2005, pp. 226-239.

[31] Mei, T., J. Roychowdhury, "An Efficient and Robust Technique for Tracking Amplitude and Frequency Envelopes in Oscillators," *Proc. IEEE/ACM International Conference on Computer-Aided Design*, San Jose, CA, Nov. 2005, pp. 599-603.

[32] Nagel, L., *Spice2: A Computer Program to Simulate Semiconductor Circuits*, Electronics Research Laboratory, University of California, Berkeley, Memo ERL-M520, 1975.

[33] Nakhla, M. S., and J. Vlach, "A Piecewise Harmonic Balance Technique for Determination of Periodic Response of Nonlinear Systems," *IEEE Transactions on Circuits and Systems*, vol. 23, no. 2, 1976, pp. 85-91.

[34] Narayan, O., and J. Roychowdhury, "Analysing Forced Oscillators with Multiple Time Scales," *Proc. 12th International Conference on VLSI Design*, Goa, Jan. 1999, pp. 621-624.

[35] Narayan, O., and J. Roychowdhury, "Analyzing Oscillators Using Multitime PDEs," *IEEE Transactions on Circuits and Systems*, vol. 50, no. 7, Jul. 2003, pp. 894-903.

[36] Ngoya, E., and R. Larchevèque, "Envelope Transient Analysis: A New Method for the Transient and Steady-State Analysis of Microwave Communications Circuits and Systems," *Proc. IEEE MTT-S International Microwave Symposium Digest*, San Francisco, CA, Jun. 1996, pp. 1365-1368.

[37] Nguyen, L., and V. Janicot, "Simulation Method to Extract Characteristics for Digital Wireless Communication Systems," *Proc. Design Automation and Test in Europe Conference*, Munich, Mar. 2001, pp. 176-181.

[38] Oliveira, J., *Métodos Multi-Ritmo na Análise e Simulação de Circuitos Electrónicos não Lineares*, Master of Science Dissertation, University of Coimbra, Coimbra, Portugal, 2005.

[39] Oliveira, J. and A. Araújo, "Envelope Transient Simulation of Nonlinear Electronic Circuits using Multirate Runge-Kutta Algorithms," *WSEAS Transactions on Electronics*, vol. 3, Issue 2, Feb. 2006, pp. 77-84.

[40] Oliveira, J., "Efficient Methods for Solving Multirate Partial Differential Equations in Radio Frequency Applications," *WSEAS Transactions on Circuits and Systems*, vol. 5, Issue 1, Jan. 2006, pp. 24-31.

[41] Pedro, J. C., and N. B. Carvalho, "Efficient Harmonic Balance Computation of Microwave Circuits' Response to Multi-Tone Spectra," *Proc. 29th European Microwave Conference*, Munchen, Oct. 1999, pp. 103-106.

[42] Pedro, J. C., and N. B. Carvalho, "A Mixed-Mode Simulation Technique for the Analysis of RF Circuits Driven by Modulated Signals," *III Conferência de Telecomunicações*, Figueira da Foz, Apr. 2001.

[43] Pedro, J. C., and N. B. Carvalho, "Simulation of RF Circuits Driven by Modulated Signals Without Bandwidth Constraints," *Proc. IEEE MTT-S International Microwave Symposium Digest*, Seattle, Jun. 2002, pp. 2173-2176.

[44] Pedro, J. C., and N. B. Carvalho, *Intermodulation Distortion in Microwave and Wireless Circuits*, Norwood, Artech House, 2003.

[45] Pina, H., *Métodos Numéricos*, McGraw Hill, Lisboa, 1995.

[46] Pulch, R., "Warped MPDAE Models with Continuous Phase Conditions," *University of Wuppertal*, Preprint BUW-AMNA 04/03, Jul. 2004.

[47] Pulch, R., "Multi Time Scale Differential Equations for Simulating Frequency Modulated Signals," *Applied Numerical Mathematics*, vol. 53, Issue 2-4, 2005, pp. 421-436.

[48] Pulch, R., "Variational Methods for Solving Warped Multirate PDAEs," *University of Wuppertal*, Preprint BUW-AMNA 05/01, Apr. 2005.

[49] Rizzoli, V., C. Cecchetti, and A. Lipparni, "A General-Purpose Program for the Analysis of Nonlinear Microwave Circuits Under Multitone Excitation by Multidimensional Fourier Transform," *Proc. 17th European Microwave Conference*, Rome, Oct. 1987, pp. 635-640.

[50] Rizzoli, V., A. Neri, "State of the Art and Present Trends in Nonlinear Microwave CAD Techniques," *IEEE Transactions on Microwave Theory and Techniques*, vol. 36, no. 2, Feb. 1988, pp. 343-365.

[51] Rizzoli, V., A. Neri, and F. Mastri, "A Modulation-Oriented Piecewise Harmonic Balance Technique Suitable for Transient Analysis and Digitally Modulated Analysis," *Proc. 26th European Microwave Conference*, Prague, Oct. 1996, pp. 546-550.

[52] Rizzoli, V., F. Mastri, F. Sgallari and G. Spaletta, "Harmonic-Balance Simulation of Strongly Nonlinear Very Large-Size Microwave Circuits by Inexact Newton Methods," *Proc. IEEE MTT-S International Microwave Symposium Digest*, San Francisco, CA, Jun. 1996, pp. 1357-1360.

[53] Rizzoli, V., F. Mastri, C. Cecchetti, and F. Sgallari, "Fast and Robust Inexact Newton Approach to the Harmonic-Balance Analysis of Nonlinear Microwave Circuits," *IEEE Microwave and Guided Wave Letters*, vol. 7, no. 10, Oct. 1997, pp. 359-361.

[54] Rizzoli, V., F. Mastri, A. Coostanzo, and E. Montanari, "Highly Efficient Envelope-Oriented Analysis of Large Autonomous RF/Microwave Systems by a Trust-Region Algorithm Coupled with Krylov-Subspace Harmonic-Balance," *Proc. 32th European Microwave Conference*, Milan, Oct. 2002, pp. 1-4.

[55] Rodrigues, P.J., "An Orthogonal Almost-Periodic Fourier Transform for Use in Nonlinear Circuit Simulation," *IEEE Microwave and Guided Wave Letters*, vol. 4, no. 3, Mar. 1994, pp. 74-76.

[56] Rodrigues, P.J., *Computer-Aided Analysis of Nonlinear Microwave Circuits*, Norwood, MA: Artech House, 1998.

[57] Roychowdhury, J., "Efficient Methods for Simulating Highly Nonlinear Multirate Circuits," *Proc. 34th Design Automation Conference*, Anaheim, Jun. 1997, pp. 269-274.

[58] Roychowdhury, J., "Analyzing Strongly Nonlinear Multitone Circuits by Multi-Time Methods," *Proc. 28th European Microwave Conference*, Amsterdam, Oct. 1998, pp. 267-271.

[59] Roychowdhury, J., "Analyzing Circuits with Widely Separated Time Scales Using Numerical PDE Methods," *IEEE Transactions on Circuits and Systems*, vol. 5, no. 48, May 2001, pp. 578-594.

[60] Roychowdhury, J., "A Time-Domain RF Steady-State Method for Closely Spaced Tones," *Proc. 39th Design Automation Conference*, New Orleans, Jun. 2002, pp. 510-513.

[61] Saad, Y., and M. Schultz, "GMRES: A Generalized Minimal Residual Method for Solving Nonsymmetric Linear Systems," *SIAM Journal on Scientific and Statistical Computing*, vol. 7, Jul. 1986, pp. 856-869.

[62] Schiesser, W. E., *The Numerical Method of Lines*, New York: Academic Press, 1991.

[63] Sharrit, D., "Method for Simulating a Circuit," U.S. Patent 5588142, December 24, 1996.

[64] Smith, J. D., *Numerical Solution of Partial Differential Equations: Finite Difference Methods*, Oxford Applied Mathematics and Computing Science Series, Oxford University Press, Oxford, 1993.

[65] Sorkin, G., K. Kundert and A. Sangiovanni-Vincentelli, "An Almost-Periodic Fourier Transform for Use with Harmonic Balance," *Proc. IEEE MTT-S International Microwave Symposium Digest*, Las Vegas, Jun. 1987, pp. 717-720.

[66] Staszewski, R., et al., "All-Digital PLL and Transmitter for Mobile Phones," *IEEE Journal of Solid-State Circuits*, vol. JSSC-40, no. 12, Dec. 2005, pp. 2469-2482.

[67] Thomas, J. W., *Numerical Partial Differential Equations: Finite Difference Methods*, Texts in Applied Mathematics 22, Springer-Verlag, New York, 1995.

[68] Trefethen, L., and D. Bau, *Numerical Linear Algebra*, Society for Industrial and Applied Mathematics, Philadelphia, 1997.

[69] Wang, F., et al., "An Improved Power-Added Efficiency 19-dBm Hybrid Envelope Elimination and Restoration Power Amplifier for 802.11g WLAN Applications," *IEEE Transactions on Microwave Theory and Techniques*, vol. 54, no. 12, Dec. 2006, pp. 4086-4099.

[70] Yang, B., and Dan Feng, "Efficient Finite-Difference Method for Quasi-Periodic Steady-State and Small Signal Analyses," *Proc. IEEE/ACM International Conference on Computer Aided Design*, San Jose, CA, Nov. 2000, pp. 272-276.

[71] Zhu, L., and C. Christoffersen, “Adaptive Harmonic Balance Analysis of Oscillators Using Multiple Time Scales,” *Proc. 3rd International IEEE Northeast Workshop on Circuits and Systems*, Québec City, Jun. 2005, pp. 187-190.